NANOCOMPOSITES BASED ON BLENDS OF POLYETHYLENE

**A THESIS SUBMITTED TO
THE GRADUATE SCHOOL OF NATURAL AND APPLIED SCIENCES
OF
MIDDLE EAST TECHNICAL UNIVERSITY**

BY

FATMA IŞIK

**IN PARTIAL FULFILLMENT OF THE REQUIREMENTS
FOR
THE DEGREE OF MASTER OF SCIENCE
IN
CHEMICAL ENGINEERING**

JULY 2005

Approval of Graduate School of Natural and Applied Sciences

_____

Prof. Dr. Canan Özgen
Director

I certify that this thesis satisfies all the requirements as a thesis for degree of Master of Science.

_____

Prof. Dr. Nurcan Baç
Head of the Department

This is to certify that we have read this thesis and that in our opinion it is fully adequate, in scope and quality, as a thesis for the degree of Master of Science.

_____

Prof. Dr. Ülkü Yılmazer
Supervisor

Examining Committee Members

Prof. Dr. Nurcan Baç	(CHE)	———————————
Prof. Dr. Ülkü Yılmazer	(CHE)	———————————
Prof. Dr. Leyla Aras	(CHEM)	———————————
Assoc. Prof. Dr. Göknur Bayram	(CHE)	———————————
Assoc. Prof. Dr. Cevdet Kaynak	(METE)	———————————

I hereby declare that all information in this document has been obtained and presented in accordance with academic rules and ethical conduct. I also declare that, as required by these rules and conduct, I have fully cited and referenced all material and results that are not original to this work.

Name, Last name : Fatma Işık

Signature

ABSTRACT

NANOCOMPOSITES BASED ON BLENDS OF POLYETHYLENE

Işık, Fatma

M.S., Department of Chemical Engineering

Supervisor: Prof. Dr. Ülkü YILMAZER

July 2005, 164 pages

In this study the effects of compatibilizer type, organoclay type, and the addition order of components on the morphological, thermal, mechanical and flow properties of ternary nanocomposites based on low density polyethylene, LDPE were investigated. As compatibilizer, ethylene/methyl acrylate/glycidyl methacrylate, ethylene/glycidyl methacrylate, and ethylene/butyl acrylate/maleic anhydride; as organoclay Cloisite® 15A, Cloisite® 25A and Cloisite® 30B were used. All samples were prepared by a co-rotating twin screw extruder, followed by injection molding.

Before producing the ternary nanocomposites, in order to determine the optimum amount of the organoclay and compatibilizer, binary mixtures of LDPE/organoclay and LDPE/compatibilizer blends with different compositions were prepared. Based on the results of the mechanical tests, compatibilizer and organoclay contents were determined as 5 wt. % and 2 wt % respectively. After that, ternary nanocomposites were prepared with each compatibilizer/organoclay system and characterization of these nanocomposites was performed.

Among the investigated addition orders, mechanical test results showed that the best sequence of component addition was (PCoC), in which LDPE, compatibilizer and organoclay were simultaneously compounded in the first run of the extrusion. Considering the ternary nanocomposites, compositions of LDPE/E-MA-GMA/15A, LDPE/E-GMA/15A and LDPE/E-nBA-MAH/30B showed the highest improvement in mechanical properties.

According to the DSC analysis, addition of organoclay and compatibilizer does not influence the melting behavior of the compositions and both compatibilizers and organoclay types have no nucleation activity in LDPE.

In the X-Ray analysis, the highest increase of the basal spacing for ternary nanocomposites obtained for LDPE/E-nBA-MAH/organoclay nanocomposites. This increase was 83 %, 198 %, and 206 % for samples containing 15A, 25A and 30B respectively.

Keywords: low density polyethylene, compatibilizer, organoclay, nanocomposites, extrusion

ÖZ

POLİETİLEN ALAŞIMLARI BAZLI NANOKOMPOZİTLER

Işık, Fatma

Yüksek Lisans, Kimya Mühendisliği

Tez Yöneticisi: Prof. Dr. Ülkü Yılmazer

Temmuz 2005, 164 sayfa

Bu çalışmada, uyum sağlayıcı çeşidi, organik kil çeşidi ve bileşenlerin ekleme sırasının alçak yoğunluklu polietilen bazlı nanokompozit sistemlerinin morfolojik, ısıl, mekanik ve akış özellikleri üzerindeki etkileri incelenmiştir. Uyum sağlayıcı olarak, etilen/metil akrilat/glisidil metakrilat (E-MA-GMA), etilen/glisidil metakrilat (E-GMA), ve etilen/bütil akrilat/maleik anhidrit (E-nBA-MAH) terpolimerleri; organik kil olarak Cloisite® 15A, Cloisite® 25A ve Cloisite® 30B kullanılmıştır. Tüm numuneler aynı yönde dönen çift vidalı ekstrüder ve bunu takiben enjeksiyonlu kalıplama yöntemi kullanılarak hazırlanmıştır.

Üçlü nanokompozit sistemleri hazırlanmadan önce, en uygun uyum sağlayıcı ve organik kil miktarını belirlemek için, değişik kompozisyonlarda ikili AYPE/organik kil nanokompozitleri ve AYPE/uyum sağlayıcı alaşımları hazırlanmıştır. Mekanik test sonuçlarına göre uyum sağlayıcı ve organik kil konsantrasyonları sırası ile ağırlıkça % 5 ve % 2 olarak belirlenmiştir. Bundan sonra, herbir uyum sağlayıcı/organik kil sistemi

ile üçlü nanokompozitler hazırlanmış ve bunu takiben bu nanokompozitlerin karakterizasyonu yapılmıştır.

Mekanik test sonuçları incelenen bileşen ekleme sıraları arasında AYPE, uyum sağlayıcı ve organik kilin ilk ekstrüzyon sırasında hep beraber karıştırıldığı (PCoC) yönteminin, en iyi ekleme sırası olduğunu göstermiştir. Üçlü nanokompozit sistemleri dikkate alındığında, AYPE/E-MA-GMA/15A, AYPE/E-GMA/15A ve AYPE/E-nBA-MAH/30B sistemleri mekanik özelliklerde en yüksek gelişmeyi göstermiştir.

DSC analizine göre, alçak yoğunluklu polietilene organik kil ve uyum sağlayıcı eklenmesi, bileşiklerin erime özelliklerini etkilememiştir ve uyum sağlayıcı ve organik kil çeşitleri, AYPE içinde kristallenmeyi başlatıcı özelliğe sahip değildirler.

X-ışını kırınımı analizinde, üçlü nanokompozit sistemleri arasında tabaka aralığındaki en fazla artış, AYPE/E-nBA-MAH/organik kil nanokompozitlerinde elde edilmiştir. Bu artış 15A, 25A ve 30B içeren numunelerde sırasıyla % 83, % 198, ve % 206' dır.

Anahtar Kelimeler: Alçak yoğunluklu polietilen, uyum sağlayıcı, organik kil, nanokompozitler, ekstrüzyon

To my family & My little nephew, M.Efe Işık

ACKNOWLEDGEMENTS

It is with immense pleasure that I dedicate this dissertation to each and every member of my family who always offered their advice, love, care and support. My family's absolute unquestionable belief in me, have been a constant source of encouragement and have helped me achieve my goals. I also express my sincerest love and thanks to Fatih Coşkunses for his love, patience, support and understanding and encouragement in every step of this study. It would not have been possible without their love and support to complete this study.

TABLE OF CONTENTS

CHAPTER

LIST OF TABLES

TABLE

LIST OF FIGURES

FIGURE

NOMENCLATURE

A_0 Original, undeformed cross-sectional area, mm2

b   Width of beam tested, mm

d   Depth of beam tested, mm

d   Plane spacing, Å

E   Modulus of Elasticity, MPa

F   Tensile Load, N

L   Support span, mm

L_0 Initial gauge length, mm

ΔL Change in sample length, mm

m   Slope of the tangent to the initial straight-line portion of the load deflection curve, N/mm

n   Order of diffraction

P   Load at a given point on the load-deflection curve, N

R   Maximum strain in the outer fibers, mm/mm

S   Stress in the outer fibers at midspan, MPa

T   Thickness, mm

Tc   Crystallization temperature, °C

Tg   Glass transition temperature, °C

Tm   Melting temperature, °C

Greek Letters

Є   Tensile strain, mm/mm

λ   Wavelength, nm

σ   Tensile stress(nominal), MPa

σ_m Tensile strength, MPa

θ   Scattering angle, °

Abbreviations

ASTM	American Society for Testing and Materials
CEC	Cation Exchange Capacity
DSC	Differential Scanning Calorimetry
E-GMA	Ethylene-Glycidyl Methacrylate
E-MA-GMA	Ethylene-Methyl Acrylate-Glycidyl Methacrylate
E-nBA-MAH	Ethylene-Butyl Acrylate-Maleic Anhydride
GMA	Glycidyl Methacrylate
HDPE	High Density Polyethylene
HT	Hydrogenated Tallow
LDPE	Low Density Polyethylene
MFI	Melt Flow Index
MMT	Montmorillonite
PE	Polyethylene
PLS	Polymer Layered Silicate
SEM	Scanning Electron Microscopy
T	Tallow
TEM	Transmission Electron Microscopy
XRD	X-Ray Diffraction

CHAPTER 1

INTRODUCTION

Composites usually consist of proper volume fractions of high strength, high stiffness reinforcing materials embedded in a lower modulus matrix [1]. Properties of the constituents, their relative amounts, and the geometry of the dispersed phase determine the unique properties of the new materials. Composites are used in variety of applications in industry due to the improved material properties such as strength, stiffness or toughness, and low processing cost.

The most common matrix materials used for composites are polymers, which are lightweight materials with high strength and modulus values. One reason for their growing use is that their processing is relatively simple and does not require very high temperatures and pressures. Moreover, problems associated with the degradation of the reinforcement material during manufacture are less significant for polymer matrix composites -PMC's- than for composites with other matrices, such as ceramic and metal. Design flexibility, variety of processing techniques for producing PMC parts, are also advantages of these materials.

Nanocomposites are a special class of polymer matrix composites, containing fillers, at least one dimension of which is in the nanometer (10^{-9}) range [2]. Due to the structural properties gained by well dispersion of the nanosized fillers, nanocomposites posses highly improved mechanical, thermal, physical, and barrier properties when compared to pristine polymer and conventional composites [3].

Among the inorganic fillers, layered silicates are widely used in nanocomposites owing to the high aspect ratio. In the case of well dispersion of the silicate layers throughout

the polymer matrix, interaction of the filler and polymer increases significantly and improves material properties.

Montmorillonite which belongs to the general family of 2:1 layered silicates is the most commonly used smectite clay in nanocomposites. The structure of montmorillonite consists of an octahedral alumina sheet between two tetrahedral silica sheets. The layer thickness of the crystal structure is around 1 nm, and the lateral dimensions of these layers may be in the range of 30 nm to several microns or larger [4]. Natural montmorillonite is quite hydrophilic material, thus incompatible with many hydrophobic engineering polymers. So the layered silicates are not easily dispersed in most polymers. In order to overcome this problem, a simple cation exchange process is applied to montmorillonite to make the clay organophilic.

LDPE is one of the major class of the polyethylenes. Its unique properties such as toughness, high impact strength, low brittleness temperature, flexibility, processability, chemical resistance to polar compounds, low permeability to water, and outstanding electrical properties make it in request in industry [5].

Incompatibility of organoclay and polyethylene which is non-polar, brings out the necessity of using a third material in nanocomposites, called compatibilizer. There are several studies in the literature that emphasize the effect of the compatibilizer on dispersion of organoclay in the matrix [6-16].

Mainly, there are three methods of synthesizing nanocomposites: In-situ intercalative polymerization method, solution intercalation method and melt intercalation method. Melt intercalation method is relatively easier than the other methods due to the absence of organic solvents and compatible with various industrial processes such as extrusion and injection. Thus it is the mostly used method for commercial applications [17]. In this study nanocomposites were produced by means of a co-rotating twin screw extruder with a two step mixing procedure.

The objective of this study is to investigate the effects of compatibilizer type, organoclay type, addition order of the components on the final properties of ternary

nanocomposites containing low density polyethylene, compatibilizer, and organically modified clay. Three types of compatibilizers, terpolymer of ethylene – methyl acrylate – glycidyl methacrylate (E-MA-GMA), copolymer of ethylene – glycidyl methacrylate (E-GMA), and terpolymer of ethylene – n-butyl acrylate – maleic anhydride (E- nBA-MAH), and organoclays, Cloisite® 15A, Cloisite® 25A and Cloisite® 30B were used during the experiments.

First, the concentrations of the compatibilizer and organoclay in nanocomposites were determined by melt compounding of binary LDPE/compatibilizer blends and LDPE/organoclay nanocomposites. After determining the optimal compatibilizer and clay content, ternary nanocomposites were produced by means of a co-rotating twin screw extruder with a two step mixing procedure. Finally, in order to characterize the nanocomposites, all standard test specimens were prepared by injection molding.

X-Ray Diffraction (XRD) and Scanning Electron Microscopy (SEM) analyses were performed in order to investigate the extent of dispersion of the organoclay in the matrix. Thermal characterization of the nanocomposites was performed by Differential Scanning Calorimetry (DSC), and flow properties were determined with Melt Flow Index measurements. Mechanical characterization of the nanocomposites included the investigation of tensile strength, tensile modulus, tensile strain at break, flexural strength and flexural modulus of the all samples.

CHAPTER 2

BACKGROUND

2.1 Composites

A composite is defined as a combination of two or more components differing in form or composition on a macroscale, with two or more distinct phases having recognisable interfaces between them [1]. The constituents of composites retain their identities which mean that, they do not dissolve or merge completely into one another although they act together and also the components can be physically identified [18].

The first composite materials may have been bricks fashioned by the ancient Egyptians from mud and straw [19]. Reinforced concrete which was invented by Romans and natural fiber reinforced clay used before the invention of iron are also the essence of the composite materials [18]. In the early 1960's, there has been an increasing demand for materials that are stiffer and stronger, yet lighter, in aeronautic, energy, civil engineering and various structural applications. Unfortunately, no monolithic material is available to satify them. This need and demand certainly led to the concept of combining different materials in an integral composite structure [1].

The new material obtained by mixing the proper combinations of the materials has highly improved properties than the individual constituents of composites can attain [1]. The concept of improved performance is broad and includes increased strength or reinforcement of one material by the addition of another material [20]. The high performance of the obtained composites results in the usage of these new materials

in a wide range of applications such as automotive, aerospace, chemical, marine, sports, electrical and electronics, construction, etc. industries [21].

The composites are usually blends of two different phases, one of which is a resinous binder or matrix, which surrounds and holds the reinforcing material, dispersed phase, in place. The dispersed phase is strong and stiff relative to the continuous phase [22]. The final properties of the composites depend on not only the properties of each phases but also the relative amounts of the constituents, the geometry of the dispersed phase which includes the shape, particle size, orientation and dispersion of reinforcing material as well as on the reinforcement-matrix interface [23]. Interface is the region through which material properties such as concentration of an element, crystal structure, elastic modulus, density, thermal expansion coefficient change from one side to another [24]. The interface plays an important role in controlling the failure mechanism, fracture toughness, and overall stress-strain behavior of material, although it is small in size [25].

2.1.1 Matrix Phase

Matrix is the continuous phase of the composites and usually occupies 30% -40% of composite structures. Some of the main functions of the matrix are that, it holds the components together and determines the thermo-mechanical stability of the composite, protects the reinforcements from environment, accepts the load over a large surface area, and then transfers it to the reinforcement material, which can resist a greater load [1].

2.1.2 Reinforcement Phase

The reinforcement material determines the strengthening mechanism of a composite. It can be in the form of either continuous (long fibers, sheets) or discontinuous (particles, short fibers, etc.). It is also possible to classify composites according to the characteristics of the reinforcement. The following three categories are the commonly used type of composites [1].

- Fiber Reinforced: The fiber is the primary load-bearing component.
- Dispersion Strengthened: The matrix is the major load-bearing component.
- Particle Reinforced: The load is shared by the matrix and the particles.

The choice of reinforcement for a particular engineering application depends on a large number of parameters, including strength, stiffness, environmental stability, and cost [20].

2.1.3 Types of Composites

Composites can be classified according to the material type of matrix phase. The matrix can be metal, ceramic, wood, polymer, etc. The most common composites are metal-matrix composites (MMC), ceramic-matrix composites (CMC), and polymer-matrix composites (PMC).

2.2 Polymer Matrix Composites

Polymers are mostly organic compounds based on carbon, hydrogen, and other non metallic elements. PMC are in general a synergistic combination of high performance reinforcing material and matrix and moreover they are the most developed composite materials group and they have found widespread applications [1]. The main reasons for being most preferable composite type are the versatility of their properties, such as light weight, easy processing, corrosion resistance and low processing cost [26].

There are two different alternatives in matrix selection, thermoplastic and thermoset, and there are matrix choices available within the two main divisions. The basic difference between the two is that thermoplastic materials (polyolefinics, polystyrene, polyamides, etc.) can be repeatedly softened by heat, and thermosetting polymers (epoxy resins, polyester, polyimides, phonolics, etc.) can not be changed after the chemical reaction since their cure has been completed. Thermoplastics and thermosets differ profoundly in terms of manufacturing, processing, physical and

6

mechanical properties of product, and the environmental resistance of the resultant composite [22].

Thermoplastics polymers have linear or branched structures that soften upon heating. The chains of the thermoplastics are tied together with secondary bonds such as Van der Waals forces [20]. These bonds can be broken temporarily upon heating and the polymer chains can slide past one another easily and can move to form a different shape. When thermoplastics are cooled the weak bonds reform and the thermoplastic material keeps its new shape.

The structure of thermoset materials similar to those of thermoplastic materials but processing develops permanent cross-links between adjacent molecules, forming complex networks that prevent relative movement between the chains of the thermoset resins. This means that the thermosetting material always keeps its shape. Heating a thermoset degrades the material so that it cannot be reprocessed satisfactorily [27].

2.3 Nanocomposites

Nanocomposites are one of the most interesting and potentially important new areas of polymer research. These are composites including less than 6 % inorganic reinforcements with high aspect ratio with dimensions in the area of 1 to 100 nm [19]. Due to their nanometer size features, nanocomposites have unique properties typically not shared by conventional composites, and therefore offer new technology and business opportunities [3].

Improved mechanical properties, reduced gas and water permeability for barrier applications, increased thermal stability, flame resistance, elevated heat-distortion temperature, recyclability, and improved processability are some of the attractive properties of nanocomposites. Moreover usage of inexpensive naturally-occurring materials for reinforcement phase makes these materials more preferable than the conventional composites [19].

Nanocomposites can be divided into three groups according to number of nano-size dimensions of the dispersed particles. The first group is *isodimensional nanoparticles* of which three dimensions are in the order of nanometers. Spherical silica nanoparticles are one example of this group. When two dimensions of the particles are in the nanometer scale and the third dimension is larger, the structure is *elongated structure* and includes nanotubes and whiskers. The third type of nanocomposites is called *polymer-layered crystal nanocomposites* correspond to the case where reinforcements are in the shape of platelets and have only one dimension in the nano level. In this type, the filler has a very high aspect ratio owing to a few nanometer thickness to hundreds to thousands nanometers length. Polymer-layered crystal nanocomposites are obtained by the insertion of the polymer inside the galleries of the reinforcements which can be either natural or synthetic crystalline. Graphite, carbon oxides, metal phosphates, clays and layered silicates are some examples of fillers used in producing nanocomposites [2].

This study is based on the polymer-layered silicate nanocomposites which belong to this third class.

2.3.1 Polymer-Layered Silicate Nanocomposites

Main reinforcement materials used in nanocomposites are clay and layered silicates since clay materials are easily available and according to previous studies it was seen that using these materials results in highly improved properties.

It was 1950's that polymer layered silicate nanocomposites were first reported in the patent literature [28]. However this type of nanocomposites became more widely studied in academic, government and industrial laboratories after the Toyota researchers obtained a well dispersion of nano-sized particles(clay) in the matrix (nylon) and the obtained nanocomposites exhibited dramatically improved mechanical, thermal, optical and physico-chemical properties compared to the pristine polymer or conventional composites [2,28].

Polymer layered silicate nanocomposites usually exhibit properties superior to conventional composites such as strength, stiffness, thermal and oxidative stability, barrier properties with very little amount of filler content in comparison to glass- or mineral- reinforced polymers. Moreover, these nanocomposites are lighter in weight than the conventional composites. The fabrication techniques of polymer layered silicate nanocomposites are much easier and cheaper than the fabrication of conventional composites since they can attain the composite properties with low volume fraction of reinforcement [3].

Some application areas of polymer layered silicate nanocomposites are aerospace, automotive, electronics and biotechnology industries [29].

2.3.2 Layered Silicates

Among the large number of inorganic layered materials that have the capability of intercalation, layered silicates are one of the most typical because of the versatility of reactions [30].

The commonly used layered silicates in preparation of polymer layered silicate nanocomposites belong to the 2:1 layered or phyllosilicates family [31]. The crystalline structure of phyllosilicates has one octahedral layer sandwiched between two tetrahedral layers. In the structure of 2:1 layered family, two tetrahedrally coordinated silicon atoms are fused to an edge-shared central octahedral sheet of either aluminum or magnesium hydroxide. The oxygen atoms of the octahedral sheet also belong to the tetrahedral sheets [32].

The layer thickness of the crystal structure is around 1 nm, and the lateral dimensions of these layers may be in the range of 30 nm to several microns or larger. Stacking of the layers leads to a regular Van der Waals gap between the layers called interlayer or gallery. Isomorphic substitution within the layers (for example, Al^{+3} replaced by Mg^{+2} or Fe^{+2}) generates negative charges that are counterbalanced by alkali and alkaline earth cations placed inside the galleries. This type of layered silicate is characterized by the cation exchange capacity (CEC). Since this charge is not constant for each layer, an

average value of CEC is determined for a whole crystal. The structure of 2:1 phyllosilicates is given in Figure 2.1.
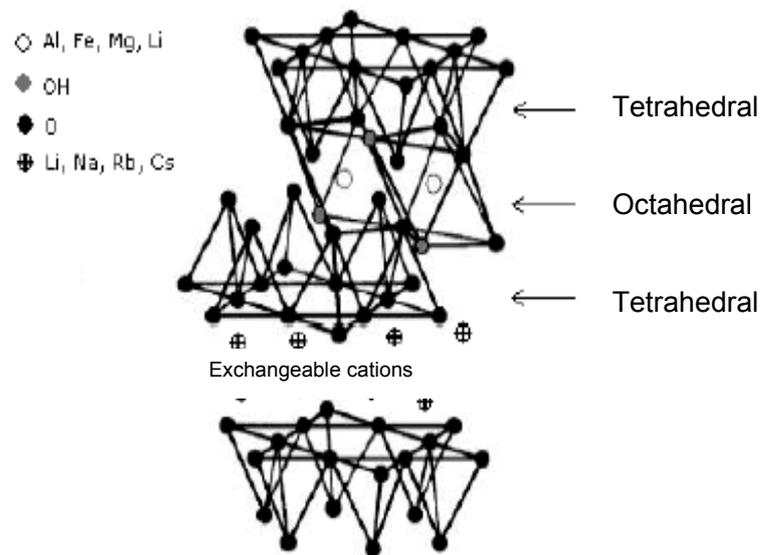
Figure 2.1 Structure of 2:1 layered phyllosilicates [33].

Two main characteristics of layered silicates are the ability of the silicate particles to disperse individual layers and to fine-tune their surface chemistry through ion exchange reactions with organic and inorganic cations.

The most commonly used layered silicates are montmorillonite, hectorite and saponite.

2.3.2.1 Montmorillonite (Smectite clay)

Montmorillonite is a naturally-occurring 2:1 phyllosilicate, which has the same layered and crystal structure as talc and mica but a different layer charge. The structure of montmorillonite consists of an octahedral alumina sheet between two tetrahedral silica sheets. Generally, the alumina sheet has some replacement of the aluminum cations

by magnesium cations which results in a net negative charge to the layers. This negative charge is balanced by having hydrated Na^+, Li^+, Mg^{+2}, Ca^{+2}, K^+ cations situated in the galleries between the aluminosilicate layers [19].

The most important aspect of the smectite group is the ability for water molecules to be absorbed between the layered sheets, causing the volume of the minerals to increase when they come in contact with water. Thus montmorillonite can expand by several times its original volume when it comes in contact with water which makes it useful for several applications.

2.3.3 Organically Modified Layered Silicates

In its pristine form the clay is present as a crystal which is made up of stack of layered silica sheets (platelets). Silicate nanolayers are ideal for reinforcement due to the high aspect ratios. Moreover the presence of positive ions on the surface of the silica sheets increases the d-spacing of the clay crystal which generally varies from 1.0-1.3 nm, but it also makes the clay crystal planes hydrophilic and thus incompatible with many hydrophobic engineering polymers [4]. So the layered silicates are not easily dispersed in most polymers.

In order to make layered silicates miscible with polymers, naturally hydrophilic silicate surface can be converted to organophilic surface easily by ion-exchange reactions with cationic surfactants including primary, secondary, tertiary, and quaternary alkylammonium cations [31]. The choice of the ammonium ion depends on its chemical compatibility with the polymer matrix. The cation-exchange process between the alkylammonium ions and the cations initially intercalated between the clay layers is shown in Figure 2.2.
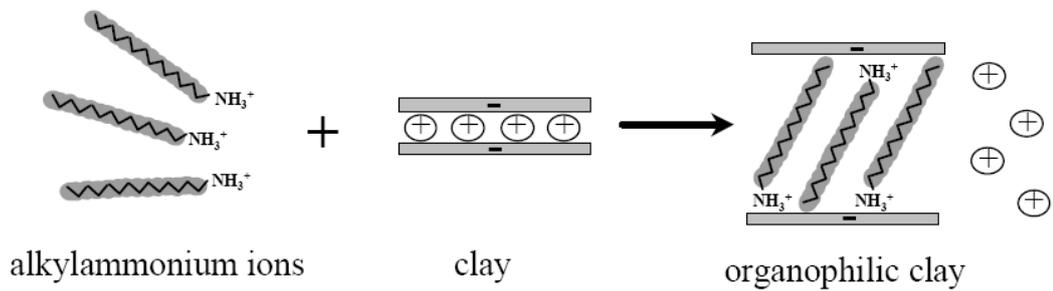
Figure 2.2 The cation-exchange process between alkylammonium ions and cations initially intercalated between the clay layers [35].

According to charge density of the clay and the onium ion surfactant, different arrangements of the onium ions as monolayer, lateral bilayer, pseudo-trimolecular layer, and inclined paraffin structure, are possible [34].

The replacement of inorganic exchange cations by organic onium ions on the gallery surfaces of smectite clays not only helps to match the polarity of the clay surface with the polarity of the polymer, but it also increases the d-spacing of the layered silicates [34]. Moreover the alkylammonium cations can have functional groups that can react with the polymer matrix and improve the interface between the layered silicates and the matrix.

2.3.4 Types of Polymer Layered Silicate Nanocomposite Structures

The structures of the polymer layered silicate nanocomposites depend on the nature of the components used, synthesizing methods, and strength of the interfacial interactions between the clay and the polymer, and the clay loading. There are mainly three types of composites; phase separated composites (microcomposite), intercalated nanocomposites, and exfoliated nanocomposites. Figure 2.3 shows the types of nanocomposites structures.
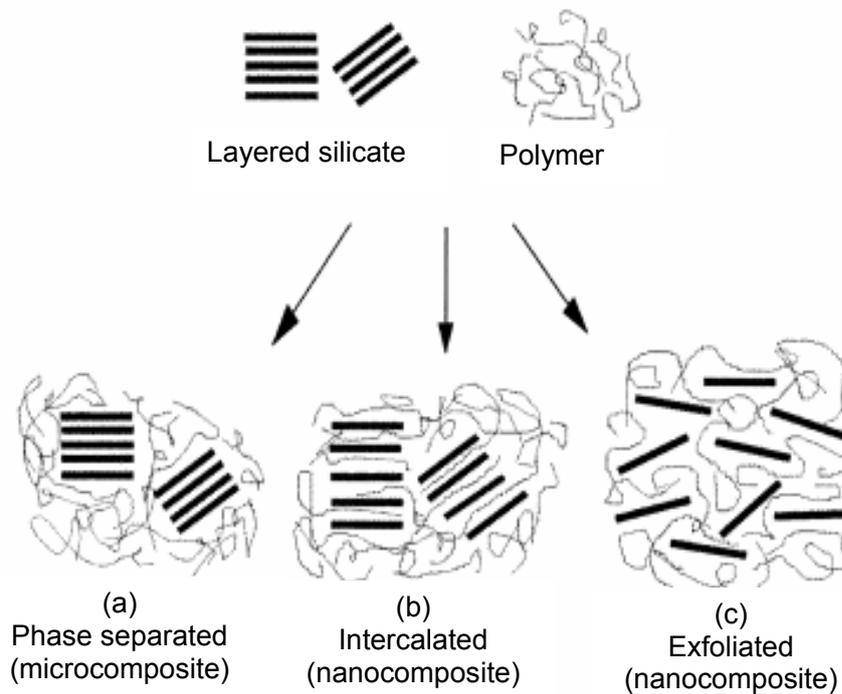
Figure 2.3 Scheme of different types of composites arising from the interaction of layered silicates and polymers: (a) phase-separated microcomposite; (b) intercalated nanocomposite and (c) exfoliated nanocomposite [2].

If the polymer and clay are not compatible, and the clay platelets remain as large stacks without any polymer chains entering the region between the clay platelets the resulted structure is the phase separated microcomposite (Figure 2.3a). This type of composites behave as conventional composites and the incomplete and non-uniform dispersion of clay layers creates large regions of pure polymer in the nanocomposite leading to poor properties.

In the intercalated nanocomposites, a single or sometimes several polymer chains enter the clay gallery, but the platelets still remain as a stack and well ordered multilayer structures (Figure 2.3b).

In an exfoliated nanocomposite, the individual clay layers are completely separated throughout the polymer matrix (Figure 2.3c). This structure can be obtained if both the polymer and the clay layers have polar groups that have favorable interaction and the greatest property enhancement in polymer layered silicate nanocomposites systems is obtained with the exfoliated nanocomposite structures. Usually, the clay content of an exfoliated nanocomposite is much lower than that of an intercalated nanocomposite.

2.3.5 Synthesis of Polymer Layered Silicate Nanocomposites

Three main processes used for preparing polymer layered silicate nanocomposites are; *In-Situ Intercalative Polymerization Method, Solution Intercalation Method* and *Melt Intercalation Method.*

2.3.5.1 In-Situ Intercalative Polymerization Method

This process involves mechanical mixing of the clay mineral with the required monomer. The layered silicate is swollen within the liquid monomer (or a monomer solution) and then the monomer intercalates within the interlayer and promotes delamination. Polymerization follows, initiated by a number of ways such as heat or radiation, the diffusion of a suitable initiator, an organic initiator or catalyst fixed through cationic exchange inside the interlayer before the swelling step by the monomer, to yield linear or cross linked polymer matrices. Usually the clay mineral needs to be dispersed by a pre-swelling step of long-chain alkylammonium ion intercalation to aid exfoliation [2].

The first US patent (#4739007) for the development of nylon-clay nanocomposites by in-situ polymerization route was filed by Okada et.al. from Toyota Motor Company in 1988.

Nanocomposites prepared by this method have showed remarkably improved properties but the batch size achieved by this method in a laboratory is limited due to small sized reactors. Presence of additives in the system leads to complicated reaction conditions making the production of these materials very complicated in the large

reactors used in industry. Thus bulk production of the nanocomposites by this method is very unlikely in industry [4].

2.3.5.2 Solution Intercalation Method

In this synthesizing method, the polymer is first dissolved in a solvent and then the modified layered silicate is added to the system. The solvent used in this method should dissolve the polymer and also swell the layered silicates. The layered silicates can be easily dispersed in an adequate solvent due to the weak forces that stack the layers together. The process includes the swelling of the clay layers by the solvent and then intercalation of the polymer chains into the expanded clay galleries and removal of the solvent molecules out of the gallery. After the solvent is completely displaced out of the galleries the system is heated to evaporate the solvent from the system. The layers of the clay do not collapse back since they have been dispersed enough during the process and at the end intercalated nanocomposites are obtained.

It is possible to synthesize nanocomposites from polymers that have little polarity with this method but since large amounts of organic solvents are used it is not preferable commercially because of the environmental and economical concerns.

2.3.5.3 Melt Intercalation Method

In melt intercalation method, the layered silicate is mixed with the polymer matrix in molten state. If the layer surfaces are compatible enough with the polymer matrix, the polymer can easily enter into the layered silicates as shown in Figure 2.4 and form either intercalated or exfoliated nanocomposites.
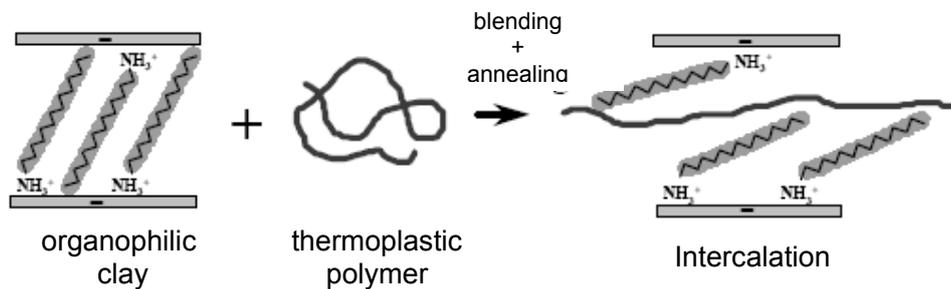
Figure 2.4 Melt Intercalation Method [35].

Extrusion process is generally used for obtaining melt intercalated nanocomposites. Vaia et al. first synthesized polymer-clay nanocomposites with this method by using a twin screw extruder in 1993. The layered silicate and polymer can be simultaneously or separately fed to the twin screw extruder [36]. The heat and the shear generated by the screws of the extruder help to disperse the layered silicates throughout the polymer matrix. The stepwise mechanism of clay platelets dispersion during melt blending is shown in Figure 2.5.
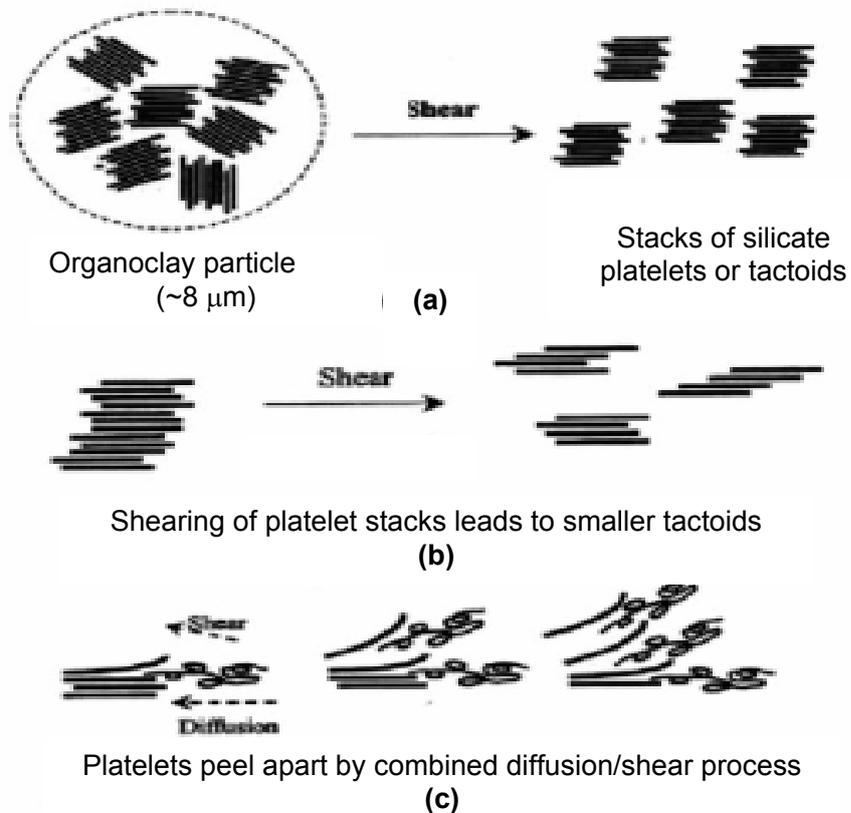
Figure 2.5 The stepwise mechanism of clay platelets dispersion during melt blending: (a) Organically modified layered silicates breakup, (b) Intercalated organically modified layered silicate tactoids breakup, and (c) platelet exfoliation [31].

Melt intercalation method is relatively easier than the in-situ method and solution intercalation method and environmentally benign due to the absence of organic solvents and compatible with various industrial processes such as extrusion and injection. So that it is the mostly used method for commercial applications. In addition to these, melt intercalation method is quite an effective technology for the synthesis of polyolefin-based nanocomposites [17].

In this study, nanocomposites have been synthesized by melt intercalation method by using a twin screw extruder.

2.4 Polyethylene

Polyethylenes are major olefin polymers achieving significant growth each year [37]. The merits of polyethylene are its low price, good processability, excellent electrical insulation properties, good chemical resistance, toughness, light weight, and flexibility. On the other hand the hydrophobicity of PE prevents its usefulness considerably [38]. The classification of polyethylene is based on two parameters that could be easily measured in 1950's in a commercial environment with minimum instrumentation: the resin density and its melt index [39]. According to this classification three major groups are as follows:

- Low density polyethylene (LDPE)
- High density polyethylene (HDPE)
- Linear low density polyethylene (LLDPE).

Table 2.1 shows the classifications of PE resins with respect to density.

Table 2.1 Commercial classification of Polyethylenes [39]

Designation	Acronym	Density (g/cm^3)
High density polyethylene	HDPE	≥ 0.941
Medium density polyethylene	MDPE	0.926-0.940
Linear low density polyethylene	LLDPE	0.915-0.925
Low density polyethylene	LDPE	0.910-0.940

Some typical applications for PE are: LDPE- bags, textile products, moisture barriers, greenhouses, cable insulation; HDPE- bottles, pails, tubes, caps, uses where injection molding of complex shapes is required but low load is applied, film, sheet, wire and cable insulation, pipes and drums [4].

This study is based on LDPE.

2.4.1 Low Density Polyethylene

The first high molecular weight crystalline polyolefin was produced in 1933 by Imperial Chemical Industries, Ltd. through the high pressure process [40]. Low density polyethylene can also be called high pressure - low density polyethylene because of its production conditions. LDPE is produced by a free-radical catalyzed reaction using oxygen or other free radical initiators such as organic peroxides at high temperature and high pressure. Temperature range is 150-300°C and pressures range from 103-345 MPa [37]. The residence time of the material is usually about 10-50 seconds [38]. The heat of ethylene polymerization is high as 105 kJ/mol, and needs to be controlled during the process [19].

 The Figure 2.6 shows simply the mechanism of polymerization of ethylene that forms LDPE.
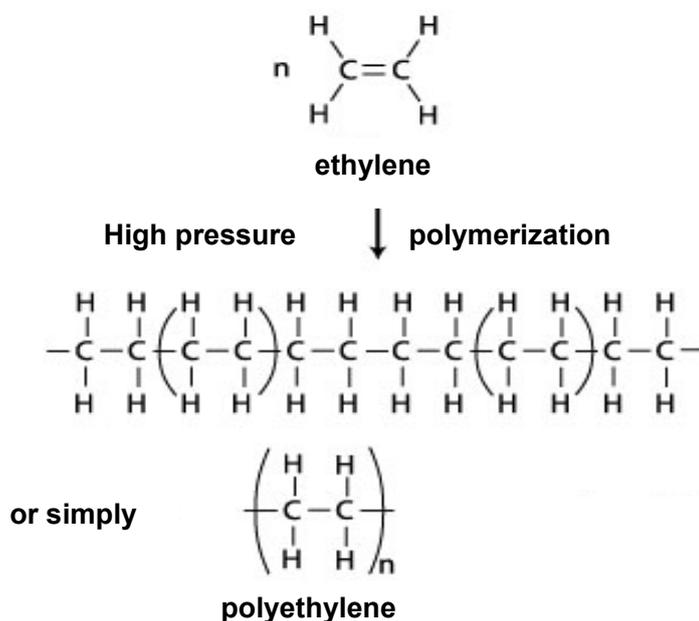
Figure 2.6 Schematic of polymerization of ethylene [41]

The resultant polymer is a highly branched long-chain thermoplastic polymer with a density of 0.915 - 0.925 g/cm^3 and molecular weight up to 4 x 10^6.

LDPE is used in a wide range of applications: the largest segment is taken up by end uses requiring processing into thin film. The film products include food packaging, nonfood packaging, stretch and shrink film, carry out bags. In addition to these, injected molded LDPE is used in making house wares, can lids, toys and pails. Other important uses for LDPE are wire and cable jacketing, carpet backing, and foam for life preserves or package cushioning material [40, 42].

2.4.2 Polymerization of LDPE

The polymerization process involves three basic steps: initiation, propagation, and termination [42].

Initiation requires an initiator, usually a peroxide that thermally decomposes into free radicals, which reacts with ethylene

Initiator $(R)_2$ ………………………………………….2 R' (2.1)

R' + CH_2CH_2 ………………………………………..RCH_2CH_2' (2.2)

Propagation

RCH_2CH_2' + CH_2CH_2 ………………………………$RCH_2CH_2CH_2CH_2$' (2.3)

Termination occurs when two free radical groups combine or when a hydrogen radical transfers from one chain to another.

RCH_2CH_2'+ 'CH_2CH_2R ……………………………$RCH_2CH_2CH_2CH_2R$ (2.4)

RCH_2CH_2'+ 'CH_2CH_2R ……………………………RCH_2CH_3 + $RCHCH_2$ (2.5)

2.4.3 Properties of LDPE

Toughness, high impact strength, low brittleness temperature, flexibility, processability, film transparency, chemical resistance to polar compounds, low permeability to water, and outstanding electrical properties are some unique properties of LDPE [5].

The mechanical properties of LDPE fall somewhere between rigid polymers such as polystyrene and soft polymers such as polyvinyls. Table 2.2 summarizes the properties of LDPE.

Table 2.2 Properties of LDPE [19].

Property	ASTM	LDPE
Specific gravity	D792	0.91-0.93
Crystallinity, %	-	50-70
Melt temperature, °C	-	98-120
Tensile strength, MPa	D638	4.1-16
Tensile modulus, MPa	D638	100-260
Elongation-to-break, %	D638	90-800
Impact strength, notched Izod	D256	No break

LDPE is highly resistant to penetration by most chemically neutral or reactive substances which is an important property for packaging applications. Also its high impermeability makes it useful for producing containers to transport many kinds of chemicals without leak hazards. In addition, LDPE is resistant to penetration from most polar liquids, water, and aqueous acids. Water absorption value of LDPE is less than 0.01 wt. %. However, it can be easily penetrated by nonpolar liquids such as hydrocarbons.

The excellent electrical properties make LDPE extremely well suited for wire and cable insulation for electrical power supplies at high frequency, applications in electronics. It is also the universal insulating material for television lead-in wire.

LDPE may have molecules that range in length from a few thousands carbons to a million or more carbons. Melt viscosity is directly related to the average molecular weight of the polymer. Increase in molecular weight results in increase in melt viscosity, tensile strength, flexural stiffness, on the other hand it decreases the transparency, haze and gloss [40].

The thermal properties of LDPE include a melting range 106-112 °C [41]. Its relatively low melting point and broad melting range result in easy process applications. The glass transition temperature of LDPE is well below the room temperature (~ -120 °C), accounting for the polymer's soft and flexible nature. Also, LDPE does not break when subjected to the Izod impact test [43].

The environmental properties of LDPE are subjected to thermal and ultraviolet degradation. However, this can be controlled with available additives and degradation can be prevented up to several years.

2.4.4 Polyethylene – Organoclay Interaction

Polyolefines (PE, PP), can not make strong interaction with polar, hydrophilic layered silicates because of their nonpolar, hydrophobic structures during melt blending process. This prevents the homogeneous dispersion of the silicate layers in the matrix and thus the intercalation and exfoliation. It is known that modification of clay increases the intercalation of polymer into the clay galleries since the modifier opens the galleries to some extent. But this does not favor the intercalation of non-polar polymers like polyethylene (PE) and polypropylene (PP) because the long alkyl tail displays only a limited compatibility with the polymer chains [44]. In order to increase the polymer clay interaction, a third component, compatibilizer is necessary to enhance the intercalation of nonpolar polymer throughout the silicate layers [6]. Usually maleic anhydride grafted polyethylene is used as the compatibilizer to increase the miscibility of the polyethylene and the clay. This increase, in interaction originates from the strong hydrogen bonding between the maleic anhydride groups and the oxygen atoms on the clay surfaces.

Compatibilizers that are used in this study include functional groups: methacrylate (MA), glycidyl methacrylate (GMA) and maleic anhydride (MAH). There is also a possibility of the glycidyl methacrylate (GMA), to react with the hydroxyl groups that may be present on the organophilic clay. On the other hand, acrylic group imparts thermal stability, flexibility and polarity. Increasing the polarity of the compatibilizer also increases the interaction of polymer matrix and the layered silicates. Also the bulky nature of the compatibilizer increases the d-spacing of the layers and allows the polymer matrix to enter the galleries. The following figure shows the action of the compatibilizer for the exfoliation of clay sheets within a polymer matrix.
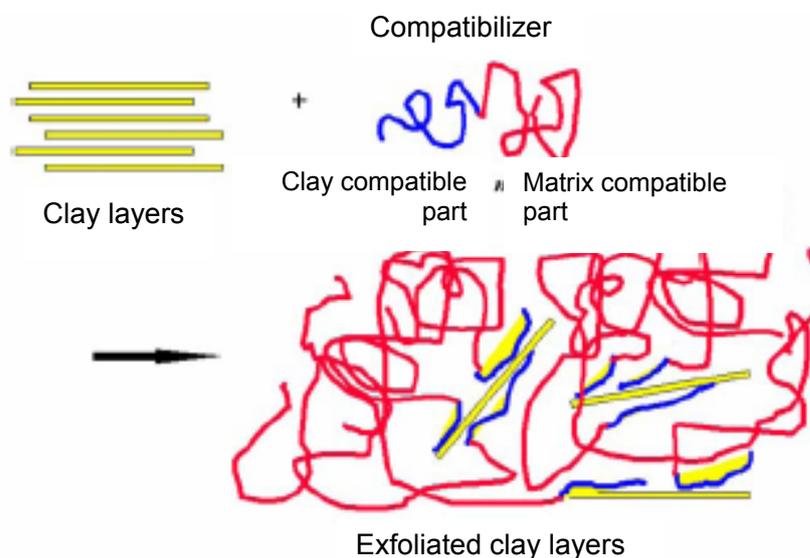
Figure 2.7 Schematic picture of the action of compatibilizer for an exfoliation of clay layers within a polymer matrix [44].

There have been several studies in the literature on the effect of the addition of a compatibilizer such as maleated polyolefines on dispersion of clay platelets in polyolefines [6, 16].

In this study, terpolymer of Ethylene – Methyl Acrylate – Glycidyl Methacrylate (E-MA-GMA), copolymer of Ethylene – Glycidyl Methacrylate (E-GMA), and terpolymer of Ethylene – nButyl Acrylate – Maleic Anhydride (E- nBA-MAH) have been used as compatibilizer in order to enhance the intercalation and exfoliation of LDPE through the organoclay layers.

2.4.4.1 Glycidyl Methacrylate (GMA) Functionality

Glycidyl Methacrylate (GMA) monomer contains both epoxy and acrylic groups, providing the flexible design conditions which are required for the most demanding coating and resin applications. Figure 2.8 shows the chemical structure of GMA.
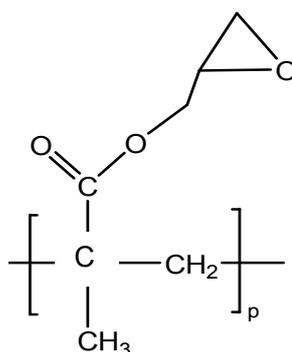
Figure 2.8 Chemical structure of GMA

The GMA monomer can react with a variety of monomers and functionalized molecules due to the functional groups of epoxy and acrylic. Acrylic and vinyl functionalities provide the copolymerization with a variety of other vinyl monomers in aqueous and non aqueous systems. The obtained polymers have a unique combination of epoxy functionality with an acrylic backbone. Moreover, wide co-monomer selection provides easy control of physical and chemical properties such as glass transition temperature.

Due to the epoxy functionality, crosslinking reactions with amines, carboxylic acids, anhydrides and hydroxyl containing polymers can be obtained. Also, the choice of polymer accelerator / catalyst allows use of a wide range of cure temperatures. In addition to these, this functionality allows structural modification of the polymer backbone that can result in different properties and higher performance.

Both acrylic and epoxy functionality provides several benefits to the polymer systems such as; improved impact resistance, improved adhesive strength, excellent acid resistance (epoxide reactions only), improved water and heat resistance, and improved thermoplastic polymer blend compatibility [45].

2.4.4.2 Maleic Anhydride (MAH) Functionality

Maleic anhydride increases the adhesion onto polar substrates and allows the creation of chemical bonds. Chemical reaction occurs between the hydroxyl groups of the organoclay and the maleic anhydride groups of maleated polyethylene. By the help of this reaction, maleated polyethylene can move into the clay galleries and expand the distance between the layers. Thus the maleated polyethylene serves as a useful compatibilizer for the nanocomposite systems. Figure 2.9 shows the reaction mechanism between the maleic anhydride and the hydroxyl group.

Maleated polyethylene
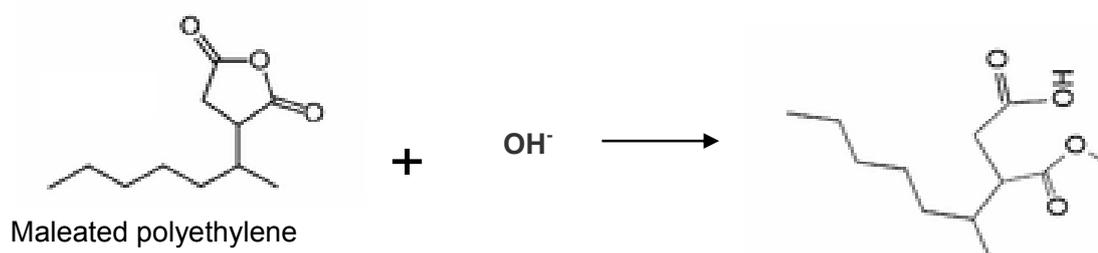
Figure 2.9 Reaction of Maleic Anhydride with Hydroxyl group of clay

2.5 Polymer Processing

Processing involves the conversion of the solid polymer into a desirable size and shape. There are number of methods to shape the polymer, including extrusion and injection molding.

2.5.1 Extrusion

Extrusion process is one of the oldest manufacturing processes. This process is used to obtain significant quantities of plastic products, such as plastic film, sheet, and profiles, but it is also used to produce the plastic pellets that are later used by all the other plastics manufacturing processes [46].

In typical plastics extrusion processing, a viscous melt under pressure is forced through a shaping die in a continuous stream. The feedstock may enter the extruder in the molten state, but more commonly, it consists of solid particles that must be subjected in the extruder to melting, mixing and pressurization. The solid feed may be in the form of pellets, powder beads, flakes, or reground material. It may also be a combination of these which may be premixed or fed separately at one or more feeders [5].

In extrusion process, the materials are fed into the cavity between the screw and extruder barrel and, as the screw rotates they are dragged forward, compressed, and heated by conduction through the barrel walls and through frictional heating. During the dragging the materials are melted, and forced under pressure through a die that forms the molten material.

Figure 2.10 shows schematic drawing of the extruder used to obtain nanocomposites in this study.
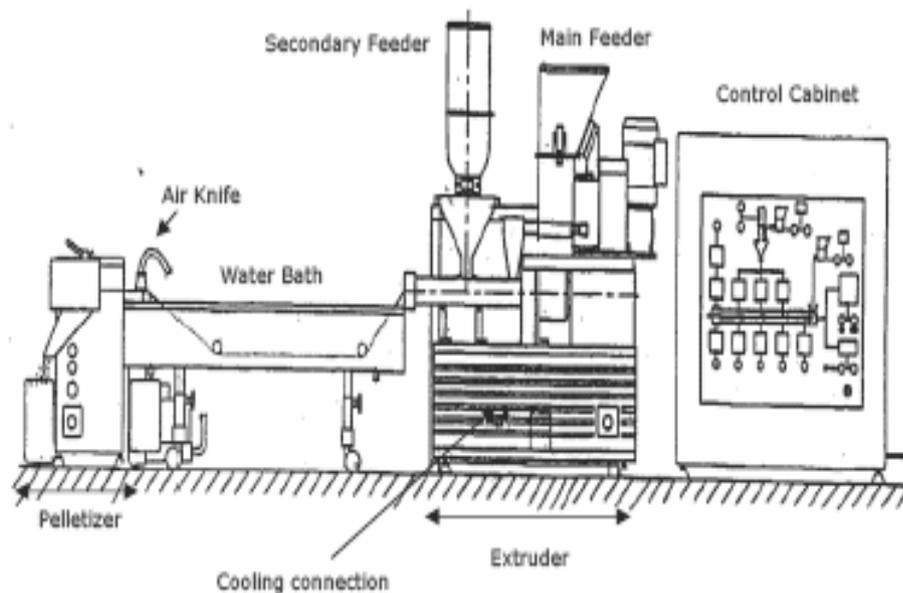
Figure 2.10 The extruder, used to obtain nanocomposites in this study.

The components of the extruder are, control panel, feeders, screw, barrel and die.

The control panel consists of different indicators to control the extrusion process. It is possible to adjust the temperature, screw speed and feeding rate with the control panel. Moreover, pressure of the die, temperature of the zones and torque can be monitored.

The screw is the main part of the extruder which directly affects the performance of the machine. It performs a number functions such as; conveying the plastic pellets, melting the material, conveying the molten material, and mixing the plastic melt to obtain homogeneity.

The screw is placed inside the cylinder extruder barrel. It provides the bearing surface where shear is imparted to the plastic granules. The barrel consists of cast or fabricated steel sections and a smooth inner liner, often made of a wear-resistant

material. Heating and cooling media surrounds the barrel to keep it at the desired temperatures.

The polymer is shaped in the die zone so the die is one of the most important parts of the extruder. The objective of an extrusion die is to distribute the polymer melt in the flow channel in such a way that the material exits from the die with a uniform velocity. The polymer melt is forced through the die by means of the diehead pressure. The pressure is not determined by the extruder but by the extruder die [48].

There are tremendous die design and applications such as compounding, (coloring and blending of melts, additives, and fillers), sheet, film, coatings, pipe, and rod [5].

Screw extruders are divided into single screw and multi screw extruders.

2.5.2 Twin Screw Extrusion

Although twin-screw extruders are used less than single-screw extruders they are widely employed for difficult compounding applications, devolatilization, chemical reaction, and profile extrusion of thermally sensitive materials in the polymer processing industry [5].

The complex flow patterns in twin screw extruders have several advantages, such as good mixing, good heat transfer, large melting capacity, good devolatilization capacity, and good control over stock temperatures [47].

Type of transport in extruder is different in single screw and twin screw extruders. Material transport in single screw extruder is by frictional drag in solid conveying zone and viscous drag in the melt conveying zone. On the other hand, the transport in an intermeshing twin screw extruder is a positive displacement type of transport [47].

There is a tremendous variety of twin screw extruders, with vast differences in design, principle of operation, and field of applications. The twin screw construction substantially increases the number of design variables, such as direction of rotation,

(co-rotating, counter rotating), intermeshing, non-intermeshing, etc. [48]. Figure 2.11 shows the different screw configurations of twin screw extruders.
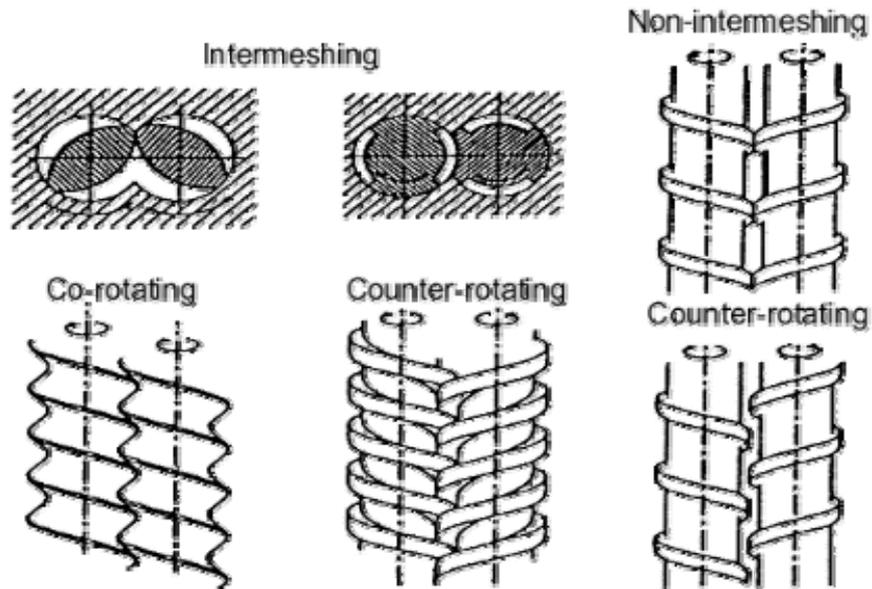
Figure 2.11 Types of twin screw extruders according to screw design [49].

There are two different patterns for intermeshing twin screw extruders according to the direction of rotation of the screws: co-rotating, and counter rotating twin screw extruders.

Co-rotating twin screw extruders in which both screw rotate in the same direction, are typically used in applications where mixing and compounding need to be accomplished in addition to the molding of the plastic melt. They are highly capable of dispersing small agglomerates such as carbon black or clay [22]. The following figure shows the co-rotating twin screw extruder and its zones.

Solids Conveying　　Melting　　Melt Pumping
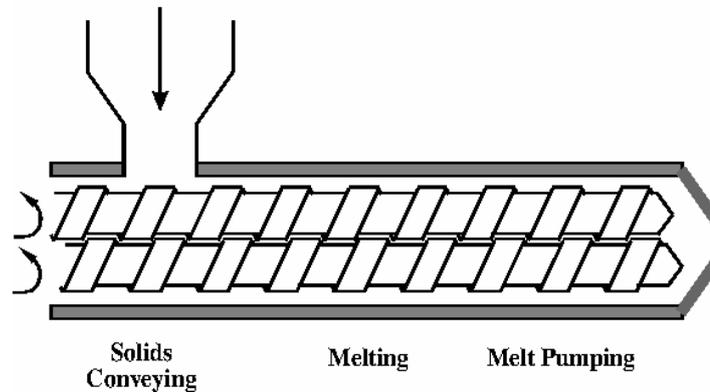
Figure 2.12 Co-rotating twin screw extruder and its zones [50].

In the other intermeshing type, the screws rotate counter to each other, one rotates clockwise and the other counterclockwise thus it is called counter rotating extruder. In this type, material is brought to the junction of the two screws and a material bank occurs on the top of the junction. Only a small amount of material passes between the screws so the total shear applied to material is lower than the single screw extruders and co-rotating twin screw extruders.

2.5.3 Injection Molding

Injection molding is a widely used process to produce parts with variable dimensions. It is a major processing technique for converting thermoplastic and thermosetting materials into all types of products [48].

The injection molding process cycle includes melting of plastic resin, injection of melt into the mold under high pressure, cooling of the mold, and removing the part. Cycle time depends on the cooling time of the thermoplastic or the curing time of the thermosetting plastic.

The injection unit may be ram fed or screw fed. The ram fed injection molding machine uses a hydraulically operated plunger to push the material through a heated region.

The reciprocation single screw injection molding machine is the most common injection unit used. In this system, the screw rotates and axially reciprocates. A hydraulic motor produces the rotation and acts to melt, mix, and pump the polymer. In addition to the material properties, the injection molding process itself has a large influence on the final properties of the material, since the polymer chains undergo orientation in the flow direction during the melt-filling phase of the injection cycle [22].

Injection molding produces parts in large volume at high production rates and the parts need little or no finishing. The system is usually highly automated which reduces the labor costs. Injection molding process allows the parts be molded in a combination of plastics and fillers such as glass, and carbon. Also, parts can be molded with metallic and nonmetallic inserts. Moreover, it is possible to produce very small parts that are almost impossible to fabricate in quantity by other methods. On the other hand, the plastic industry has very low profit margins. The molds, machinery and auxiliary equipment are expensive, the initial equipment investment is high, thus in effective molding, it is necessary to design the parts more carefully [48].

2.6 Characterization of Nanocomposites

2.6.1 Morphological Analysis

X-ray diffraction (XRD) and transmission electron microscopy analyses are the mostly used methods to investigate the dispersion of the clay particles in the polymer matrix. In this study, only x-ray diffraction analysis has been used for this purpose.

2.6.1.1 X-Ray Diffraction (XRD)

The method of X-ray diffraction and scattering is one of the oldest and most widely used techniques available for investigating the orderly arrangements of atoms and molecules of the polymer structures. X-rays are electromagnetic radiation of very short wavelength (0.01 to 100 nm), produced when an electron hits a piece of metal in an evacuated tube. A beam of x rays incident to a material is partly absorbed and partly scattered, and the rest is transmitted unmodified. Diffraction occurs as waves interact with a regular structure whose repeat distance is about the same as the wavelength [5].

X-ray diffraction relies on Bragg's law:

$$n\lambda = 2d \sin \theta \qquad (2.6)$$

where, n is degree of diffraction, λ is wavelength, θ is the measured diffraction angle, and d refers to the interlayer spacing.

Figure 2.13 shows the principal of the X-ray diffraction method.
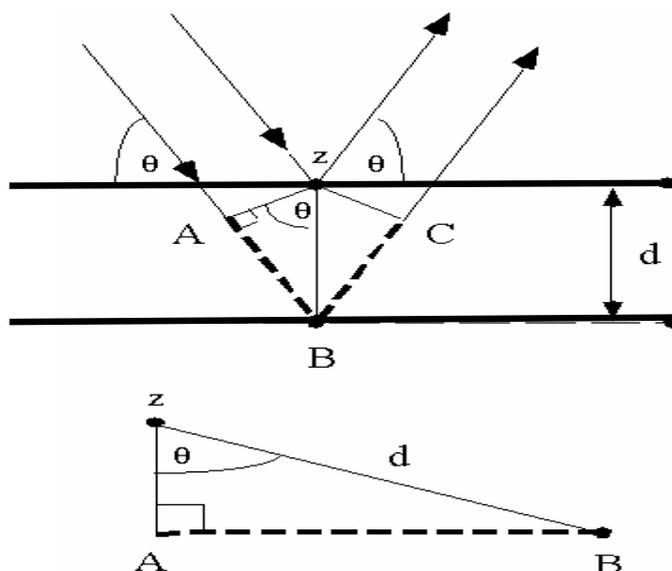
Figure 2.13 Principal of X-ray diffraction [53].

XRD gives quantitative data on the dispersion of the clay platelets. In intercalated systems, the platelets are arranged periodically so a reflection from the clay platelets can be observed in the XRD pattern. If more polymer chains enter the clay gallery, the d spacing of the clay platelets increases, and the clay peak is shifted to lower angles ($2\theta < 2°$). In addition to this, the separation of the layers also decreases the periodicity and hence reduces the intensity of the clay peak. In exfoliated systems, the clay platelets are randomly dispersed throughout the polymer matrix and in the X-ray pattern no clay peak is observed. But the lack of a Bragg's peak in the diffraction pattern does not always mean that the clay is exfoliated. A disordered and immiscible sample, or low concentration of the clay in the region where the x-ray beam hits a non-uniformly dispersed sample, could fail to produce a Bragg's reflection [4].

2.6.1.2 Scanning Electron Microscopy (SEM)

The scanning electron microscope is a microscope that uses electrons instead of light to form an image. As in any microscope, the main objective of SEM analysis is magnification and focus for clarity. In scanning electron microscopy, a fine beam of electrons is scanned across the surface of an opaque specimen to which a light conducting film (gold, platinum, silver) has been applied by high vacuum evaporation. SEM is limited to a surface view only. It does not provide information about the interior of the specimen. But the surface can be monitored as black and white images which can be fitted to a x-ray instrument and elemental analysis can be made. Also, the images can be used to make accurate conclusion about the morphology of the polymer systems.

2.6.2 Mechanical Tests

Most plastic materials are used in industry because they have the desirable mechanical properties at an economical cost [54]. So the mechanical properties can be considered to be the most important of all physical and chemical properties of polymers for most applications. There are various number of mechanical tests and testing instruments in order to investigate the properties of polymers and some of

these tests including tensile and flexural, have been standardized and described in the publications of ASTM [55].

2.6.2.1 Tensile Test

Tensile tests are performed in order to measure the force required to break a specimen and the extent to which the specimen elongates to that breaking point. The test is applied according to standardized testing method [56]. According to this standard, the specimens are rectangular or in the shape of dogbone, as seen in Figure 2.14.

The ends of the specimen are clamped into the jaws of the testing machine and the jaws are separated by the application of a known force. Since the specimen is pulled up, it elongates or breaks when the load applied is higher than the load which the specimen can resist. The tensile test mechanism is given in Figure 2.14. Tensile test provides a stress-strain diagram, which is used to determine the tensile modulus. Stress-strain tests not only give the modulus and an indication of the strength of the material but also toughness which is an indication of the energy that a material can absorb before breaking [48].
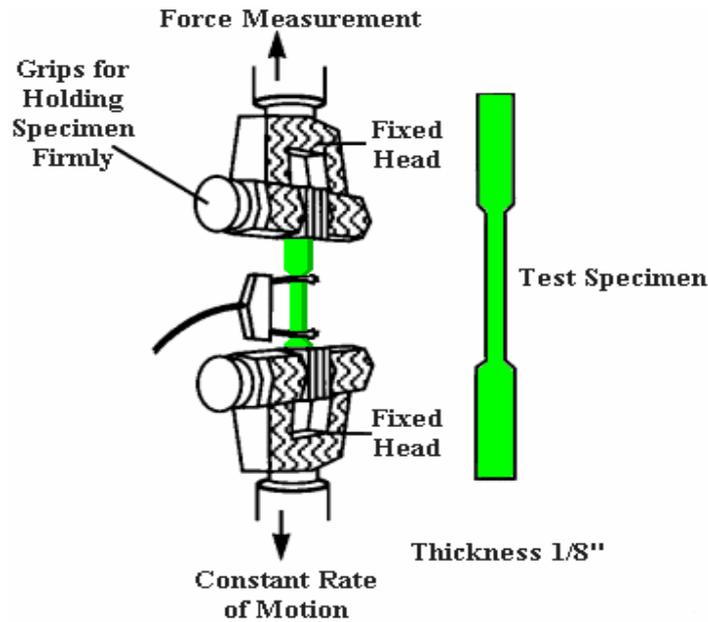
Figure 2.14 Tensile specimen and tensile test procedure [57].

Tensile stress, σ is the tensile load per unit area perpendicular or normal to the applied force (Equation 2.7), and *tensile strain*, ϵ is the ratio of change in gage length of a specimen in the direction of applied load stress to its original gage length (Equation 2.8).

$$\sigma = \frac{F}{A_0} \tag{2.7}$$

$$\varepsilon = \frac{\Delta L}{L_0} \tag{2.8}$$

where, F is the measured value at the fixed end as a function of elongation (N), and A_0 is the original, undeformed cross-section area of the gage region (mm^2), ΔL is the change in gage length (mm), and L_0 is the original gage length of the specimen (mm).

The tensile strength, σ_m of a material is the maximum amount of tensile stress that it can be subjected to before it breaks during a tensile test and is reported in MPa' s. If the maximum stress occurs at break, it is called tensile strength at break.

The ratio of the stress to strain in the proportional region of the stress-strain curve is the measure of the stiffness and called as Young's modulus or tensile modulus as given in the Equation 2.9.

$$E = \frac{\sigma}{\varepsilon} \qquad\qquad (2.9)$$

Tensile modulus and elongation values are determined by using the stress-strain diagrams. Tensile modulus is the slope of the initial straight line portion of the stress-strain diagram and may be expressed in MPa' s [55]. Figure 2.15 represents several polymeric materials properties according to stress-strain curves.

Soft and weak   Hard and brittle   Soft and tough

Hard and strong   Hard and tough
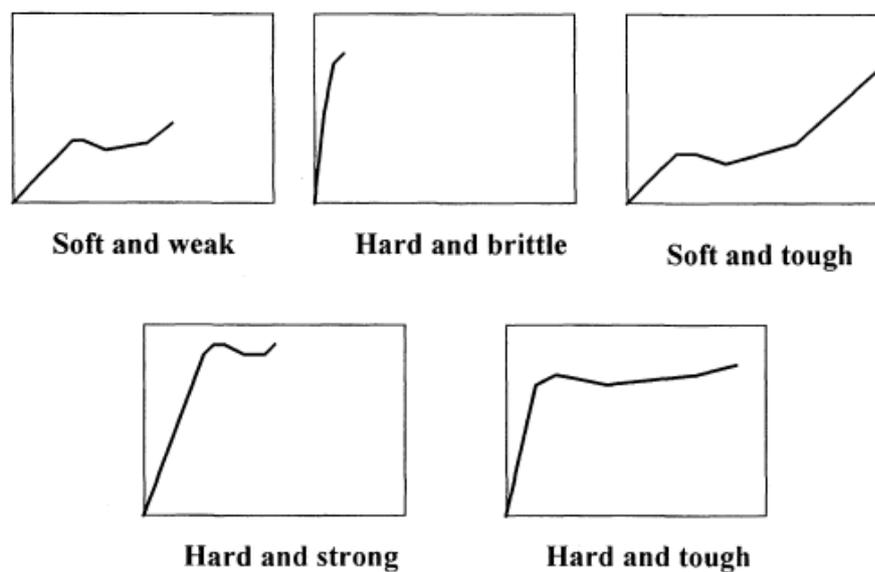
Figure 2.15 Stress –strain curves of several polymeric materials [58]

2.6.2.2 Flexural Test

The flexural test is performed according to ASTM D790M-92 test method [59]. In this study three point loading system is applied in order to determine the flexural properties of the specimens. Three point loading system bases on a center loading of a simply supported beam. Due to this procedure, specimen lies on a support span and the load is applied to the center of the specimen as shown in Figure 2.16. The support span and the speed of loading are two parameters of flexural test and the specimen deflection is usually measured by the crosshead position.
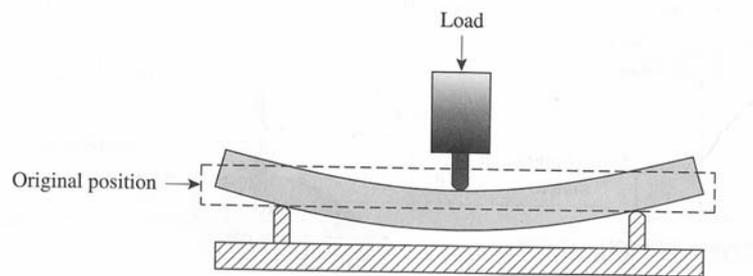
Figure 2.16 Flexural test procedure [51]

Flexural test results include flexural strength, flexural modulus and strain.

Maximum fiber stress developed in a specimen just before it cracks or breaks in a flexure test is called the flexural strength It is the ability of the material to resist bending forces applied perpendicular to its longiditual axis and can be calculated for any point on the load-deflection curve by using Equation 2.10:

$$S = \frac{3PL}{2bd^2}$$

(2.10)

where; S is the stress in the outer fibers at midspan and may be represented in MPa, P is the applied load at a given point on the load-deflection curve (N), L is the length of support span (mm), b is the width of the specimen (mm), and d is the depth of the

specimen (mm). For materials that do not crack in the flexure test, flexural yield strength is reported instead of flexural strength. In this study, flexural yield strength values have been reported.

The maximum strain in the outer fibers at midspan is calculated as follows:

$$r = \frac{6Dd}{L^2}$$

(2.11)

where; r is the maximum strain, D is the maximum deflection of the center of the beam(mm), and L is the length of the support span (mm), and d is the depth of the specimen (mm).

Flexural modulus is used as an indication of a material's stiffness when flexed. It is the ratio, within the elastic limit of stress to corresponding strain and determined by drawing a tangent line to the initial straight-line portion of the load-deflection curve and using Equation 2.12.

$$E_b = \frac{L^3 m}{4bd^3}$$

(2.12)

where; E_b represents the flexural modulus (MPa), L is the support span (mm), m is the slope of the tangent to the initial straight-line portion of the load-deflection curve (N/mm), b is the width of beam tested (mm), and d is the depth of the beam (mm).

2.6.3 Thermal Analysis

In thermal characterization, a controlled amount of heat is applied to a sample and its effect is measured and recorded.

2.6.3.1 Differential Scanning Calorimetry Analysis (DSC)

Differential scanning calorimetry is the dominant technique for the thermal analysis of polymeric materials. The working principal of a differential scanning calorimeter is based on measurement of the difference in energy inputs into a substance and a reference material as they are subjected to a controlled temperature range. Its measurement process is quantitative [5].

In DSC analysis, two small metal containers, one containing polymer sample and the other either empty or a control substance, are heated by individual electric heaters. Both the sample and reference are maintained at the same temperature throughout the experiment and temperature of each container is monitored by a heat sensor. Usually the temperature of the system increases linearly as a function of time during the experiment. When the sample suddenly absorbs heat during a transition, this additional heat is detected by the sensor, since this sample results in a greater current flow and change in electrical current can be monitored accurately which means sensitive measurement can be made by DSC analysis. A recorder prints out the data as a plot of increase in heat per increase in temperature, versus temperature. Exothermic and endothermic processes within the sample result in a significant deviation in the difference between the two heat flows.

The result is a peak in the DSC curve and the differential heat flow is calculated by subtracting the sample heat flow from the reference heat flow. According to this , exothermic processes show up as positive peaks (above the baseline) while peaks resulting from endothermic processes are negative (below the baseline). The area under the resulting curve is a direct measure of heat of transition [52]. A representative drawing of DSC and the output of analysis are seen in Figure 2.17.
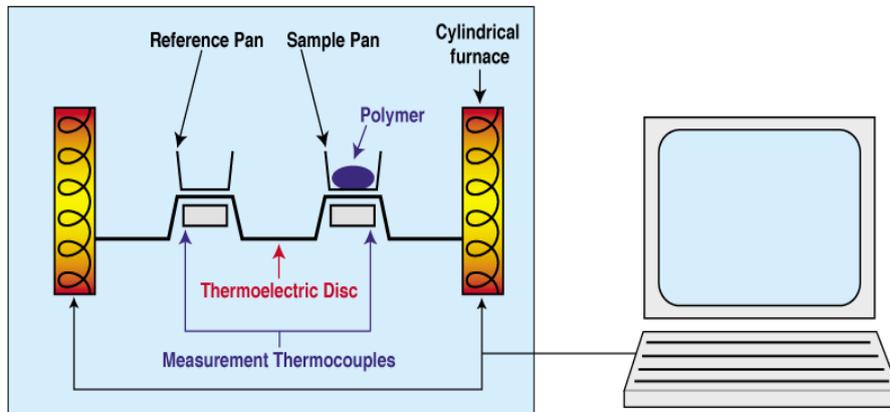
(a)
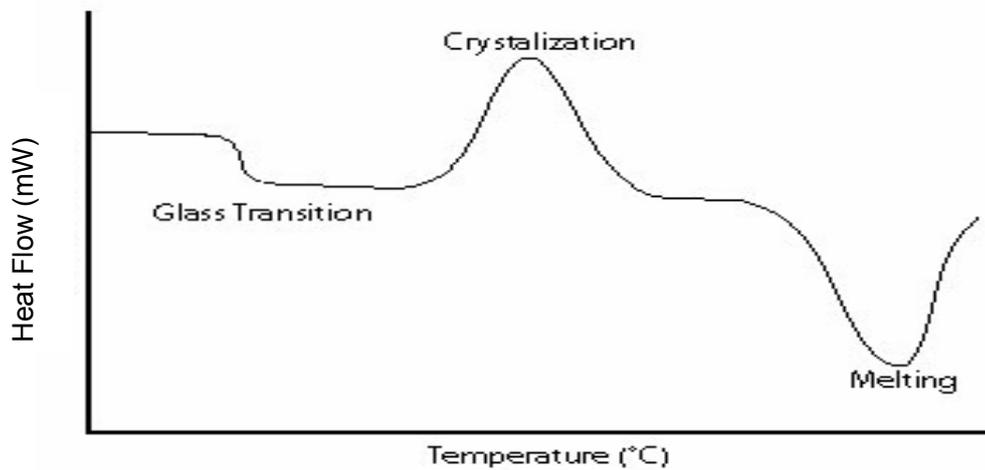
(b)

Figure 2.17 A representative drawing of a) DSC, b) output of analysis [51].

It is possible to determine the heat capacity, heats of transition, heats of reaction, temperature of transition (melting temperature, glass transition temperature, and crystallization temperature), for polymeric materials by DSC instruments. One of the main advantages of using DSC is its speed. Furthermore accuracy of measurement of very small specimens is usually sufficient for many fundamental studies [5].

2.6.4 Flow Characteristics

2.6.4.1 Melt Flow Index (MFI) Test

The melt flow index is one of the indices used to characterize the behavior of molten plastic [38]. It is not an intrinsic property of polymers (which limits its usefulness), but is nearly always specified when a polymer is requested due to its ability to predict general behavior properties of the polymer. It describes the flow behavior of a polymer at a specific temperature under specific pressure. If the melt flow index is low, then its melt viscosity or melt flow resistance is high.

The melt index machine is a simple ram extruder. The polymer is placed in the barrel which is heated to the appropriate temperature that is required to provide the flow of polymer. When the polymer is molten and free of bubbles, the polymer is forced to flow from the die by the help of the ram and a weight which is placed on the top of the ram. After a set amount of time, usually 10 minutes, the polymer that was extruded is weighed and the melt index is expressed as grams polymer/10 minutes.

2.7 Previous Studies

Wang et al. [7] prepared maleated polyethylene/clay nanocomposites by melt compounding method. They investigated the effect of the maleic anhydride grafting level and organic modifier of clay on the morphology of linear low density polyethylene/clay nanocomposites. It was concluded that maleic anhydride grafting level of polyethylene should be higher than 0.1 wt % and organic modifiers should contain higher methylene groups in order to obtain better exfoliation of LLDPE/clay nanocomposites. After this study, in 2002 Wang and co-workers studied the morphology and physical properties of polyethylene/silicate nanocomposites prepared by melt intercalation method.

Li et al. [8] reported the effect of blending sequence on the microstructure and properties of ternary nanocomposites that consist of poly(butylene terephtalate), maleic anhydride grafted polyethylene-co-vinyl acetate and organically modified

montmorillonite. They applied four different blending sequences in a Haake records mixer and investigated that mixing sequence significantly influenced the microstructure of the prepared nanocomposites, dispersion of the organoclay and thus the mechanical properties.

Jog and co-workers in 2002 investigated the effect of the compatibilizer on the thermal, crystallization and dynamic mechanical behavior of polypropylene / clay nanocomposites. They used three grades of PP with different molecular weights, two different organo-modified montmorillonites and two grades of maleic anhydride modified PP. It was reported that the extent of intercalation or exfoliation depends on the type of compatibilizer [6].

Gopakumar et al. [9] studied the influence of clay exfoliation on the physical properties of montmorillonite/polyethylene composites. They prepared conventional composites and nanocomposites of two different montmorillonite clays, high density polyethylene and 1 wt % maleic anhydride grafted polyethylene by melt compounding method and concluded that it is necessary to modify both the montmorillonite clay and polyethylene in order to prepare polyethylene nanocomposites and resulting rheological, mechanical and thermal properties of these nanocomposites depend on the structure of the composite and clay content. In addition to this, improved rheological, mechanical and thermal properties observed for the nanocomposites were shown to be the evidence of the exfoliation of clay.

Kato et al. [10] prepared different compositions of nanocomposites by melt compounding with maleic anhydride grafted polyethylene, organophilic clay and polyethylene. In this study, silicate layers were exfoliated and dispersed which led to superior mechanical and gas barrier properties. They obtained nanocomposites which have 1.4 times higher tensile strength and 1.8 times higher tensile modulus than the matrix and gas permeability of the nanocomposites was 30 % less than the polyethylene matrix.

Liang et al. [11] produced polyethylene/maleic anhydride grafted polyethylene/organic-montmorillonite nanocomposites by two blending processes which were direct melt blending and solution blending. They investigated the effects of polyethylene type, surfactant type for modifying montmorillonite, compositions of nanocomposites and blending process type, on the microstructure and mechanical properties of the nanocomposites. The results showed that the intercalation of nanocomposites was enhanced by increasing the amount of the compatibilizer. Maximum tensile strength was obtained when the concentration of compatibilizer was 6 % and maximum impact strength was obtained at 9 % compatibilizer content.

Zhang et al. [12] studied the flammability properties of low density polyethylene/clay nanocomposites produced by using melt blending in a Brabender mixer. Nanocomposites with different organically modified clays were prepared and it was reported that polyethylene/clay nanocomposites have a mixed immiscible-intercalated structure. Addition of maleic anhydride to polymer resulted in better intercalation and addition of 3 % clay resultrd in 30-40 % reduction in the peak heat release rate.

Hotta et al. [13] studied the effect of the number of the alkyl groups attached to the nitrogen of the organic modifier of clay and maleic anhydride grafted linear low density polyethylene (LLDPE-g-MA) on morphology, mechanical properties, rheological properties and gas permeability of nanocomposites with LLDPE matrix. They prepared nanocomposites by melt compounding method by using co-rotating twin-screw extruder. According to this study, it was seen that increase in the number of alkyl groups of organic modifier and the use LLDPE-g-MA resulted in better nanocomposites in terms of dispersion of clay and mechanical properties.

Zhai et al. [14] obtained PE and PE-g-MAH/montmorillonite nanocomposites by melt-direct intercalation method and showed that both types of nanocomposites have better thermal and crystal properties than the neat polymer matrix. Moreover, PE-g-MAH /Organo MMT nanocomposites were exfoliated and led to better thermal properties in comparison to PE / Organo MMT nanocomposites.

Morawiec et al. [15] prepared nanocomposites based on low density polyethylene, containing 3 or 6 wt. % of organo-modified montmorillonite clay and maleic anhydride grafted low density polyethylene as a compatibilizer by melt blending. According to this study, it was concluded that the mechanical performance of the system did not only depend on the exfoliation of clay and the clay content, but it was also affected by the presence of a significant amount of the compatibilizer. The results showed that maleic anhydride grafted polyethylene promoted the exfoliation of the clay and its good adhesion to LDPE and moreover it toughened the polymer matrix.

Zhong et al. [16] studied the effects of clay, polymer matrix, and compatibilizer on the morphology, flow behavior and mechanical properties of nanocomposite blown films prepared by melt compounding of organoclay, maleic anhydride grafted polyethylene as compatibilizer with ethylene vinyl acetate, low density polyethylene, and high density polyethylene respectively.   As in the previous studies, it was concluded that compatibilizer is required to obtain improved properties in nanocomposites.

CHAPTER 3

EXPERIMENTAL

3.1 Materials

3.1.1 Polymer Matrix

Low density polyethylene was purchased from Petkim Petrokimya Holding A.Ş, İzmir, Turkey. The trade name of the LDPE used is Petilen G03-5 and it is sold in the form of pellets in a 25 kg white colored PE bags. Properties of LDPE obtained from the company are given in Table 3.1.

Table 3.1 Properties of polymer matrix, LDPE

Property	Unit	Value
Melt Flow Rate (MFR) (2160 g, 190°C)	g/10 min	0.2-0.4
Density, 23°C	g/cm^3	0.919-0.923

3.1.2 Organoclays

Three different natural montmorillonites modified with a quaternary ammonium salt were used in this study as filler. These organoclays, namely Cloisite® 15A, Cloisite® 25A, and Cloisite® 30B, were purchased from Southern Clay Products, Texas-U.S.A. They are all additives for plastics to improve various plastic physical properties, such as mechanical, thermal, and barrier properties.

3.1.2.1 Cloisite® 15A

The cation of Cloisite® 15A is dimethyl, dehydrogenated tallow, quaternary ammonium and the anion is chloride. Figure 3.1 shows the chemical structure of organic modifier of Cloisite® 15A. Physical properties obtained from manufacturer are listed in Table 3.2.

$$CH_3 - \overset{\overset{\displaystyle CH_3}{|}}{\underset{\underset{\displaystyle HT}{|}}{N^+}} - HT \qquad \qquad Cl^-$$

Figure 3.1 Chemical structure of organic modifier (2M2HT*) and anion (Cl⁻) of Cloisite® 15A.

*2M : Dimethyl
HT : Hydrogenated Tallow (Alkyl chain), (~65% C18; ~30% C16; ~5% C14)

Table 3.2 Physical properties of Cloisite® 15A

Properties	Cloisite® 15A
Organic Modifier (1)	2M2HT
Modifier Concentration	125 meq/100g clay
% Moisture	< 2%
% Weight Loss on Ignition	43%
Typical Dry Particle Sizes:	10% less than: 2μ
(microns, by volume)	50% less than: 6μ
	90% less than: 13μ
Color	Off white
Loose Bulk, lbs/ft^3	10.79
Packed Bulk, lbs/ft^3	18.64
Specific Gravity, g/cc	1.66
d- spacing (X-Ray)	31.5Å

3.1.2.2 Cloisite® 25A

The organic modifier of Cloisite® 25A is dimethyl, hydrogenated tallow, 2-ethylhexyl quaternary ammonium and its anion is methyl sulfate. Figure 3.2 shows the chemical structure of the cation of Cloisite® 25. Table 3.3 summarizes the physical properties of Cloisite® 25 .
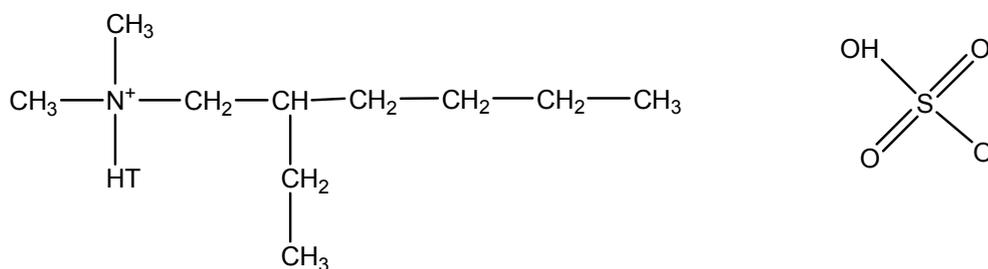
Figure 3.2 Chemical structure of organic modifier **(**2MHTL8 *) and anion (methyl sulfate) of Cloisite® 25A

* 2MHTL8: dimethyl, hydrogenated tallow, 2-ethylhexyl quaternary ammonium
  HT: Hydrogenated Tallow (~65% C18; ~30% C16; ~5% C14)

Table 3.3 Physical properties of Cloisite® 25A

Properties	Cloisite® 25A
Organic Modifier	2MHTL8
Modifier Concentration	95 meq/100g clay
% Moisture	< 2%
% Weight Loss on Ignition	34%
Typical Dry Particle Sizes:	10% less than: 2μ
(microns, by volume)	50% less than: 6μ
	90% less than: 13μ
Color	Off white
Loose Bulk, lbs/ft^3	12.08
Packed Bulk, lbs/ft^3	20.48
Specific Gravity, g/cc	1.87
d- spacing (X-Ray)	18.6Å

3.1.2.3 Cloisite® 30B

Cloisite® 30B is treated with methyl, tallow, bis-2-hydroxyethyl, quaternary ammonium by manufacturer. The anion of this clay is chloride ion. The chemical structure of organic modifier is shown in Figure 3.3. The physical properties of Cloisite® 30B are given in Table 3.4.

$$CH_3 - N^+ - T \qquad Cl^-$$

with $CH_2 - CH_2 - OH$ and $CH_2 - CH_2 - OH$ substituents
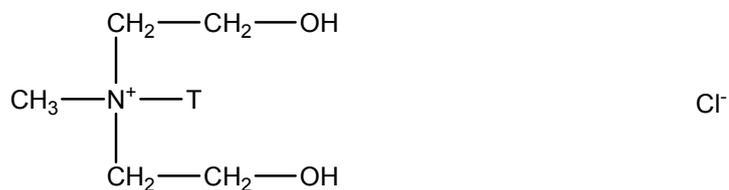
Figure 3.3 Chemical structure of organic modifier (MT2EtOH*) and anion (Cl$^-$) of Cloisite® 30B

* MT2EtOH: methyl, tallow, bis-2-hydroxyethyl, quaternary ammonium

T : tallow (~65% C18; ~30% C16; ~5% C14)

Table 3.4 Physical properties of Cloisite® 30B

Properties	Cloisite® 30B
Organic Modifier	MT2EtOH
Modifier Concentration	90 meq/100g clay
% Moisture	< 2%
% Weight Loss on Ignition	30%
Typical Dry Particle Sizes:	10% less than: 2µ
(microns, by volume)	50% less than: 6µ
	90% less than: 13µ
Color	Off white
Loose Bulk, lbs/ft^3	14.25
Packed Bulk, lbs/ft^3	22.71
Specific Gravity, g/cc	1.98
d- spacing (X-Ray)	18.5Å

3.1.3 Compatibilizers

In this study Lotader® AX8900; terpolymer of Ethylene – Methyl Acrylate – Glycidyl Methacrylate (E-MA-GMA) , Lotader® AX8840; Copolymer of Ethylene – Glycidyl Methacrylate (E-GMA), and Lotader® 2210; terpolymer of Ethylene – nButyl Acrylate – Maleic Anhydride (E- nBA-MAH), were chosen as compatibilizers. They were purchased from Arkema Inc., France. The reason for choosing Lotader® resins as compatibilizer was that, they are highly compatible with various thermoplastics including polyethylene, owing to their reactivity, crystallinity and melt fluidity characteristics. Moreover these resins have high thermal stability during processing.

Lotader® AX8900 and Lotader® AX8840 contains glycidyl methacrylate (GMA) monomer as reactive group. GMA includes both acrylic and epoxy groups which

enables the polymer to react with substances such as hydroxyl, (OH) containing materials, carboxylic acids (COOH), and amines. The chemical structure of Lotader® AX8900 and Lotader® AX8840 are given in Figure 3.4 and Figure 3.5, and Table 3.5 gives the specifications of both resins.
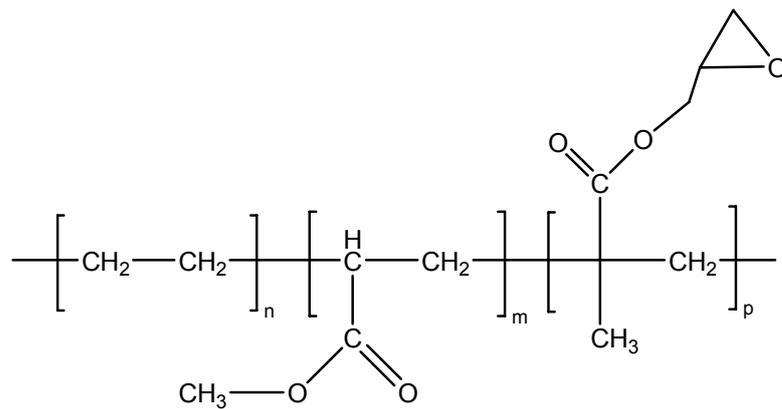
Figure 3.4 Chemical structure of Lotader® AX8900 (E-MA-GMA)
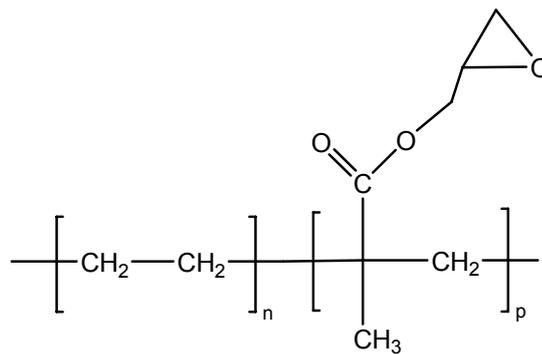
Figure 3.5 Chemical structure of Lotader® AX8840 (E-GMA)

Table 3.5 Specifications of Lotader® AX8900 and Lotader® AX8840

	Unit	Lotader® AX8900	Lotader® AX8840
Type of Polymer		E-MA-GMA	E-GMA
Methyl Acrylate Content	wt %	25	O
Glycidyl Methacrylate Content	wt%	8	8
Melt Index (190°C, 2.1kg,ASTM 1238)	g/10min.	6	5
Melting Point (DSC)	°C	60	105
Vicat Softening Point (ASTM1525-1kg)	°C	< 40	87
Tensile Strength at Break (ASTM D638)	MPa	4	8
Elongation at Break (ASTM D638)	%	1100	420
Hardness Shore A (ASTM D2240)	-	70	92

Lotader® 2210 is different from other the two resins, since it contains maleic anhydride (MAH) monomer, instead of GMA monomer, as the reactive group. The acrylic ester group of this terpolymer decreases the crystallinity and provides the prevention of mechanical properties. The reactive group, MAH, increases adhesion onto polar substrates and helps to formation of chemical bonds with substrates such as metals, polymers metallised products. Chemical structure and specifications of Lotader® 2210 are given in Figure 3.6 and Table 3.6.
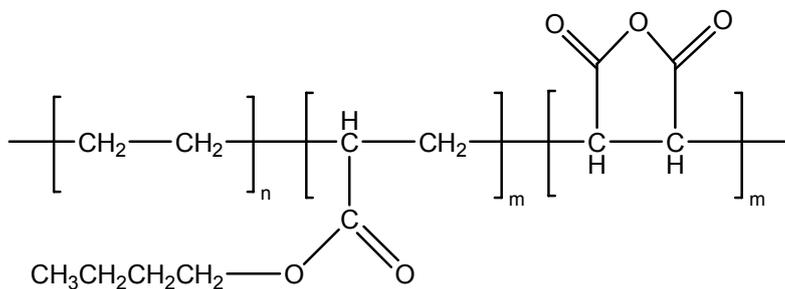
Figure 3.6 Chemical structure of Lotader® 2210 (E-nBA-MAH)

Table 3.6 Specifications of Lotader® 2210

	Unit	**Lotader® 2210**
Type of Polymer		E-nBA-MAH
Butyl Acrylate Content	wt %	8
Maleic Anhydride Content	wt%	2.6
Melt Index (190°C, 2.1kg,ASTM 1238)	g/10min.	3
Melting Point (DSC)	°C	107
Vicat Softening Point (ASTM1525-1kg)	°C	80
Tensile Strength at Break (ASTM D638)	MPa	12
Elongation at Break (ASTM D638)	%	600
Hardness Shore D (ASTM D2240)	-	46

3.2 Experimental Set-Up and Procedure

3.2.1 Melt Blending

In this study a co-rotating twin screw extruder was used in order to obtain ternary nanocomposites. The model of extruder is Thermoprism TSE 16 TC with L/D = 24. The screw diameter and the twin bore diameter of the extruder are 16 mm and 15.6 mm respectively. It has a barrel length of 384 mm and die length of 16 mm. In addition to these, maximum screw speed and maximum torque that can be achieved are 500 rpm and 12 Nm. It is possible to set barrel zones and die temperatures, screw speed and feed flow rate of main-feeder and side-feeder by using control panel with this extruder which allows us performing several experiments with different process parameters. Figure 3.7 shows the extruder and its screw configuration that was used for this study.

Figure 3.7-a Thermo Prism TSE 16 TC twin screw extruder

Figure 3.7-b Screw Configuration of Thermo Prism TSE 16 TC twin screw extruder

3.2.2 Injection Molding

The specimens for characterization were obtained by using Microinjector which is a laboratory scale injection molding machine (Daca Instruments). The molding parameters that can be controlled with this injection molding machine are, nozzle temperature, mold temperature, fill time, hold time, injection speed and injection pressure. The schematic drawing of injection molding machine is shown in Figure 3.8.
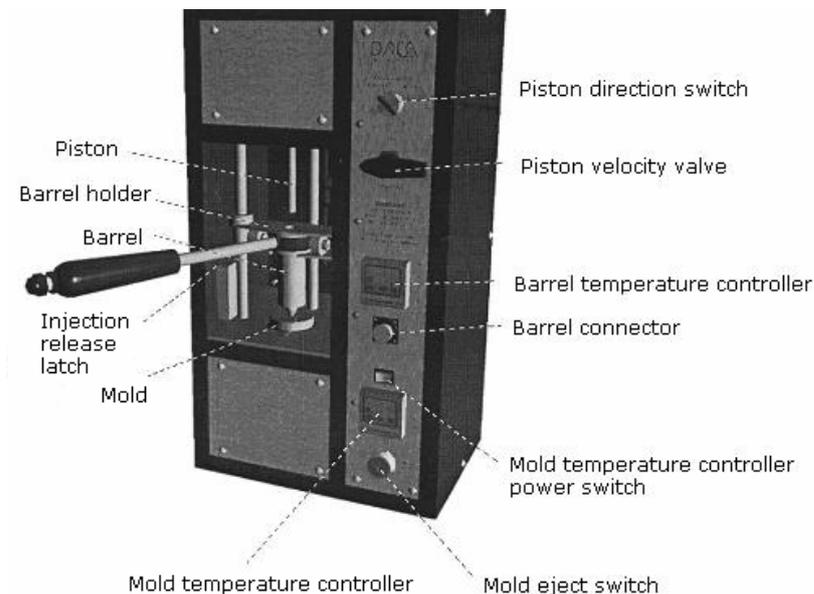
Figure 3.8 Injection Molding Machine

3.2.3 Experimental Procedure

Ternary nanocomposites of low density polyethylene/compatibilizer/clay were produced in this study. Process parameters were composition of raw materials, compatibilizer type, montmorillonite type, and addition order of materials during melt blending process. At first nanocomposites were obtained in pelletized form by two step extrusion process and then they were molded by injection molding in order to obtain specimens for mechanical, thermal and morphological characterization. Pure LDPE and binary mixtures of LDPE/Organoclay and LDPE/Compatibilizer were also prepared with the same process conditions in order to make comparison with the properties of nanocomposites. Before each run of extrusion process and molding, the raw materials and samples were dried in order to get rid of the moisture. Drying conditions were determined by considering the melting point of raw materials. Table 3.7 represents the drying conditions.

Table 3.7 Drying conditions

Materials	Drying Temperature (°C)	Drying Time (h)
Before RUN I Extrusion Process		
LDPE	-	-
Lotader® AX8900	40	12-15
Lotader® AX8840		
Lotader® 2210		
Cloisite® 15A	120	12-15
Cloisite® 25A		
Cloisite® 30B		
Before RUN II Extrusion Process		
LDPE	100	4
LDPE + Compatibilizer	100	4
LDPE + Clay	100	4
Compatibilizer + Clay	40	4
LDPE + Compatibilizer + Clay	100	4
Before Injection Molding Process		
All samples	100	12-15

Flowchart of experimental procedure and characterization of nanocomposites is shown in Figure 3.9.
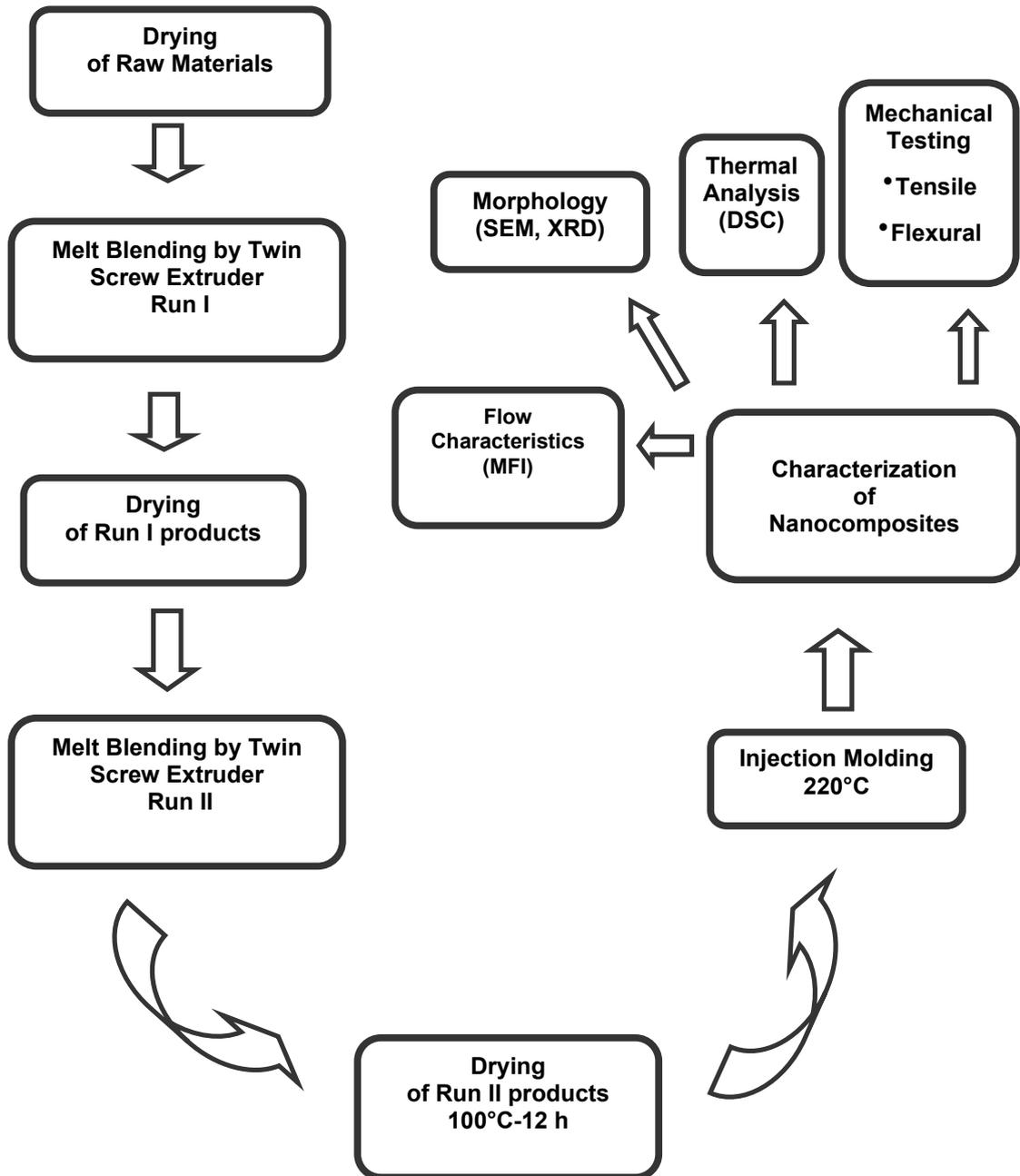
Figure 3.9 Flowchart of experimental procedure and characterization

3.2.4 Extrusion Process

During the extrusion process, temperature profile of the hopper, the mixing zones and the die was the screw speed, and the total flow rate of feed to extruder barrel were constant in all experiments. Process temperatures were 170, 210, 210, 210 ,220 °C for the hopper, the three mixing zones and the die, respectively. The screw speed and total flow rate of feed were kept constant at 200 rpm and 25 g/min throughout the experiments. In order to obtain the desired compositions, inlet flow rate of the main-feeder and the side-feeder were calibrated before each extrusion run. The molten product obtained from the extruder barrel was cooled by passing through a water bath, whose temperature was continuously controlled. At the end of the water bath, an air fan was placed in order to remove the water from the product surface and finally the product was collected in plastics bags after passing through the pelletizer.

3.2.4.1 Addition Order of Raw Materials

Addition order procedure was varied only in producing LDPE/Lotader® AX8900/Cloisite® 15A and LDPE/Lotader® 2210/Cloisite® 30B nanocomposites. Four different addition order procedures were applied to produce these products. The letters P, Co, and C represent LDPE, compatibilizer, and clay respectively.

Addition Order 1 (CoC)-P

Run I: Compatibilizer pellets were fed to the extruder from the main-feeder and organoclay was added to the system from the side-feeder. The temperature profile of this step was determined by considering the process conditions of compatibilizer so it was different from the other steps. Temperature profile was, 170, 190, 190, 190, 200 °C.
Run II: LDPE and product of Run I were mixed mechanically with desired compositions and fed to the extruder from the main-feeder.

Addition Order 2 (PC)-Co

Run I: LDPE pellets were fed to the extruder from the main-feeder and montmorillonite was fed from the side-feeder by adjusting the appropriate flow rates.

Run II: Compatibilizer pellets and precompounded LDPE-clay pellets were mixed and fed to the extruder barrel from the main-feeder.

Addition Order 3 (PCo)-C

Run I: LDPE and compatibilizer pellets were mixed mechanically and fed to the extruder barrel from the main-feeder with a flow rate of 25 g/min.

Run II: Product of Run I was fed to the system from the main-feeder and organoclay was added from the side-feeder of extruder.

Addition Order 4 (PCoC)

Run I : LDPE and compatibilizer were mechanically mixed and fed to the extruder barrel from the main-feeder, meanwhile the organoclay was fed from the side-feeder to the hopper. Total flow rate of inlet streams was adjusted to 25 g/min.

Run II: Product of Run 1 were fed to the extruder from the main-feeder after dried at determined conditions.

The reason of performing Run II, in addition order 4, was to prepare all compositions at the same experimental conditions. Pure LDPE and binary mixtures were also extruded twice. Table 3.8 summarizes all the addition order procedures and Table 3.9 and 3.10 shows all compositions produced in this study.

Table 3.8 Addition order procedures

Addition Order	RUN I		RUN II	
	Main-Feeder	Side-Feeder	Main-Feeder	Side-Feeder
1 (CoC)-P	Compatibilizer	Organoclay	Run I + LDPE {(CoC) + LDPE}	-
2 (PC)-Co	LDPE	Organoclay	Run I + Compatibilizer {(PC) + Compatibilizer}	-
3 (PCo)-C	LDPE	Compatibilizer	Run I + Clay {(PCo) + Clay}	Organoclay
4 (PCoC)	LDPE Compatibilizer	Clay	Run I (PCoC)	-

Table 3.9 Compositions of all samples

Set	Composition	Concentration wt %		
		LDPE	Compatibilizer	Organoclay
1	LDPE	100	-	-
LDPE / Organoclay Compositions				
2	LDPE+15A	98	-	2
3	LDPE+15A	96	-	4
4	LDPE+15A	94	-	6
5	LDPE+25A	98	-	2
6	LDPE+30B	98	-	2
LDPE / Compatibilizer Compositions				
7	LDPE+8900	95	5	-
8	LDPE+8900	90	10	-
9	LDPE+8900	85	15	-
10	LDPE+8840	95	5	-
11	LDPE+8840	90	10	-
12	LDPE+8840	85	15	-
13	LDPE+2210	95	5	-
14	LDPE+2210	90	10	-
15	LDPE+2210	85	15	-
Ternary Compositions (PCoC)				
16	LDPE+8900+15A	93	5	2
17	LDPE+8840+15A	93	5	2
18	LDPE+2210+15A	93	5	2
19	LDPE+8900+25A	93	5	2
20	LDPE+8840+25A	93	5	2
21	LDPE+2210+25A	93	5	2
22	LDPE+8900+30B	93	5	2
23	LDPE+8840+30B	93	5	2
24	LDPE+2210+30B	93	5	2

Table 3.10 Compositions of all samples (Cont'd)

LDPE / Lotader® AX8900 / Cloisite® 15A				
		Concentration wt %		
AO*		**LDPE**	**Compatibilizer**	**Organoclay**
1	(8900+15A)+LDPE	93	5	2
2	(LDPE+15A)+ 8900	93	5	2
3	(LDPE+8900)+15A	93	5	2
4	LDPE+8900+15A	93	5	2
LDPE / Lotader® AX8900 / Cloisite® 15A				
		Concentration wt %		
AO*		**LDPE**	**Compatibilizer**	**Organoclay**
1	(8900+15A)+LDPE	88	10	2
2	(LDPE+15A)+ 8900	88	10	2
3	(LDPE+8900)+15A	88	10	2
4	LDPE+8900+15A	88	10	2
LDPE / Lotader® 2210 / Cloisite® 30B				
		Concentration wt %		
AO*		**LDPE**	**Compatibilizer**	**Organoclay**
1	(2210+30B)+LDPE	93	5	2
2	(LDPE+30B)+ 2210	93	5	2
3	(LDPE+2210)+30B	93	5	2
4	LDPE+2210+30B	93	5	2

* AO: Addition order

3.2.5 Specimen Preparation

The specimens for characterization were molded by injection molding process. The molding conditions are summarized in Table 3.11.

Table 3.11 Molding parameters for injection molding

Parameter	Unit	Value
Nozzle Temperature	°C	220
Mold Temperature	°C	30
Fill Time	sec	30
Hold Time	min	1
Injection Speed	-	Fast
Injection Pressure	bar	8

3.3 Characterization of Specimens

In order to investigate the effect of the composition of raw materials, compatibilizer type, montmorillonite type, and addition order of materials during melt blending process on the final properties of the nanocomposites, morphological, thermal, mechanical analysis and flow characteristics were determined.

3.3.1 Morphological Analysis

3.3.1.1 X-Ray Diffraction (XRD) Analysis

The composites containing organoclay were analyzed by using a Philips PW3710 based X-Ray diffractometer. Cu-K anode radiation, generated at a generator tension of 40 kV and a generator current of 55 mA was used as the X-Ray source. The diffraction patterns were collected at a diffraction angle 2θ from 1° to 10° at a scanning rate and step size of 3°/min and 0.02°, respectively. The samples for X-Ray diffraction analysis were obtained from molded specimens.

3.3.1.2 Scanning Electron Microscopy (SEM) Analysis

Scanning electron microscopy (SEM) analysis was performed by a JEOL JSM-6400 low voltage scanning electron microscope. The fractured surfaces were obtained by using liquid nitrogen for all samples. Before SEM photographs were taken, the fractured surfaces were coated with a thin layer of gold in order to obtain a conductive surface. SEM photographs were taken for each specimen at x250 and x3000 magnifications. This analysis was used to investigate the effect of compatibilizer and organoclay on the morphology of the nanocomposites.

3.3.2 Thermal Analysis

3.3.2.1 Differential Scanning Calorimetry (DSC) Analysis

Differential scanning calorimetry was performed by using a differential scanning calorimeter General V4.1.C DuPont 2000. Measurements were carried out in the temperature range of 30 °C to 180 °C with a heating rate of 10 °C/min under nitrogen atmosphere. Melting points of samples and the degree of crystallinity was determined by using the DSC curves. The heat of fusion (ΔH) value for 100 % crystalline LDPE was taken as 293 J/g [15].

3.3.3 Mechanical Analysis

Tensile tests and flexural tests were performed at room temperature in the laboratory. At least six samples were used for each composition set and average values of test results and standard deviation values were recorded. At the end of the tests, tensile strength, tensile modulus, strain at break, flexural strength and flexural modulus of each composition were evaluated according to ASTM standards.

3.3.3.1 Tensile Tests

Tensile tests were performed for each composition according to ASTM D638M-91a (Standard Test Method for Tensile Properties of Plastics) [56], by using a Lloyd LR 30 K Universal Testing machine. The shape and dimensions of the specimens are given in Figure 3.10 and Table 3.12 respectively.
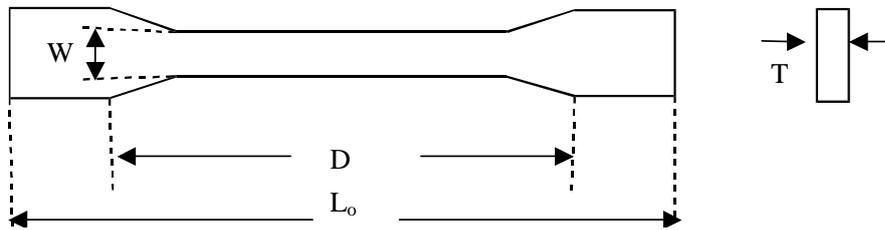
Figure 3.10 ASTM Tensile test specimen

Table 3.12 Dimensions of tensile test specimen

Symbol	Specimen Dimensions (mm)
W, Width of narrow section	7.5
D, Distance between grips	80
L_0, Total length of specimen	110
T, Thickness of specimen	2.1

The crosshead speed was calculated as 8 mm/min, based on the gauge length of 80 mm and strain rate of 0.1 min^{-1}. The test was performed by pulling the specimens from both grips until it fails. Stress versus strain diagrams were obtained from the mechanical testing device and tensile strength, tensile modulus and elongation at break values were determined by using these graphs.

3.3.3.2 Flexural Tests

Flexural tests were performed according to Test Method – I Procedure of ASTM D790M-92 (Standard Test Methods for Flexural Properties of Unreinforced Plastics and Electrical Insulating Materials) [59], with LR 30 K Universal Testing machine. Molded specimens were used for flexural tests and the thickness and width of specimens were the same as the tensile test specimens. The support span was taken as 50 mm, strain rate was 0.1 min^{-1} and the rate of cross-head was calculated as 19.84 mm/min. There was no failure of flexural test specimens so the tests were stopped when the specimens leaned against the base of the supports.

3.3.4 Flow Characteristics

3.3.4.1 Melt Flow Index (MFI) Test

Melt flow index (MFI) test was performed according to ASTM D1238-79 using an Omega Melt Flow Indexer. The measurements were carried out at 270 °C with a load of 2.16 kg. The weight of sample passing through the die in 10 min, defined as melt index, was determined for all compositions. The results were recorded as grams/10 min. The melt flow index machine used in this study is shown in Figure 3.11.

Figure 3.11 Omega Melt Flow Indexer

CHAPTER 4

RESULTS AND DISCUSSION

4. 1 Morphological Analysis

Two complementary techniques, XRD and SEM analysis, have been performed in order to characterize the morphology of nanocomposite structures.

4.1.1 X-Ray Diffraction (XRD)Analysis

XRD analysis is a convenient method for determining the crystal structure of the nanocomposites. Phase separated, intercalated and exfoliated structures can be identified according to the position, shape and intensity of the basal reflections from the silicate layers. The basal spacing (d-spacing) from XRD measurement refers to interlayer spacing of the silicate layers and calculated at peak positions according to Bragg's law.

In the case of phase separated composites, the polymer matrix is unable to enter into the clay galleries which result in no change in basal spacing. The increased basal spacing, (d_{001}), arises from the expansion of the interlayer space due to the entrance of polymer matrix into the clay galleries pushing the platelets apart, as a result, the intercalated nanocomposites can be distinguished from the difference in basal spacing [61]. When the absence of diffraction peak is observed, that means the clay platelets are completely delaminated and exfoliated nanocomposites are obtained. However, the lack of a Bragg's peak in the diffraction pattern does not necessarily mean that the clay is exfoliated. A disordered and immiscible sample, or other factors like low concentration of the clay in the region where the x-ray beam hits a non-uniformly dispersed sample, could fail to produce a Bragg's reflection [63].

67

XRD analysis was performed by setting the starting angle to 2θ = 1° in order to determine the d-spacings greater than 45 Å. Performing the analysis, at angle (2θ), greater than 2° will result in a false conclusion since no diffraction peak situation will be thought as complete exfoliation of the clay layers. The d-spacing values of samples obtained from the XRD analysis are given in Table 4.1 and the output X-ray figures are given in Appendix A.

Table 4.1 X-ray diffraction results of samples

Composition	Organoclay wt %	d- spacing (Å)	2 theta(°)
Pure Materials			
LDPE	-	-	-
Cloisite® 15A	-	31.9	2.76
Cloisite® 25A	-	20.1	4.39
Cloisite® 30B	-	17.9	4.92
LDPE / Organoclay Compositions			
LDPE+15A	2	33.3	2.65
LDPE+15A	4	30.4	2.90
LDPE+15A	6	29.9	2.95
LDPE+25A	2	28.5	3.09
LDPE+30B	2	18.80	4.70
Ternary Compositions (PCoC)[*]			
LDPE+8900+15A	2	40.3	2.19
LDPE+8840+15A	2	34.6	2.55
LDPE+2210+15A	2	32.8	2.69
LDPE+8900+25A	2	38.3	2.31
LDPE+8840+25A	2	37.4	2.36
LDPE+2210+25A	2	53.5	1.65
LDPE+8900+30B	2	59.2	1.49
LDPE+8840+30B	2	44.1	2.10
LDPE+2210+30B	2	54.8	1.61

* Ternary nanocomposites contain 5 wt % compatibilizer.

The basal spacings of neat organoclays were determined as 31.9 Å at 2θ= 2.76 °, 20.1 Å at 2θ= 4.39°, and 17.9 Å at 2θ= 4.92° for Cloisite® 15A, Cloisite® 25A and Cloisite® 30B respectively and all are in accordance with the values of basal spacings reported in the manufacturer' s datasheet.

No increase was observed in the interlamellar distance of silicate layers of nanocomposites containing only 15A with the compositions of 2 wt %, 4 wt %, and 6 wt % organoclay. However, the maximum intensity of the diffraction peaks increased sharply with increase in clay content from 2 wt % to 6 wt %. The increase in intensity is due to the high concentrations of ordered structures in the nanocomposites at high organoclay contents. In addition to these, it was seen that the increase in organoclay content also resulted in a slight decrease in basal spacing of the layers. It is easier to disrupt the stacking structure of organoclay at low concentrations during the melt blending. So the decrease in d- spacing of the layers is more likely because of the non-uniform dispersion and agglomeration of clay particles which hinder the penetration of polymer in to the clay galleries. It is concluded that the insertion of LDPE was not achieved with melt blending of LDPE and organoclay 15A and the obtained structures were not intercalated or exfoliated.

Among the LDPE and organoclay nanocomposites, the one containing 2 wt % 25A that has the peak at 3.09° in the XRD pattern, indicating the intercalated nanostructure of LDPE/25A nanocomposite with a maximum basal spacing of 28.5 Å. In the XRD pattern, it is seen that there is a broader peak between the ranges of 3.1° and 5.1° with basal spacings of 28.5 Å and 17.4 Å respectively. This shows that there are several intercalated structures with different basal spacings, which were formed during the insertion of the polymer throughout the clay galleries and resulted in more disordered structures [61]. However it was not possible to obtain complete delamination of platelets.

As in the case of LDPE/15A nanocomposites, the basal spacing of the silicate layers of organoclay 30B was unchanged, indicating that no intercalation occurred during the melt blending.

In the diffractograms of nanocomposites, secondary and tertiary peaks were also observed at high angles, and so having d-spacing values smaller than the neat organoclay's basal spacing. These peaks belong to the unintercalated organoclay. During the melt blending process, the alkyl chains of the organoclay get rearranged and due to the breakup of the electrostatic interaction between the alkyl ammonium and the negative charge of the silicate surface decrease in basal spacing occurs [62].

4.1.1.1 Effect of Compatibilizer

In this study all clay types were organically modified. The alkyl chains provide an additional distance between the interlayer of the layered silicates which makes it easy for polymer matrix to enter into the clay galleries. However, it is seen that this is not sufficient to obtain complete dispersion and delamination of layers of organoclay throughout the polymer matrix.

From Table 4.1, it is seen that addition of 5 wt % compatibilizer to the LDPE/organoclay blends resulted in a shift to lower angles of the characteristic diffraction peaks of the neat organoclay and LDPE/organoclay blends indicating a more substantial difference in the interlayer spacing of the clay layers. The results are compatible with the results reported in the literature about the effect of compatibilizer on polyolefin/clay nanocomposites [6-16].

Compatibilizers used in this study are polyethylene based therefore they are miscible with the polymer matrix of the nanocomposites and they contain functional groups of GMA, or MAH. It is possible that there are some reactions occurring between the functional groups of the compatibilizers and the hydroxyl groups of the montmorillonite. Moreover this results in the intercalation of the compatibilizer into the clay galleries and increases the possibility of the delamination of the clay structure. Also the organoclay 30B contains hydroxyl groups in its structure which provide the reaction possibility with functional groups of compatibilizers.

Since the compatibilizers have bulky functional groups such as GMA, and MAH this also increases the clay spacing and decreases the interaction between the clay layers

and enhance the intercalation of the polymer matrix. The polar structure of compatibilizers also increases the interaction between the organoclay and the polymer matrix and so favor the increase in intercalation and exfoliation [4].

Considering the LDPE/compatibilizer/15A nanocomposites, the one with compatibilizer 8900 (E-MA-GMA), has the diffraction peak at angle 2.19 ° showing that the interlayer spacing is 40.3 Å. On the other hand, XRD results of other two nanocomposites containing compatibilizer 8840 (E-GMA), and 2210 (E-nBA-MAH) show a slight increase in layer distance.

The effect of compatibilizer on the dispersion of silicate layers was observed in the case of the LDPE/compatibilizer/25A nanocomposites. XRD pattern of nanocomposite containing E-MA-GMA, showed a sharp peak at angle 2.31° and a broader one at 4.96° with the basal spacings of 38.3 Å and 17.78 Å, which indicates that the nanocomposite have an intercalated structure, however, some of the organoclay still kept its original stacking. XRD curve of nanocomposites containing E-GMA showed two broaden peaks at 2.36° and 5.0° with the resultant basal spacings of 37.4 Å and 17.65 Å which are the evidences of the intercalated structures. Even better dispersion was achieved with the nanocomposite containing E-nBA-MAH. There is a very broad peak at the position of 1.65°, corresponding to the interlayer distance 53.5 indicating that the organoclay has been significantly intercalated in the LDPE/2210/25A system.

Among all compositions, the best dispersion was achieved with LDPE/compatibilizer/30B nanocomposites. The interlayer spacings were determined as 59.2 Å, 44.1 Å, and 54.8 Å for nanocomposites containing E-MA-GMA, E-GMA, and E-nBA-MAH, respectively. Also there were basal reflection peaks around 6° indicating unintercalated clay layers.

4.1.1.2 Effect of Addition Order

X-ray diffraction analysis was performed for LDPE/8900/15A, and LDPE/2210/30B nanocomposites obtained through different addition orders. The XRD results are given in Table 4.2.

Table 4.2 X-ray diffraction results of nanocomposites produced with different addition order sequences.

Composition	Organoclay wt %	d- spacing (Å)	2 theta(°)
LDPE + 8900+ 15A Compositions [*]			
AO1 (CoC)+P	2	39.6	2.23
AO2 (P+C)+Co	2	42.5	2.07
AO3 (P+Co)+C	2	40.8	2.16
AO4 (PCoC)	2	40.3	2.19
LDPE + 2210+ 30B Compositions [*]			
AO1 (CoC)+P	2	14.7	5.98
AO2 (P+C)+Co	2	15.01	5.89
AO3 (P+Co)+C	2	15.07	5.86
AO4 (PCoC)	2	54.8	1.61

* Ternary nanocomposites contain 5 wt % compatibilizer.

Table 4.2 shows that, for LDPE/8900/15A nanocomposites, the peak of montmorillonite apparently shifts to a small angle in all the addition order sequences. All samples have diffraction peak around 2.15°, with corresponding basal spacing of 40.8 Å, indicating that intercalated nanocomposites were acquired. On the other hand, there is no a similar trend for LDPE/2210/30B nanocomposites. The XRD curve of nanocomposites obtained with AO4 sequence shows intercalated structure with a diffraction peak at 1.61°, which leads in basal spacing of 54.8 Å. In addition to these there is a broader peak at around 5.8° which is due to unintercalated clay layers.

The AO2 (PC-Co) type nanocomposite has a sharp peak at 5.89°. It can be concluded that these nanocomposites failed to have intercalated structures. Also agglomerates of clay particles are seen in SEM analysis in these nanocomposites. The other two nanocomposite types have also a broader peak at angle 5.8°, indicating the unintercalated structures.

4.1.2 Scanning Electron Microscopy (SEM) Analysis

In this study, the mixtures of polymer/organoclay, polymer/compatibilizer, and polymer/compatibilizer/organoclay have been obtained by means of twin screw extrusion process. In order to investigate the morphological properties of these samples, scanning electron microscopy analysis was performed to fractured surfaces of all samples produced. SEM images of these samples are presented here with magnifications of x250 and x3000 to provide better observation.

The SEM micrographs of ternary nanocomposites designate that compatibilizer has an important role in dispersion of the clay throughout the polymer LDPE matrix, which results in improved mechanical properties.

Figure 4.1 shows the fractured surfaces of twice extruded LDPE at magnifications of x250 and x3000. It is seen that LDPE has a smooth surface and few crack propagation lines are observed.
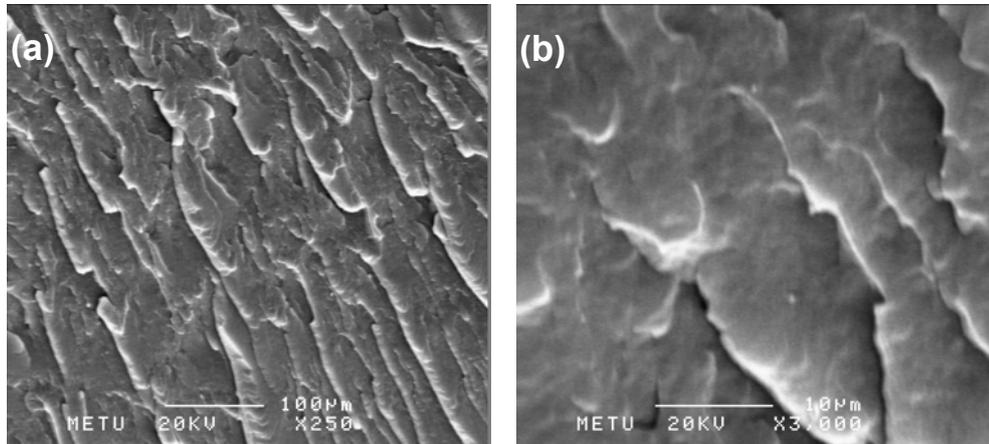
Figure 4.1 SEM micrographs of pure Low Density Polyethylene (LDPE) (a) x250 (b) x3000.

Figure 4.2 shows the fractured surfaces of nanocomposites containing 2, 4, and 6 percent of Cloisite® 15A. It is seen that addition of organoclay to neat polymer results in the disappearance of the smooth surface. In Figure 4.2 (a) and 4.2 (b) the crack propagation lines of 2 wt % organoclay containing nanocomposite can clearly be seen at x250 and x3000 magnifications. These are straight propagation lines and due to this homogeneous structure, there are no significant barriers to stop the crack propagation. The collinear position of crack lines enhances the crack growth so it is possible to obtain fracture with only small amounts of energy [49].

In Figure 4.2, it is observed that the crack propagation lines are approaching a shorter and closer structure with increasing clay loading and instead of being straight lines, they are more zigzagged and tortuous. These tortuous paths prevent the easy propagation of the cracks. Generally, as the distance between the crack lines is smaller the material can endure high impact stresses.

Figure 4.3 and 4.4 show the fractured surfaces of nanocomposites containing 2 weight % of Cloisite® 25A and Cloisite® 30B respectively. The surfaces of these nanocomposites are similar and both have tortuous crack propagation path.
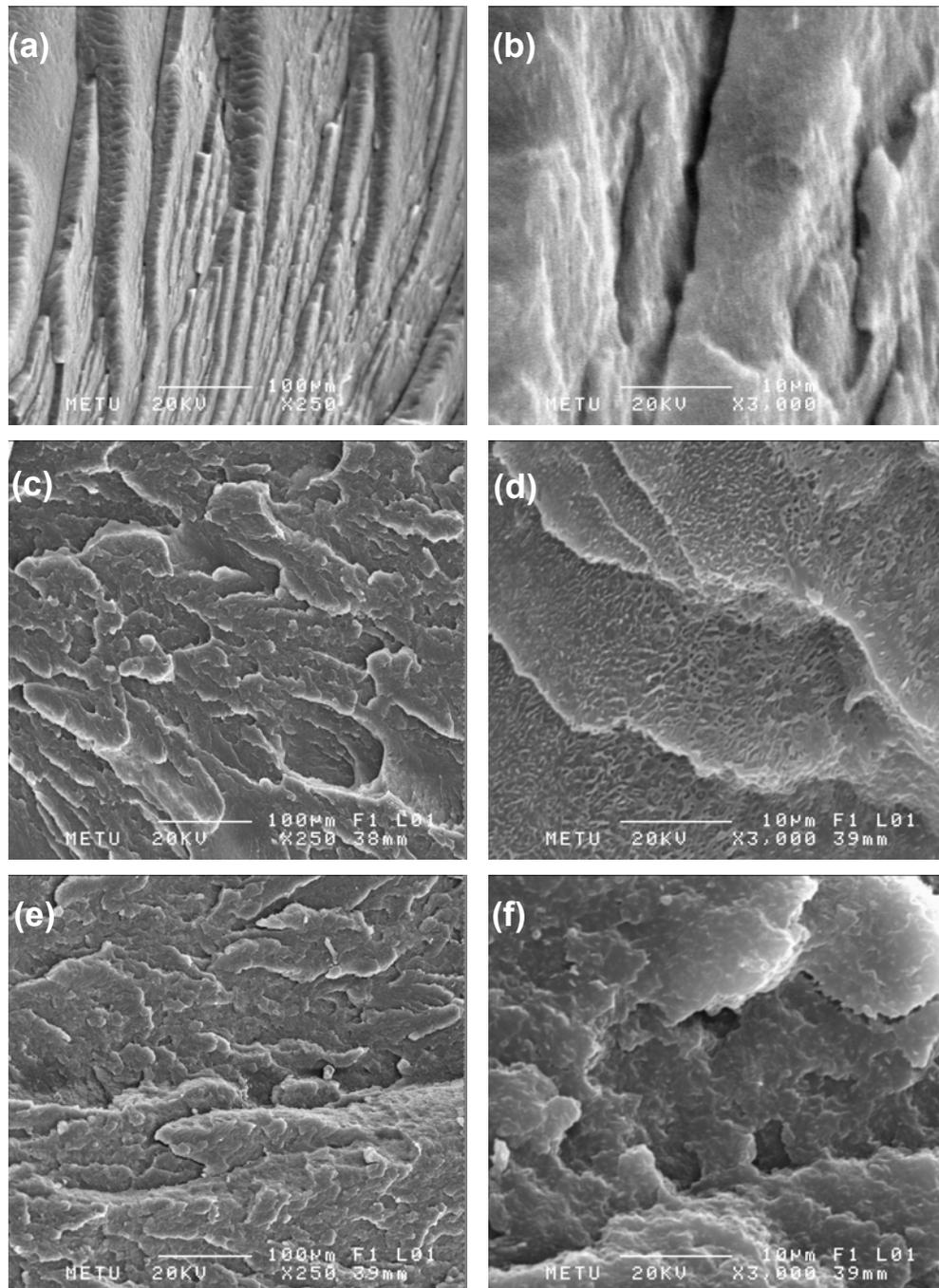
Figure 4.2 SEM micrographs of nanocomposites containing Cloisite® 15A, (a) 2 wt. % x250, (b) 2 wt. % x3000; (c) 4 wt. % x250, (d) 4 wt. % x3000; (e) 6 wt. % x250, (f) 6 wt. % x3000.
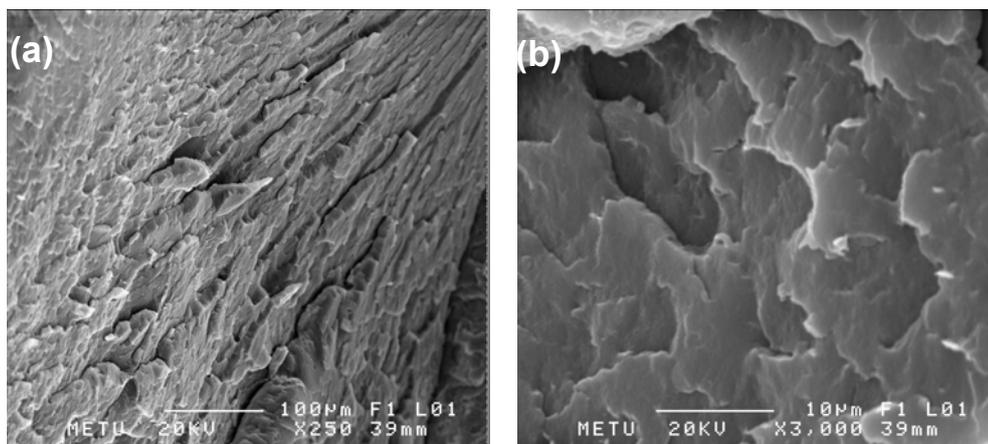
Figure 4.3 SEM micrographs of nanocomposites containing Cloisite® 25A, (a) 2 wt. % x250, (b) 2 wt. % x3000.
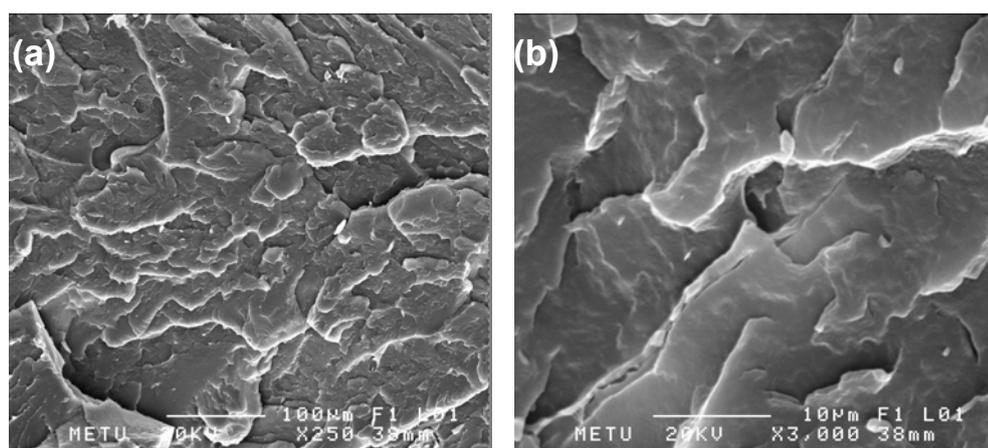
Figure 4.4 SEM micrographs of nanocomposites containing Cloisite® 30B, (a) 2 wt. % x250, (b) 2 wt. % x3000.

In Figures 4.5, 4.6, and 4.7 SEM micrographs of LDPE/ E-MA-GMA, LDPE/E-GMA, and LDPE/E-nBA-MAH blends with varying compatibilizer concentrations are shown at magnifications of x250, and x3000 respectively. Although the compatibilizer concentration is increased, no remarkable difference was observed in the morphology of LDPE/compatibilizer blends. The continuous and interpenetrated phases seen in the micrographs indicating that the compatibilizers are compatible with LDPE.
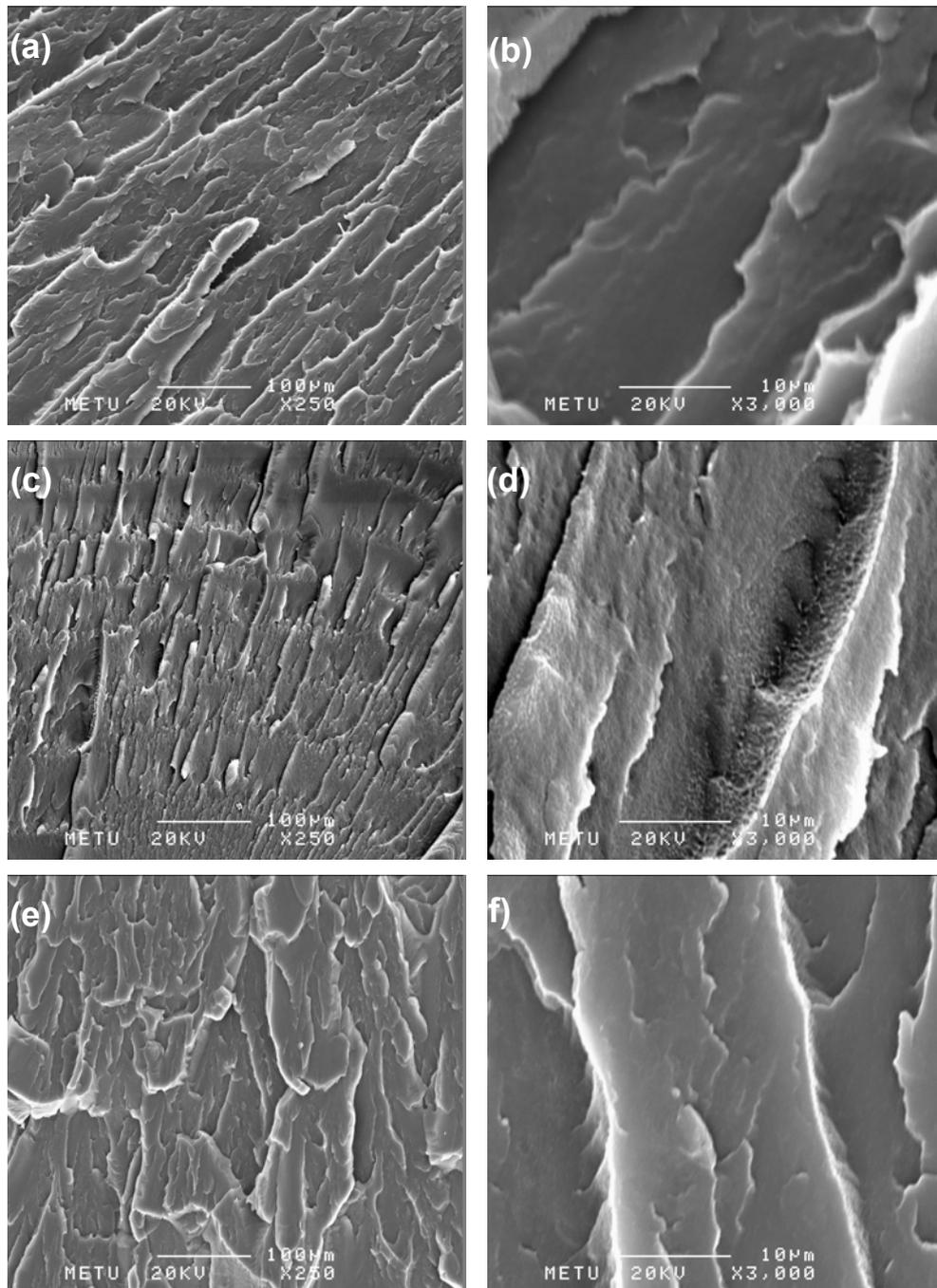
Figure 4.5 SEM micrographs of LDPE/ compatibilizer blends containing Lotader® AX 8900 (E-MA-GMA) (a) 5 wt. % x250, (b) 5 wt. % x3000; (c) 10 wt. % x250, (d) 10 wt. % x3000; (e) 15 wt. % x250, (f) 15 wt. % x3000.
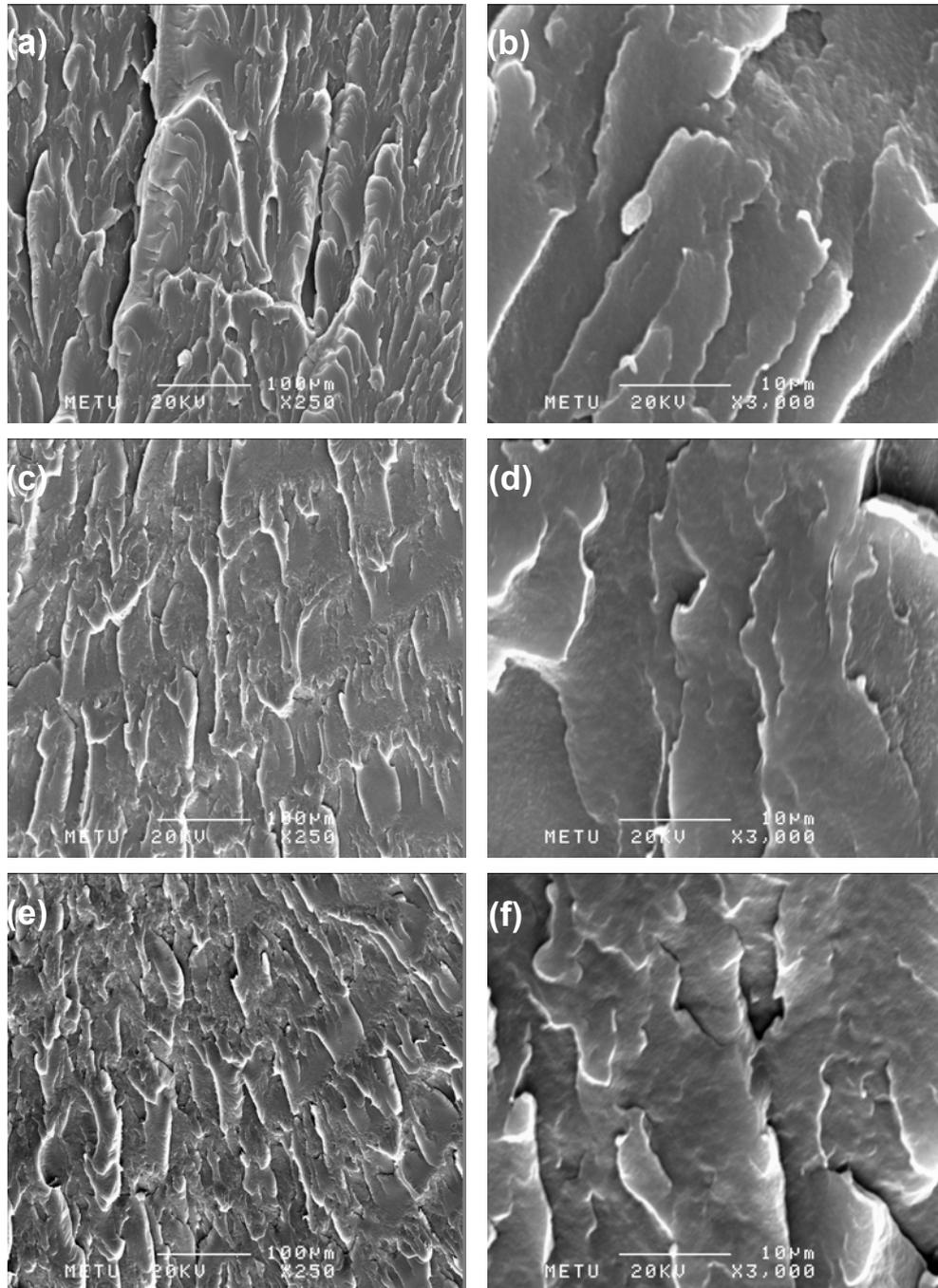
Figure 4.6 SEM micrographs of LDPE/compatibilizer blends containing Lotader® AX 8840 (E-GMA) (a) 5 wt. % x250, (b) 5 wt. % x3000; (c) 10 wt. % x250, (d) 10 wt. % x3000; (e) 15 wt. % x250, (f) 15 wt. % x3000.
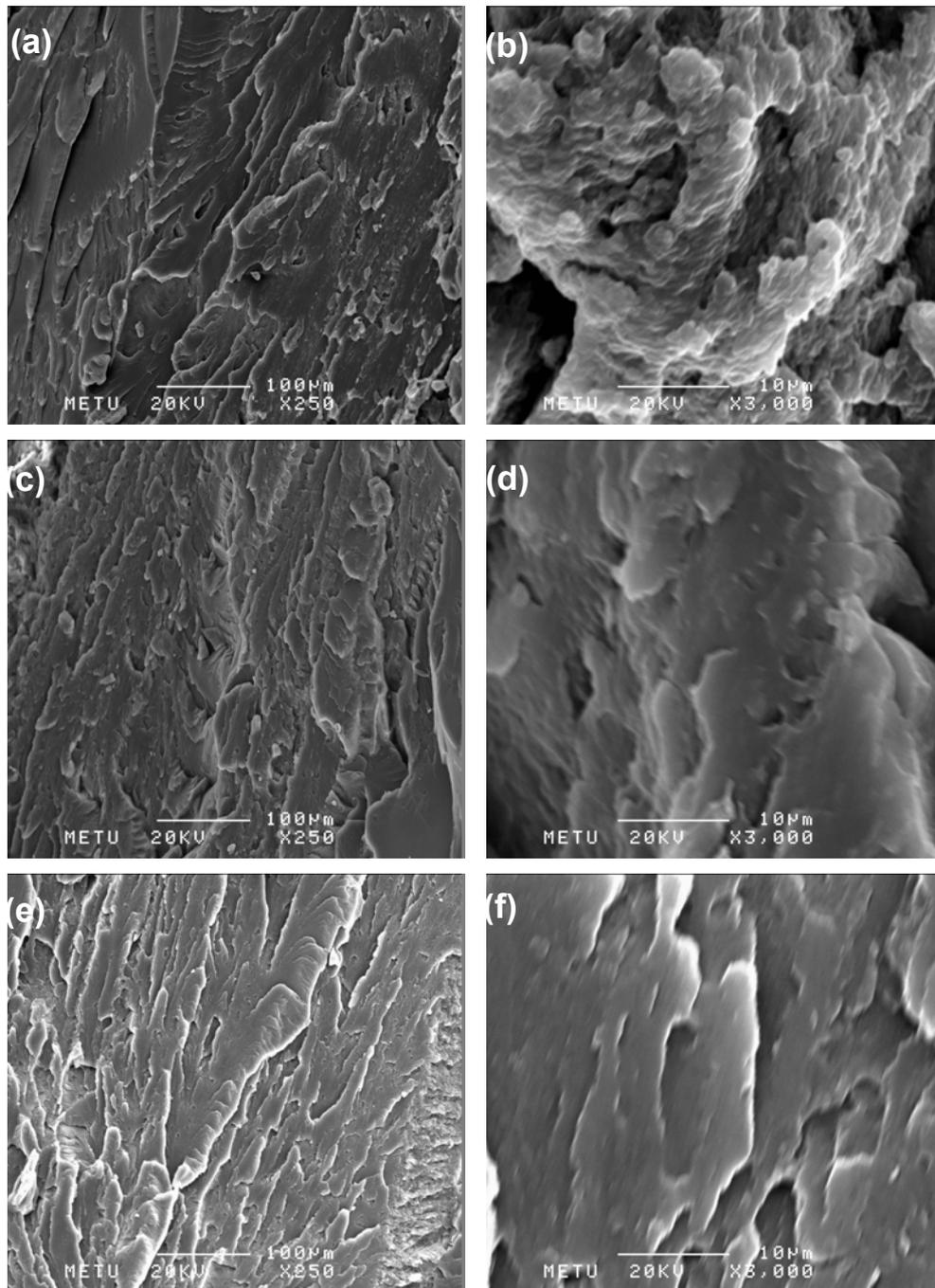
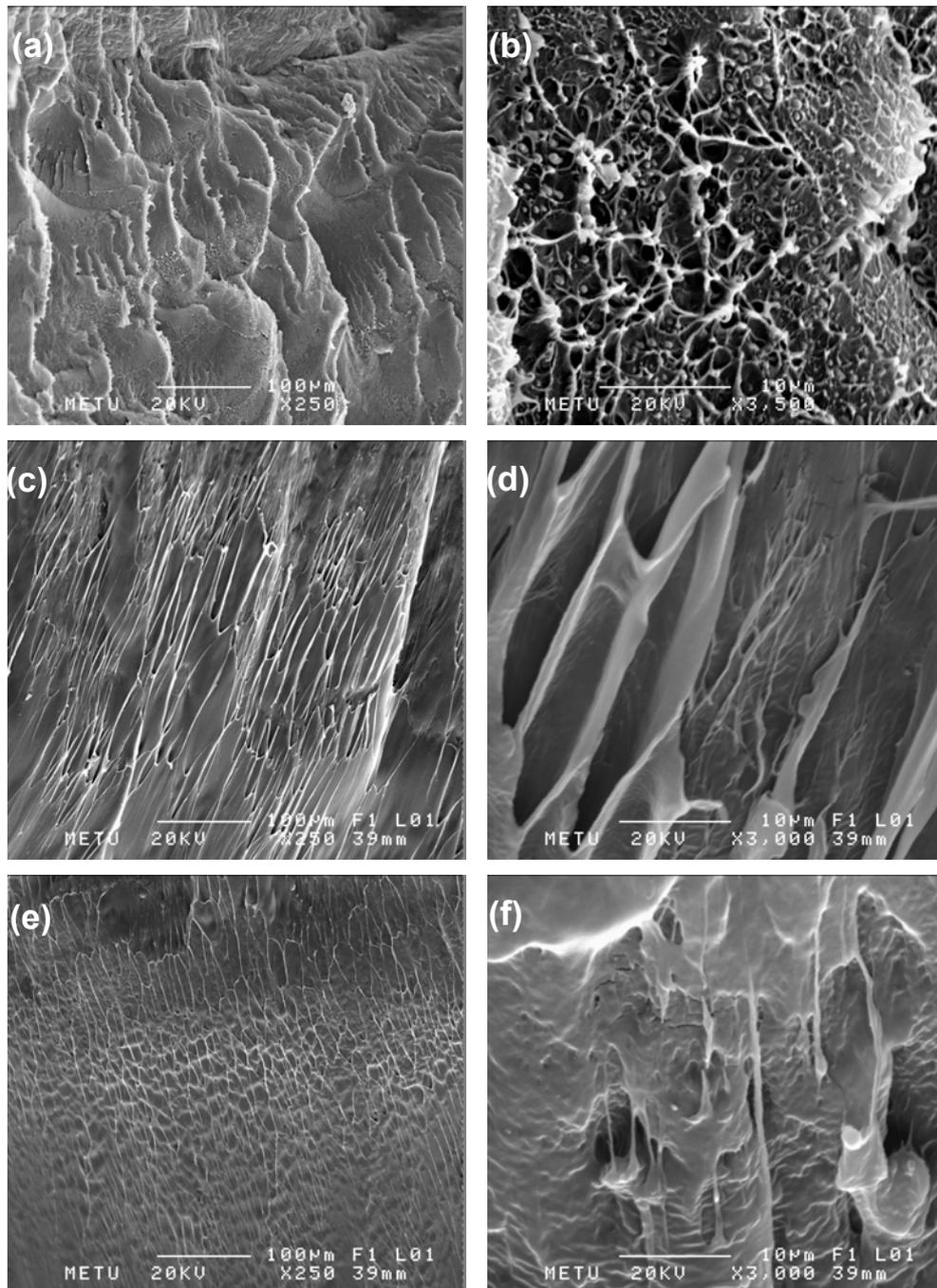**Figure 4.7** SEM micrographs of LDPE/compatibilizer blends containing Lotader® 2210 (E-BA-MAH) (a) 5 wt. % x250, (b) 5 wt. % x3000; (c) 10 wt. % x250, (d) 10 wt. % x3000; (e) 15 wt. % x250, (f) 15 wt. % x3000.

Figure 4.8, 4.9 and 4.10 are SEM micrographs of the fractured surfaces of ternary LDPE/compatibilizer/organoclay nanocomposites containing 5 weight percent compatibilizer and 2 weight percent organoclay, prepared by AO4 sequence in which all the materials were fed to extruder simultaneously at first run. It is seen that the crack propagation lines of nanocomposite surfaces are not straight lines and the smooth structure of neat LDPE is not detected in these SEM micrographs. In the case of well dispersed layered silicates, many shorter and closer, circular, nonlinear , cracks are formed simultaneously and these nonlinear cracks tend to grow until they interfere with each other. At these points, the stress fields at the tips of the crack lines interact and prevent the further growth or cracks by reducing the stress at the tips of the cracks [49]. When compared with SEM micrographs of LDPE/organoclay nanocomposites, addition of compatibilizer resulted in more miscible surfaces. The improved mechanical properties of ternary nanocomposites also support the compatibility of the phases and well dispersion of the clay particles.

When considering Figure 4.9 (a) and 4.9 (b), it is seen that agglomerates of clay particles are present on the surfaces. These agglomerates act as stress concentrator in the structure and lead in low mechanical properties of nanocomposites.

In the previous section, intercalation/exfoliation of the clay was discussed by using the XRD curves of the samples. However, a more powerful technique like transmission electron microscopy (TEM) analysis should be performed to obtain more precise observation of nanostructures, owing to high resolution obtained by TEM.

Figure 4.8 SEM micrographs of nanocomposites produced with AO4 sequence, containing 2 wt. % Cloisite® 15A and 5 wt. % compatibilizer, (a) Lotader® AX 8900 x250, (b) Lotader® AX8900 x3500; (c) Lotader® AX8840 x250, (d) Lotader® AX 8840 x3000; (e) Lotader® 2210 x250, (f) Lotader® 2210 x3000.
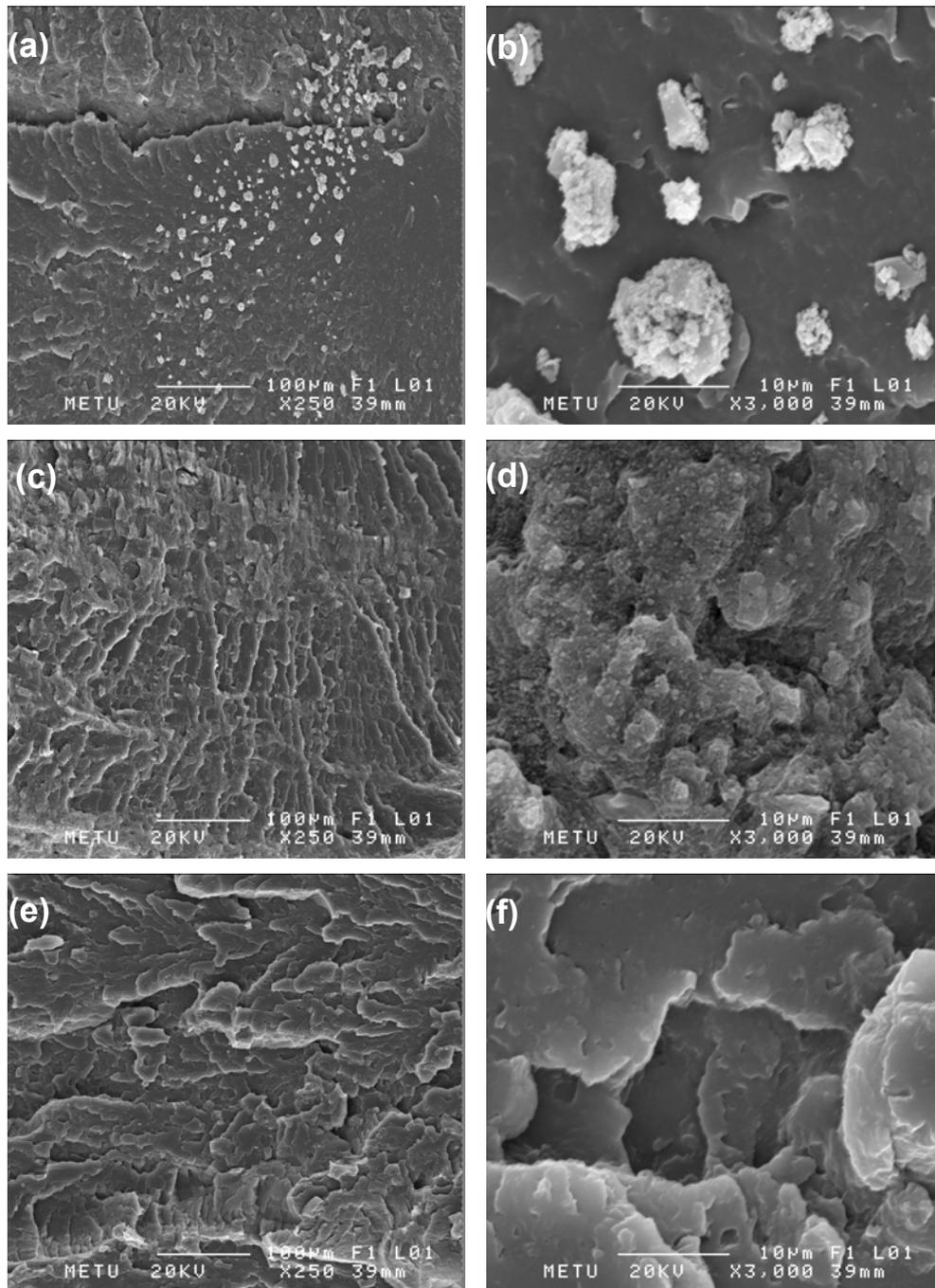
Figure 4.9 SEM micrographs of nanocomposites produced with AO4 sequence, containing 2 wt. % Cloisite® 25A and 5 wt. % compatibilizer, (a) Lotader® AX 8900 x250, (b) Lotader® AX8900 x3000; (c) Lotader® AX8840 x250, (d) Lotader® AX 8840 x3000; (e) Lotader® 2210 x250, (f) Lotader® 2210 x3000.
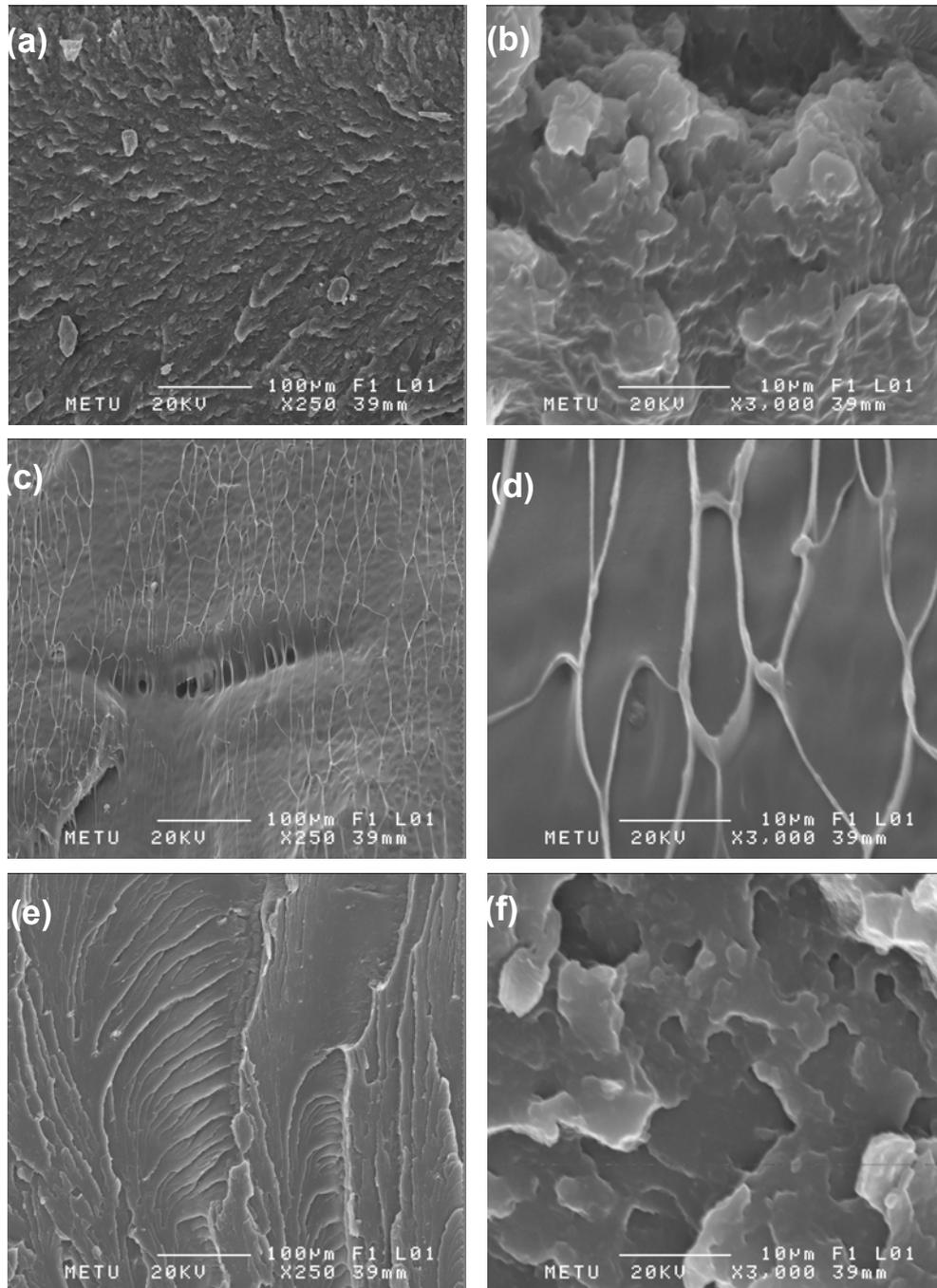
Figure 4.10 SEM micrographs of nanocomposites produced with AO4 sequence, containing 2 wt. % Cloisite®30B and 5 wt. % compatibilizer, (a) Lotader® AX 8900x250, (b) Lotader® AX8900 x3000; (c) Lotader® AX8840 x250, (d) Lotader® AX 8840 x3000; (e) Lotader® 2210 x250, (f) Lotader® 2210 x3000.

Figures 4.11 through 4.16 show the SEM micrographs of ternary nanocomposites prepared by different addition order. No significant differences were observed in the morphology of fractured surfaces. It is obviously seen that the surfaces are highly rough and the crack propagation lines are tortuous. The cracks are not far apart from each other.

The agglomerates of organoclay particles are clearly seen in Figure 4.13 (c), 4.13 (d), 4.15 (c), and 4.15 (d). Dispersion of clay particles was not achieved during melt blending of these nanocomposites. As expected, the mechanical properties of these samples are very poor.
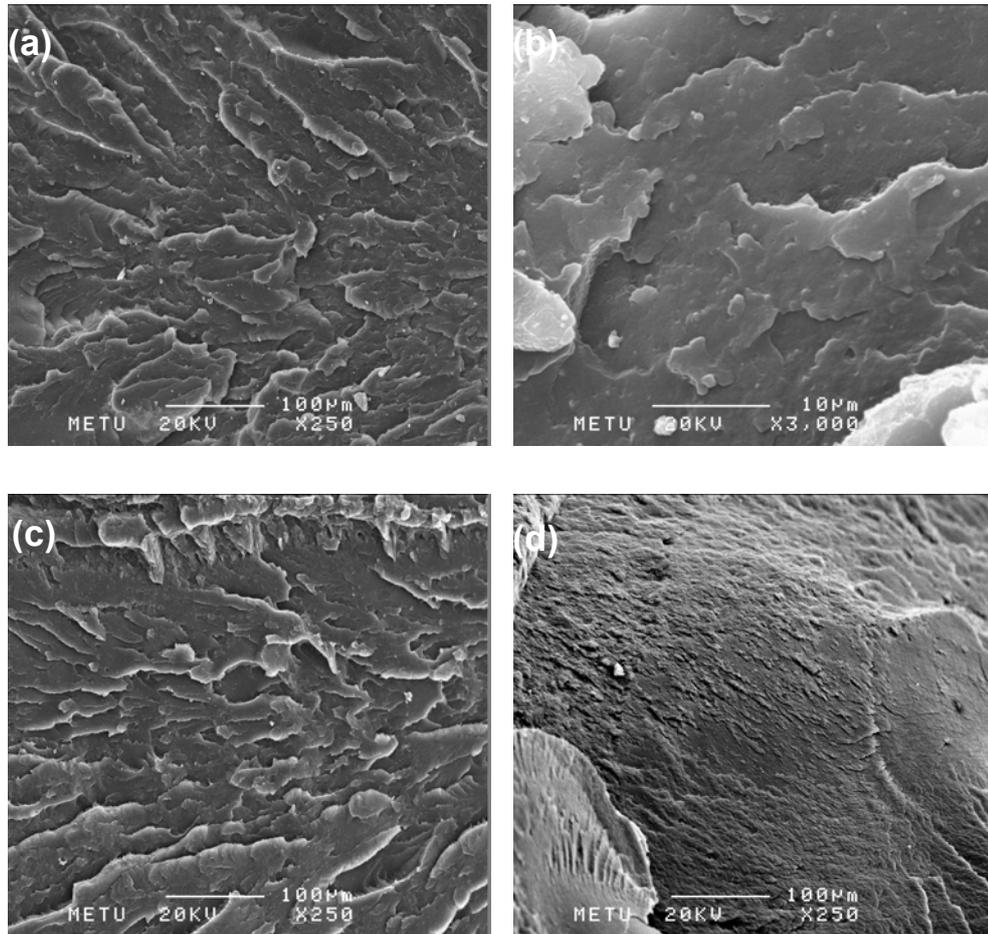
Figure 4.11 SEM micrographs of nanocomposites produced with different addition order sequences, containing 2 wt. % Cloisite® 15A and 5 wt. % Lotader® AX8900; (a) AO1 x250, (b) AO1 x3000 ; (c) AO2 x250, (d) AO2 x3000.
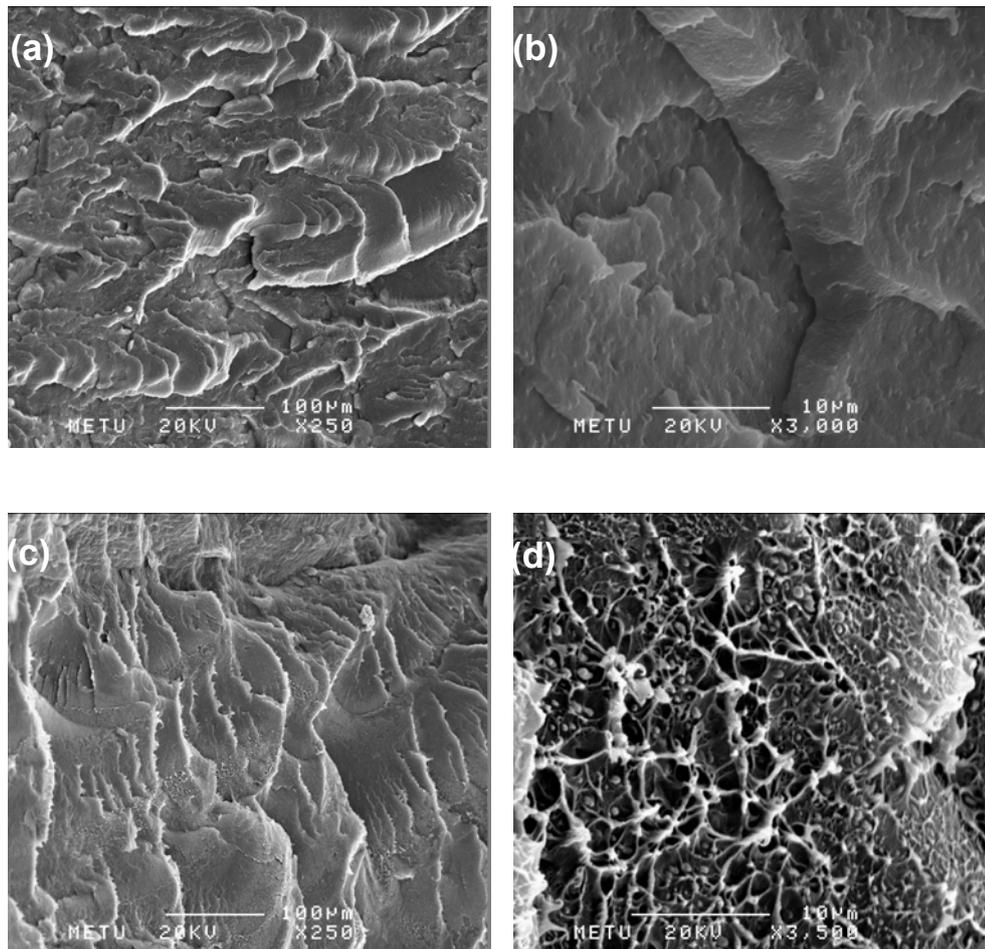
Figure 4.12 SEM micrographs of nanocomposites produced with different addition order sequences, containing 2 wt. % Cloisite® 15A and 5 wt. % Lotader® AX8900; (a) AO3 x250, (b) AO3 x3000 ; (c) AO4 x250, (d) AO4 x3500.
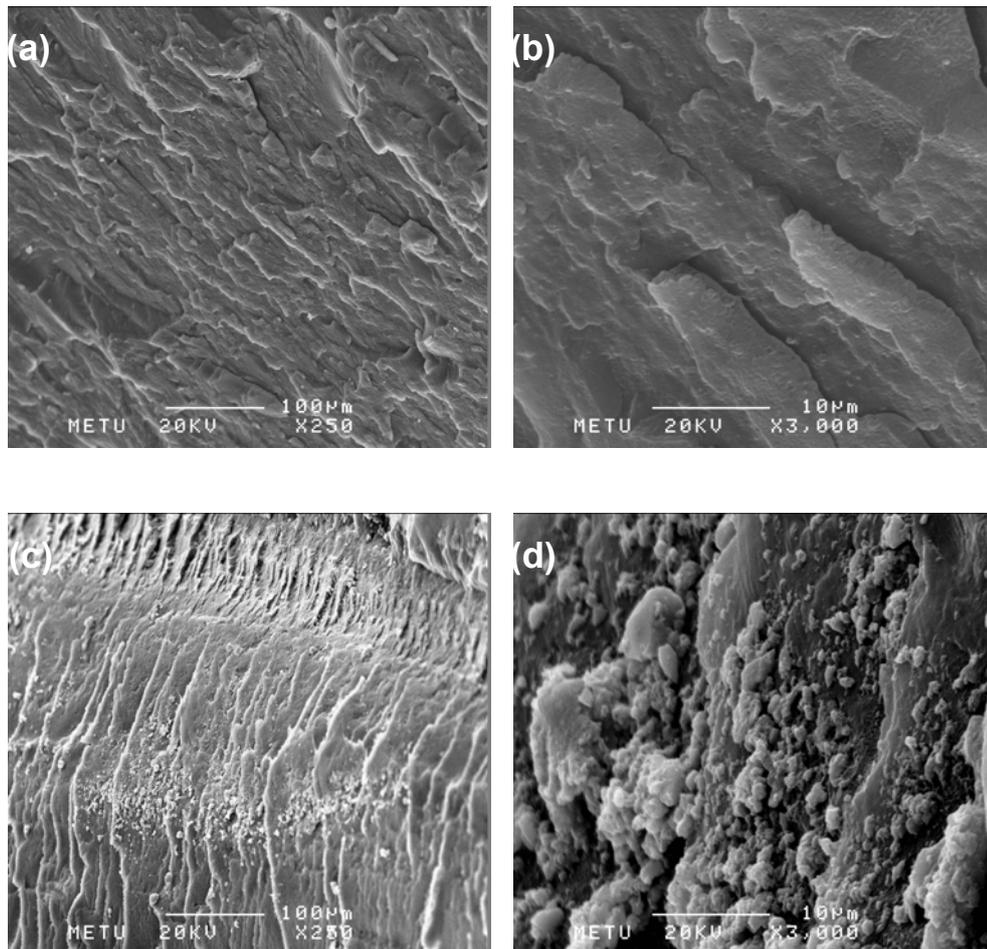
Figure 4.13 SEM micrographs of nanocomposites produced with different addition order sequences, containing 2 wt. % Cloisite® 15A and 10 wt. % Lotader® AX8900; (a) AO1 x250, (b) AO1 x3000 ; (c) AO2 x250, (d) AO2 x3000.

Figure 4.14 SEM micrographs of nanocomposites produced with different addition order sequences, containing 2 wt. % Cloisite® 15A and 10 wt. % Lotader® AX8900; (a) AO3 x250, (b) AO3 x3000 ; (c) AO4 x250, (d) AO4 x3000.

Figure 4.15 SEM micrographs of nanocomposites produced with different addition order sequences, containing 2 wt. % Cloisite® 30B and 5 wt. % Lotader® 2210 ; (a) AO1 x250, (b) AO1 x3000 ; (c) AO2 x250, (d) AO2 x3000.
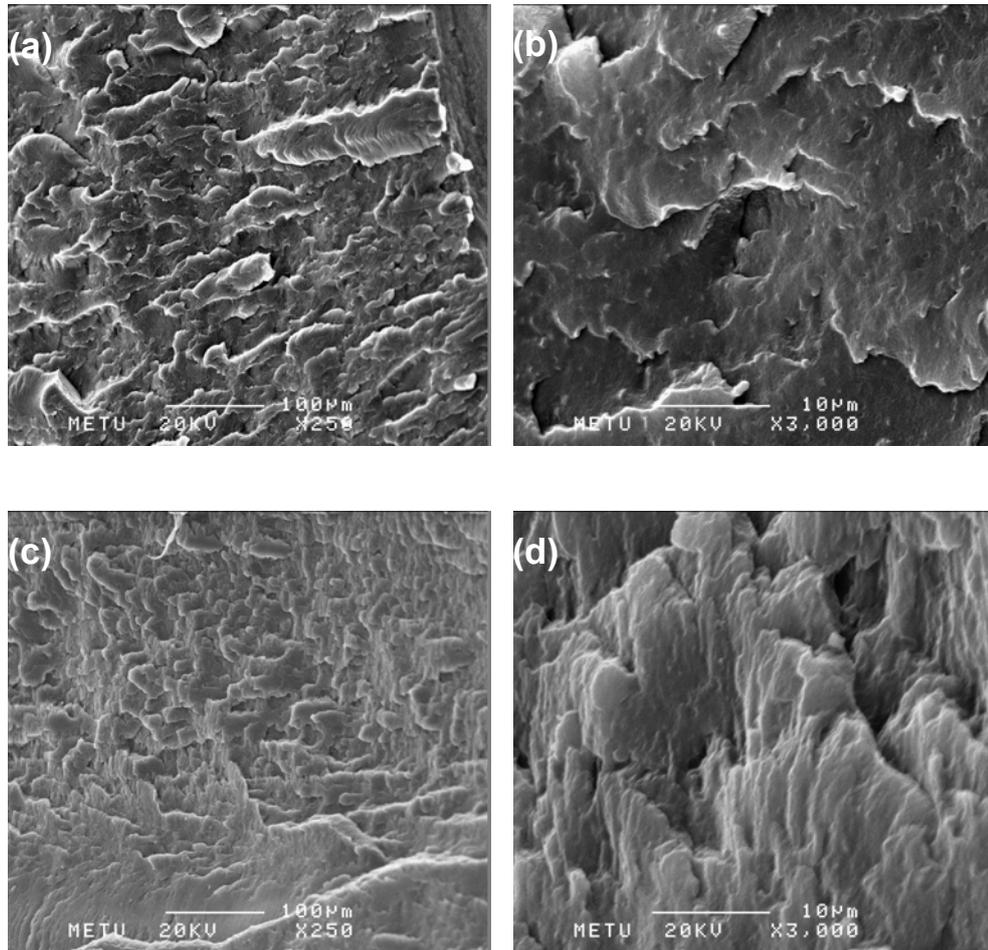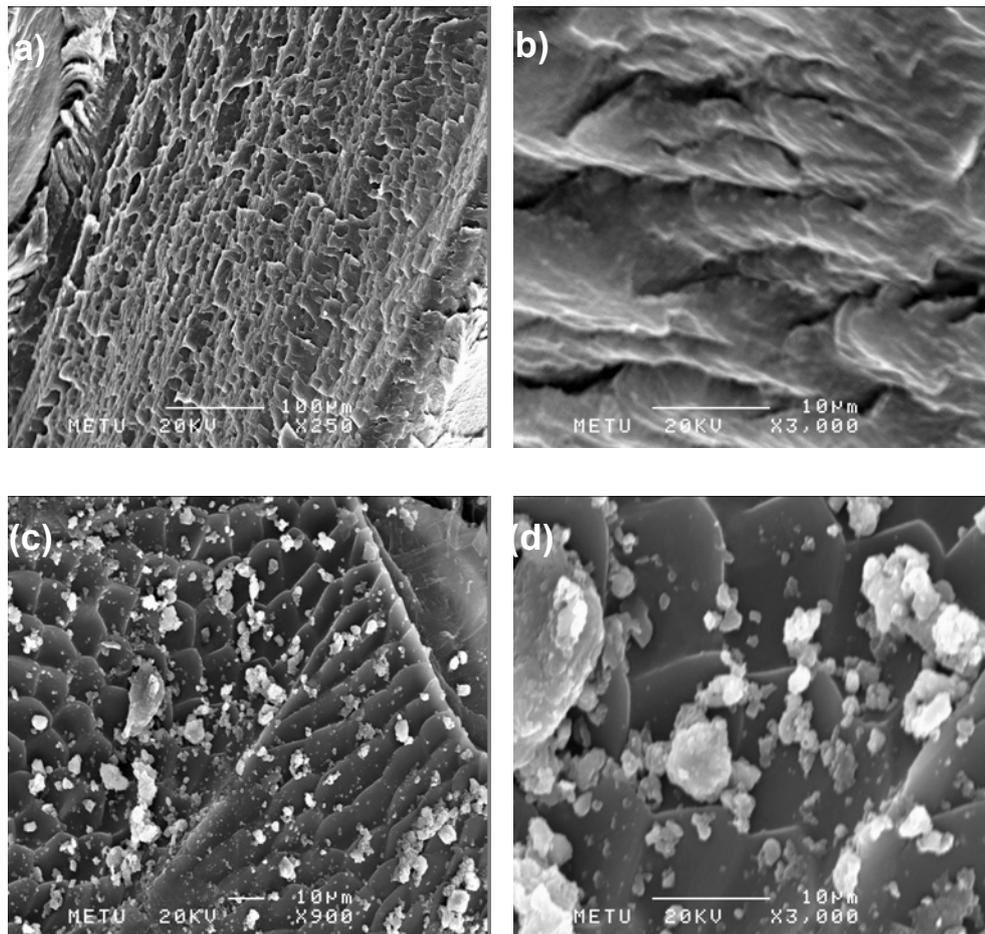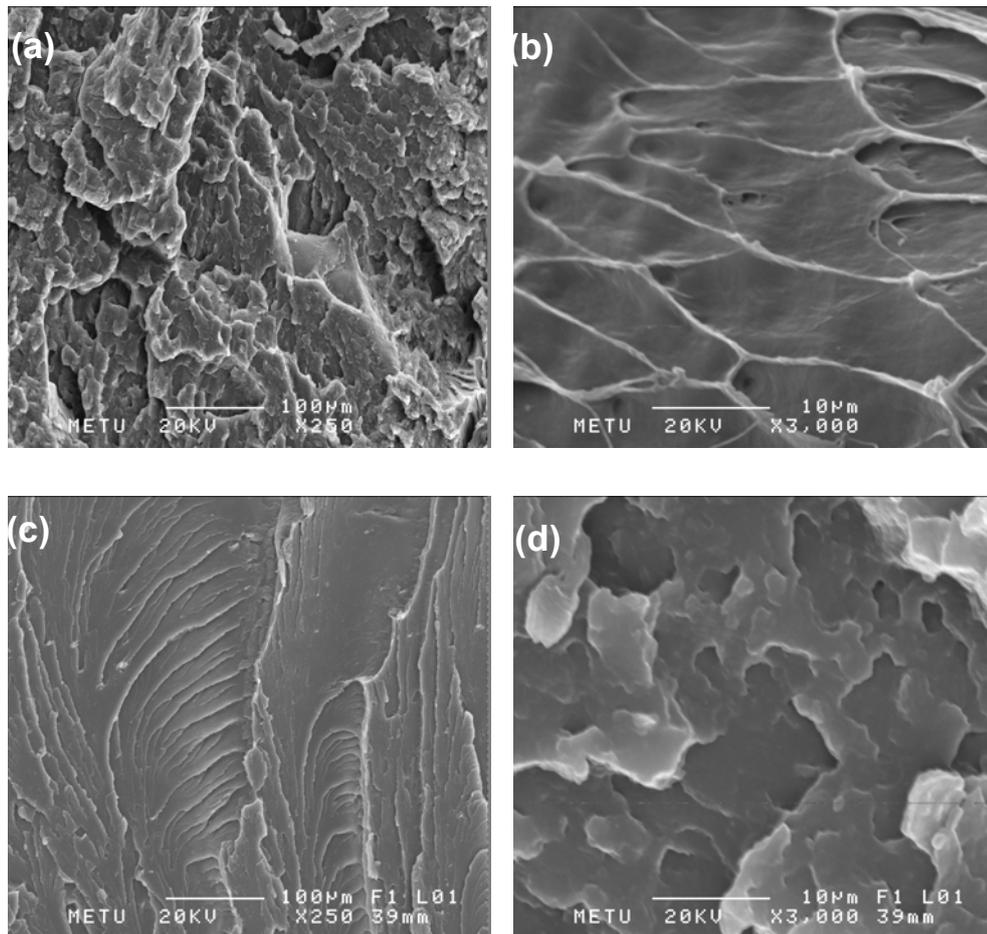
Figure 4.16 SEM micrographs of nanocomposites produced with different addition order sequences, containing 2 wt. % Cloisite® 30B and 5 wt. % Lotader® 2210 ; (a) AO3 x250, (b) AO3 x3000 ; (c) AO4 x250, (d) AO4 x3000.

4.2 Thermal Characterization

4.2.1 Differential Scanning Calorimetry (DSC) Analysis

To investigate the effect of the organoclay and compatibilizer on the thermal properties of nanocomposites in terms of melting temperature and crystallization, DSC analysis were performed. The results are presented in Table 4.3 and DSC diagrams are given in Appendix B.

The glass transition temperature of the LDPE and the compatibilizers are below the room temperature so it was not detected by DSC analysis. The melting points of compatibilizers E-MA-GMA, E-GMA, and E-nBA-MAH are, 60° C, 105° C, and 107° C respectively.

It is seen in Table 4.3 that there are no significant changes in melting point and % crystallinity of samples. The variation of melting point is only 1-2 ℃ suggesting that the addition of organoclay and compatibilizer does not influence the melting behavior of the compositions.

As far as the crystallization behavior of the samples, DSC results have not shown any remarkable differences between the samples as seen in Table 4.3. Since there is no change in crystallinity, it is concluded that, both compatibilizers and organoclays have no nucleation activity in LDPE.

Table 4.3 DSC analysis results of samples

Composition	ΔH(J/g)	LDPE wt %	% crystallinity	Tm (℃)
LDPE	79.47	100	0.27	112.18
LDPE+15A*	79.65	98	0.28	111.71
LDPE+25A*	79.05	98	0.28	111.86
LDPE+30B*	83.46	98	0.29	112.43
LDPE+8900**	83.24	95	0.30	110.88
LDPE+8840**	80.25	95	0.29	111.20
LDPE+2210**	80.76	95	0.29	110.81
LDPE+8900+15A***	73.13	93	0.27	112.11
LDPE+8840+15A***	75.02	93	0.28	114.47
LDPE+2210+30B***	79.17	93	0.29	111.33

*   organoclay concentration is 2 wt %.

**   compatibilizer concentration is 5 w %.

*** organoclay concentration is 2 wt % & compatibilizer concentration is 5 wt%.

4.3 Mechanical Analysis

In order to investigate the effects of the compatibilizer type, organoclay type, concentration of materials and addition order of materials on the mechanical properties of the produced nanocomposites, tensile and flexural tests were performed using injection molded specimens.

4.3.1 Tensile Properties

Stress – strain curves provide information about the response of the materials to applied stress during the tensile tests. In this study mechanical behavior of the binary compositions was also determined to be able to examine the effect of the third component added to the system.

Figure 4.17 and 4.18 represent the stress-strain curves of pure LDPE and LDPE/organoclay nanocomposites. As it is seen from the Figure 4.17 the virgin LDPE is very ductile at a test rate of 8mm/min. The area under the curve is the measure of the energy necessary to break the material. Addition of the organoclay to the virgin LDPE makes it more brittle and decreases the energy required to break it. Moreover, the decrease in the ultimate strain due to the increase in the clay content is clearly observed from the Figure 4.17. So with increasing clay content the ductility decreases gradually. For example, addition of only 2 wt % of Cloisite 30B resulted in decrease of the ultimate strain from 40 % to 20 % is observed in Figure 4.18.

Stress-strain curves of LDPE/compatibilizer blends and ternary nanocomposites of LDPE/compatibilizer/organoclay are given in Figures 4.19 through 4.24. Considering the blends, increase in compatibilizer concentration results in lower ultimate stress and toughness for blends containing E-MA-GMA, and E-GMA. On the other hand there was no a straight forward trend for blends containing the E-nBA-MAH. According to Figures 4.22, 4.23 and 4.24, it was concluded that compatibilizer not only favors the opening the platelets of the organoclay, and good adhesion to LDPE, but it also toughens the polymer matrix.

Effect of addition order on stress-strain behavior of the nanocomposites is shown in Figure 4.25. In comparison to the neat LDPE, AO1 (CoC)P, and AO3 (PCo)C, have shown almost the same response in tensile test. On the other hand AO2 (PC)Co, and AO4 (PCoC), showed improvement in toughness, and ultimate stress of the material.
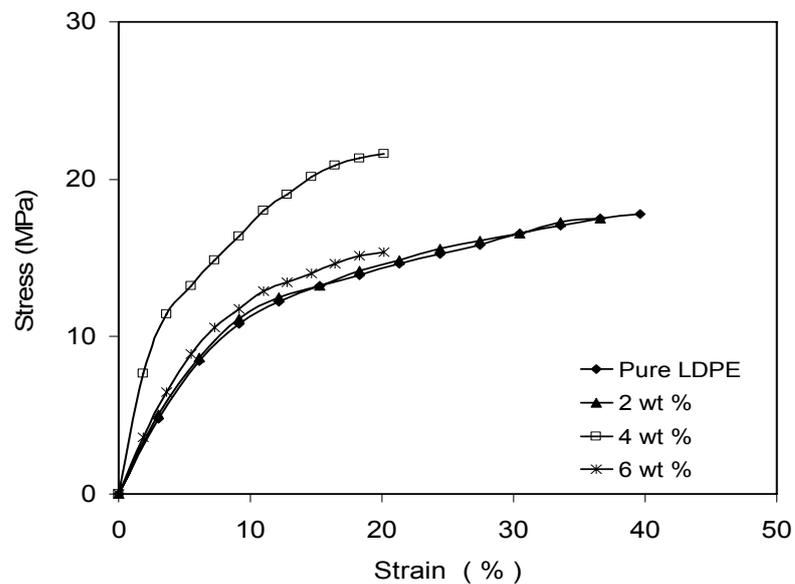
Figure 4.17 The stress-strain curves of LDPE/organoclay nanocomposites with different Cloisite® 15A content.
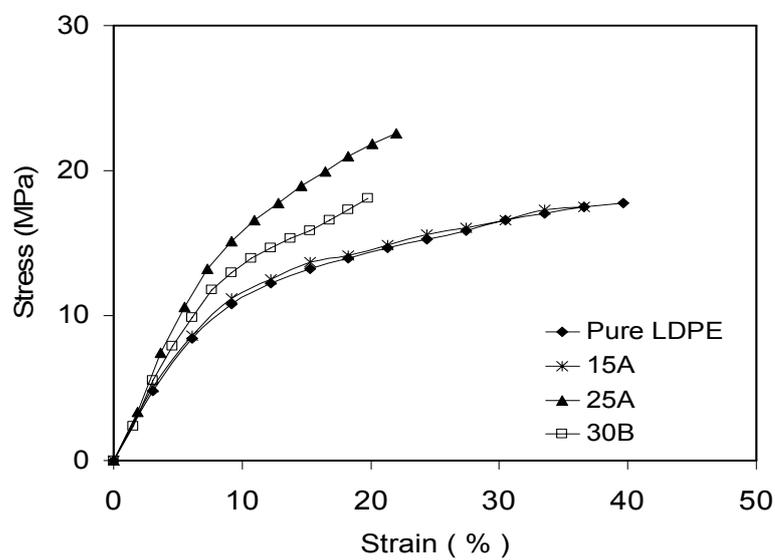
Figure 4.18 The stress-strain curves of LDPE/organoclay nanocomposites containing 2 wt % of different organoclay types.
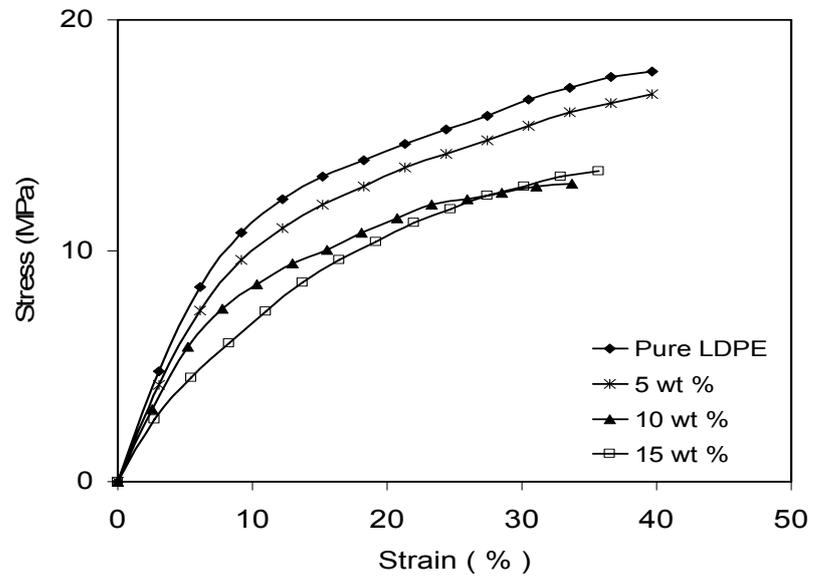
Figure 4.19 The stress-strain curves of LDPE/compatibilizer blends containing different amounts of E-MA-GMA.
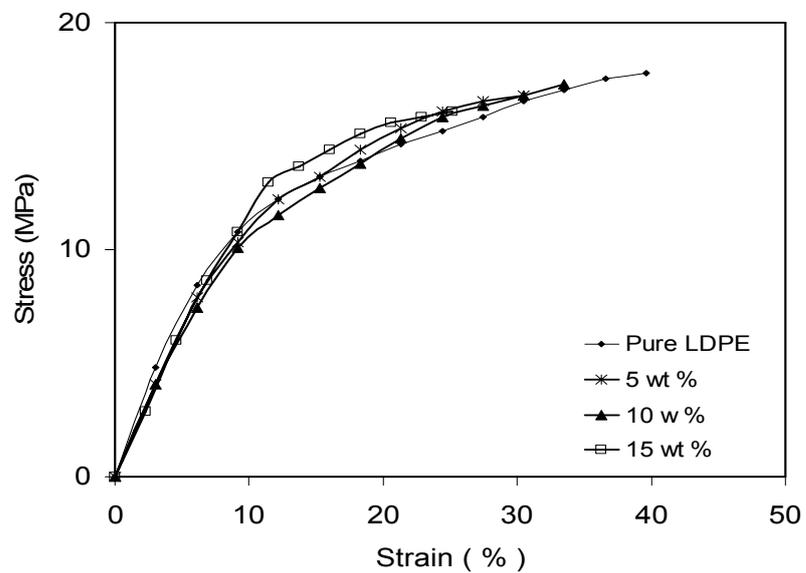
Figure 4.20 The stress-strain curves of LDPE/compatibilizer blends containing different amounts of E-GMA.
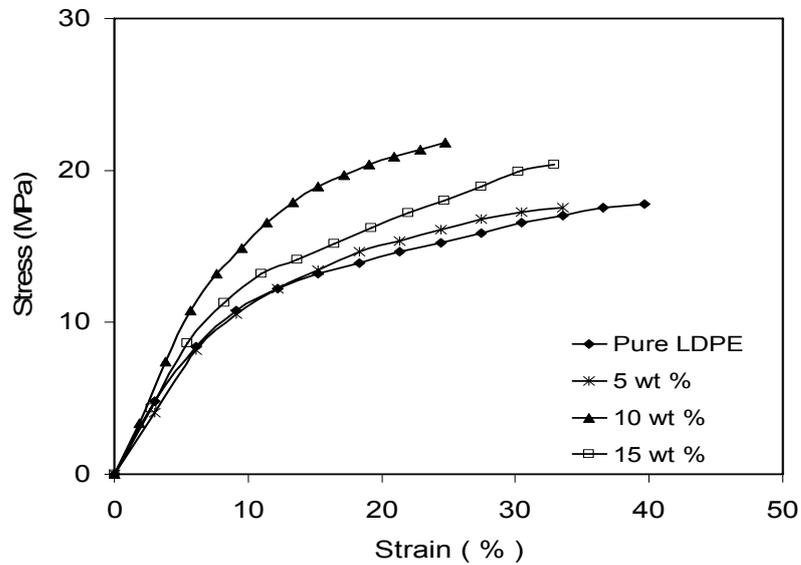
Figure 4.21 The stress-strain curves of LDPE/compatibilizer blends containing different amounts of E-nBA-MAH.
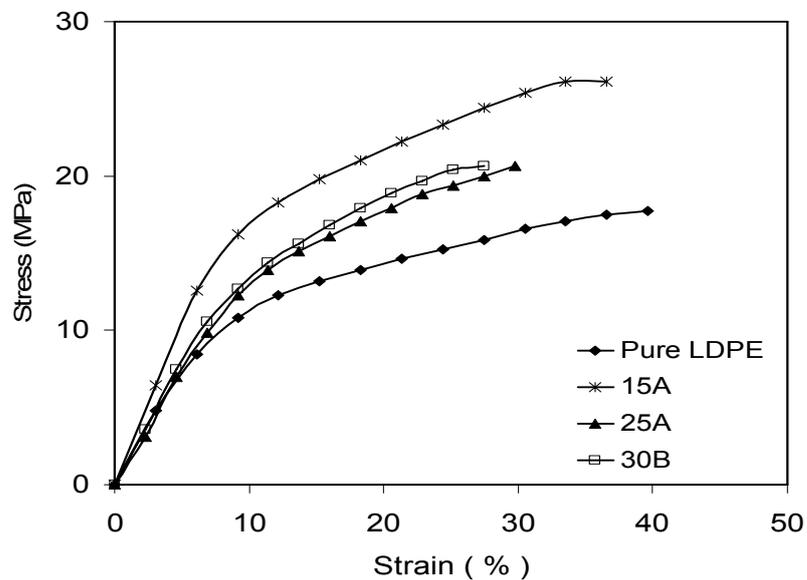
Figure 4.22 The stress-strain curves of LDPE / E-MA-GMA / organoclay nanocomposites containing 5 wt % of E-MA-GMA and 2 wt % of organoclay.
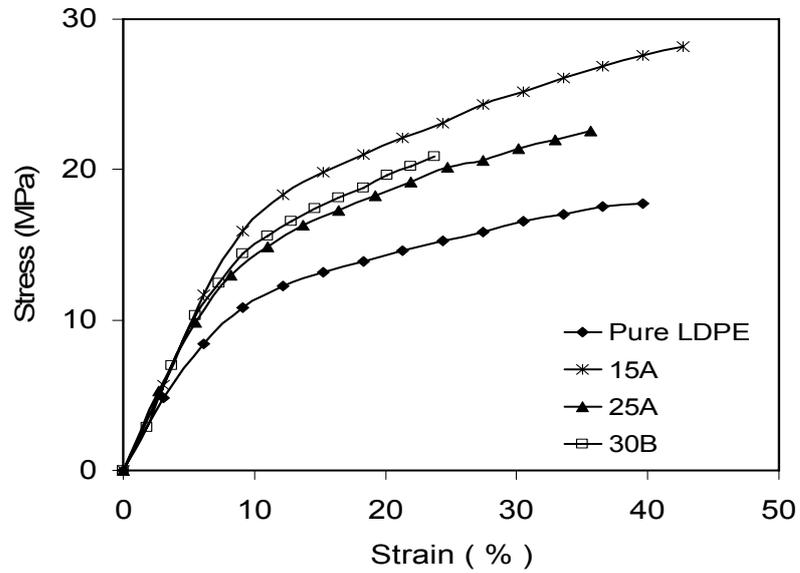
Figure 4.23 The stress-strain curves of LDPE / E- GMA / organoclay nanocomposites containing 5 wt % of E-GMA and 2 wt % of organoclay.
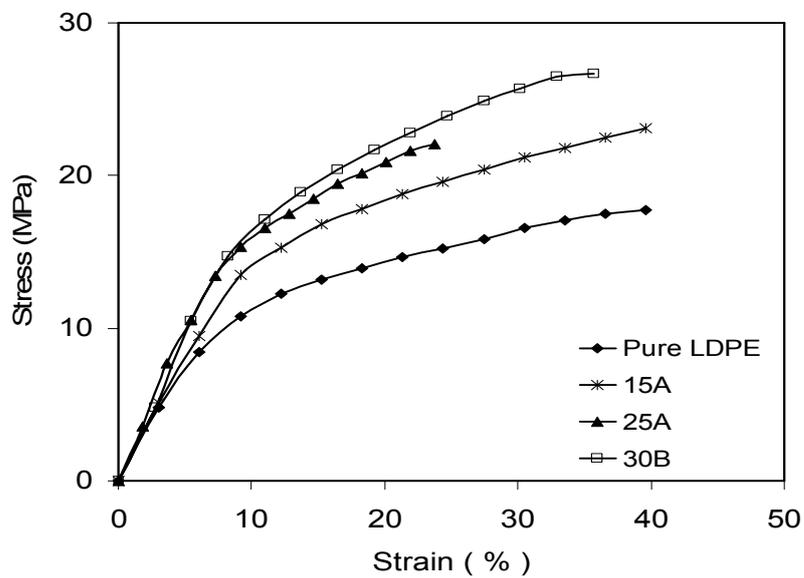
Figure   4.24   The   stress-strain   curves   of   LDPE/E-nBA-MAH/organoclay nanocomposites containing 5 wt % of E-nBA-MAH and 2 wt % of organoclay.
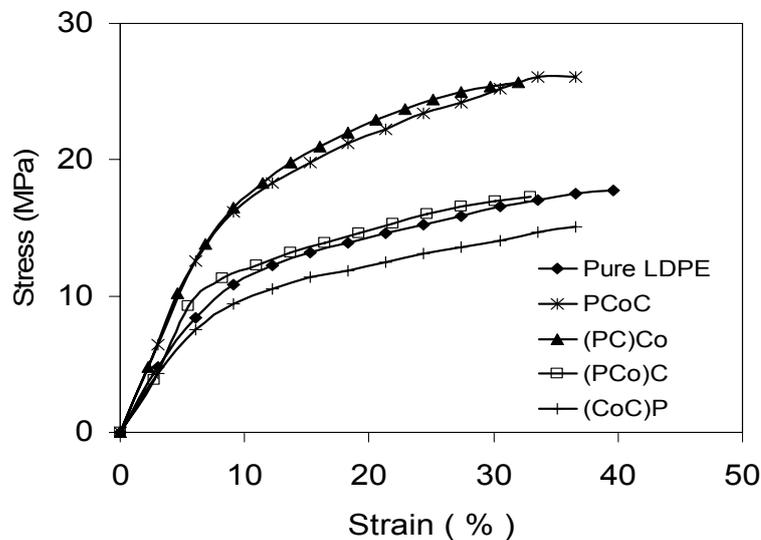
Figure 4.25 The stress-strain curves of LDPE/E-MA-GMA/15A nanocomposites produced with different addition order sequence, and containing 5 wt % E-MA-GMA, 2 wt % 15A.

The tensile strength, tensile modulus and tensile strain at break values of neat extruded LDPE were determined as 18.2 MPa, 162.6 MPa and 39.7 % respectively. The strength and modulus values are consistent with the values reported in the literature, on the other hand, measured elongation at break values are highly below the range given as 90-400 % [19]. This can be due to the high molecular weight of the LDPE used which is also supported by the very low melt flow index value of this LDPE.

The tensile properties including tensile strength, tensile modulus and tensile strain at break (%) of all binary and ternary mixtures prepared in this study are evaluated and the data are presented in Figures 4.26 through 4.43. The results are also given in Appendix C.

Figure 4.26, 4.27, and 4.28 show the effect of organoclay content on tensile properties of LDPE/15A nanocomposites. It is seen that tensile strength and tensile modulus of material increased to 19.7 MPa, and 233.2 MPa with 4 wt % of organoclay concentration. However addition of 6 wt % organoclay resulted in dramatic decrease of

both tensile strength and tensile modulus of the material. This indicates that agglomerates of organoclay did not break during the melt blending and surface interaction of polymer matrix and organoclay decreased at 6 wt % clay content. Moreover, the agglomerates act as stress concentrators. Addition of organoclay greater than 2 wt %, leads to significant decrease of the tensile strain at break value.

As seen in Figure 4.29, for the LDPE/organoclay nanocomposites, addition of 2 wt % of 15A and 30B slightly decreased the tensile strength of LDPE. This is attributed to relatively weak interaction between the polymer matrix and silicate layers. However in the case of adding 25A, tensile strength increased from 18.2 MPa to 21.5 MPa which indicates a better dispersion in comparison to the other clay types. Tensile modulus of nanocomposites containing only 2 wt % organoclay increased when compared to neat resin as shown in Figure 4.30. As in the case of in tensile strength results LDPE/25A nanocomposites possess the highest strength with an increase of 25 %. These results are also supported by the XRD results which claim the high level of intercalation of the LDPE/25A nanocomposite.

Figure 4.31 shows the tensile strain at break values of 2 wt % clay loaded LDPE/organoclay nanocomposites. There is no remarkable change in nanocomposites containing 15A. On the other hand lower tensile strain at break values are observed for the nanocomposites containing 25A and 30B indicating lower deformation of the samples.
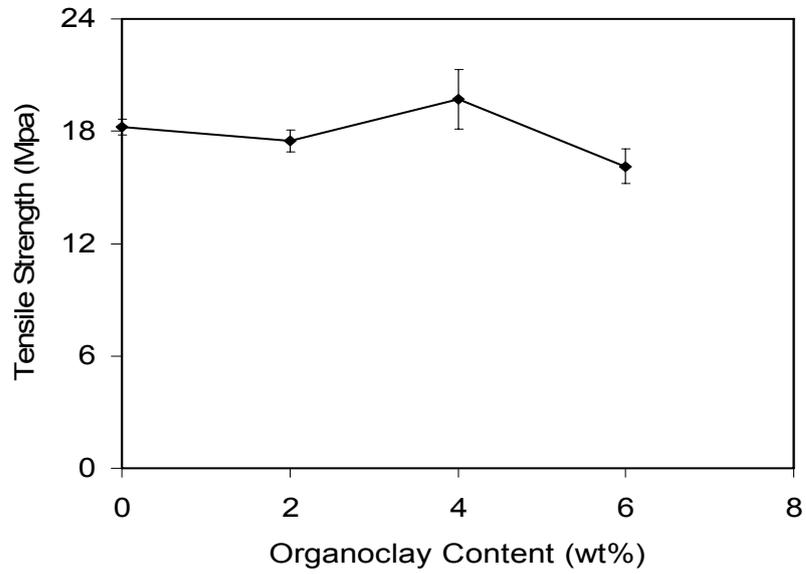
Figure 4.26 Effect of organoclay content on tensile strength of LDPE/15A nanocomposites.
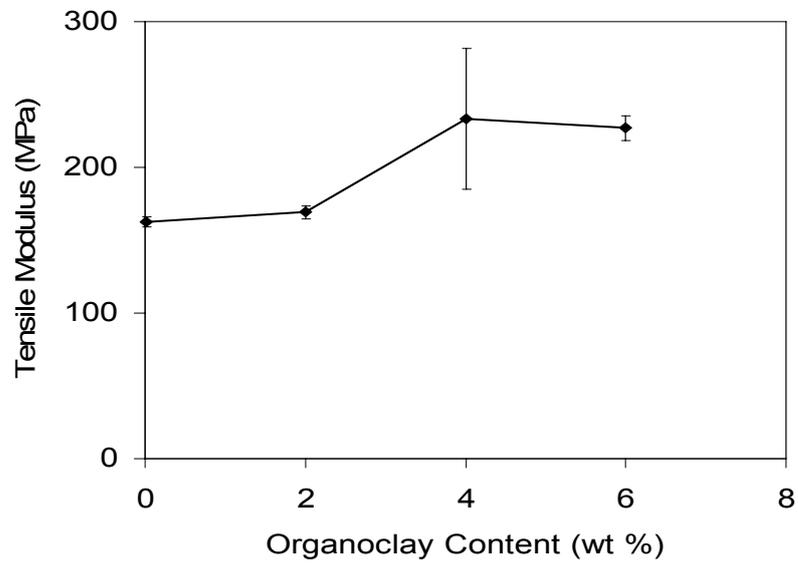
Figure 4.27 Effect of organoclay content on tensile modulus of LDPE/15A nanocomposites.
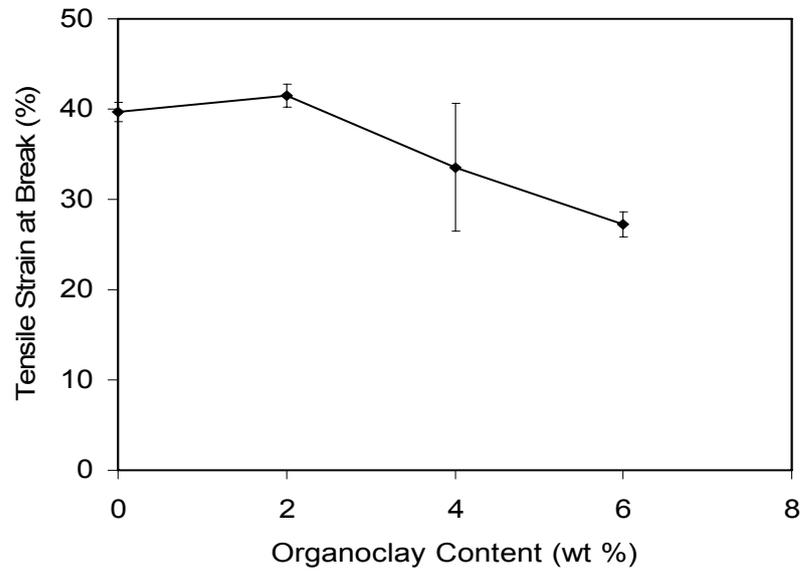
Figure 4.28 Effect of organoclay content on tensile strain at break values of LDPE/15A nanocomposites.
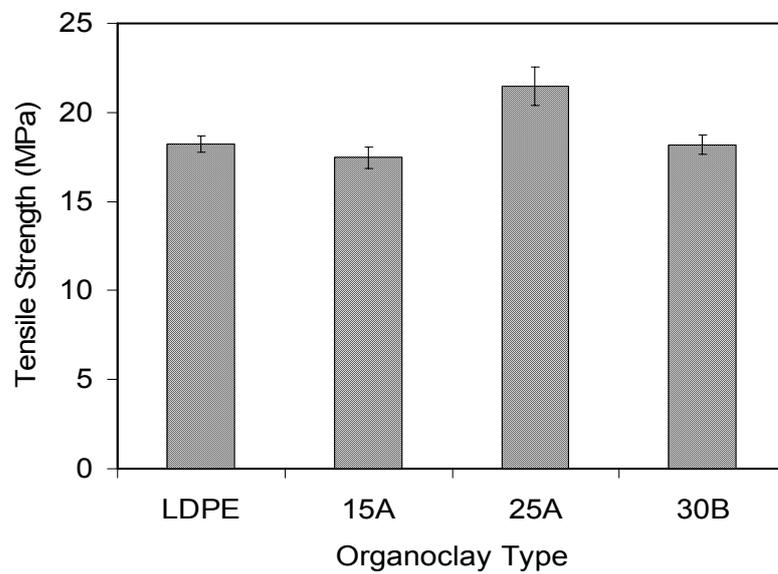
Figure 4.29 Tensile strength of LDPE/organoclay nanocomposites, containing 2 wt % organoclay.
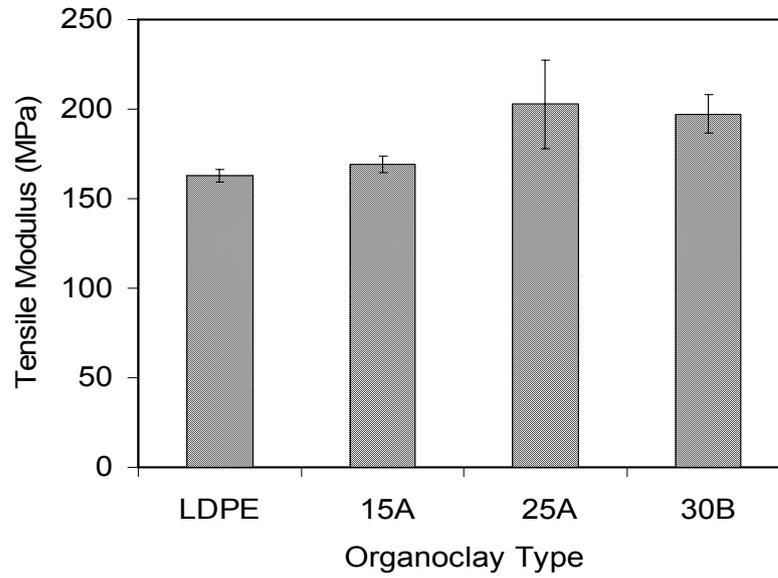
Figure 4.30 Tensile modulus of LDPE/organoclay nanocomposites, containing 2 wt % organoclay.
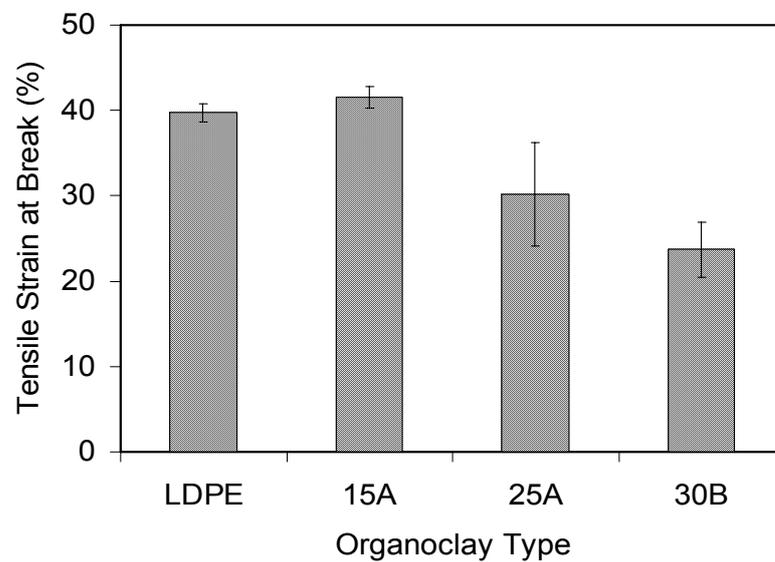
Figure 4.31 Tensile strain at break values of LDPE/organoclay nanocomposites , containing 2 wt % organoclay.

Tensile strength, tensile modulus and elongation at break values of LDPE/compatibilizer blends are shown as a function of compatibilizer content in Figures 4.32, 4.33, and 4.34. According to technical data sheet reported by the producer, tensile strength values of E-MA-GMA, E-GMA, and E-nBA-MAH are 4 MPa, 8 MPa and 12 MPa, respectively. For blends containing E-MA-GMA, increase in compatibilizer content resulted in decrease in both tensile strength and tensile modulus. On the other hand, for other compatibilizer types, at 10 wt % loading, both tensile strength and tensile modulus values increased. The maximum tensile strength and tensile modulus values were 21.6 MPa, and 221.4 at 10 wt % loading of E-nBA-MAH. However additional loading of compatibilizer caused remarkable decreases. In addition to these, Figure 4.34 shows that, at 10 wt % loading of compatibilizer, deformation of blends are much lower when compared with the neat resin and 5 wt % loading. The lowest tensile strain at break value is observed as 27.9 % at 10 % of E-nBA-MAH loading.
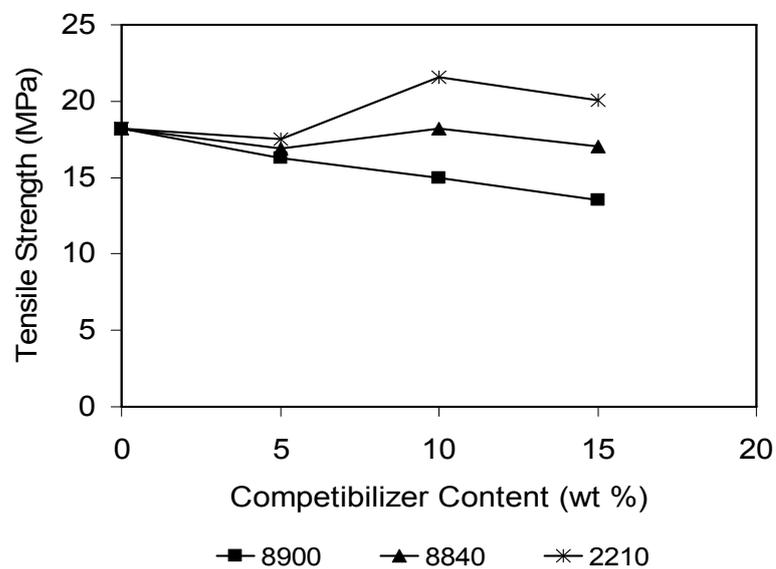
Figure 4.32 Effect of compatibilizer content on tensile strength of LDPE/compatibilizer blends.
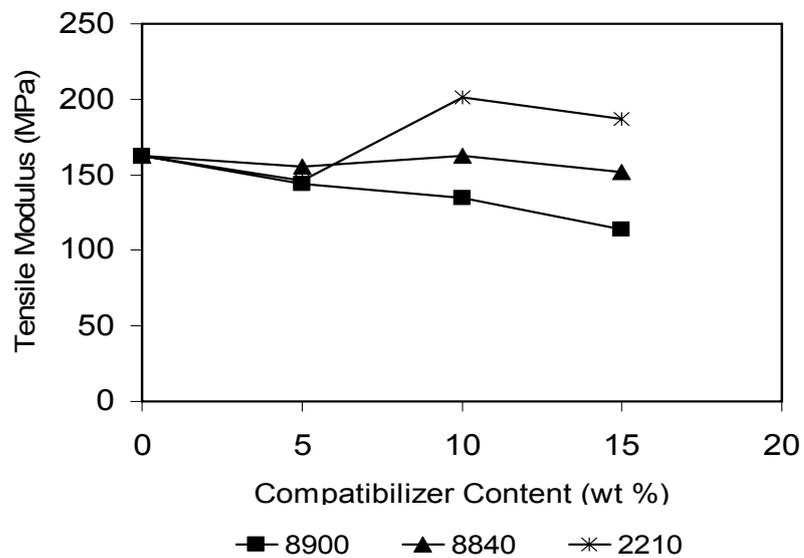
Figure 4.33 Effect of compatibilizer content on tensile modulus of LDPE/compatibilizer blends.
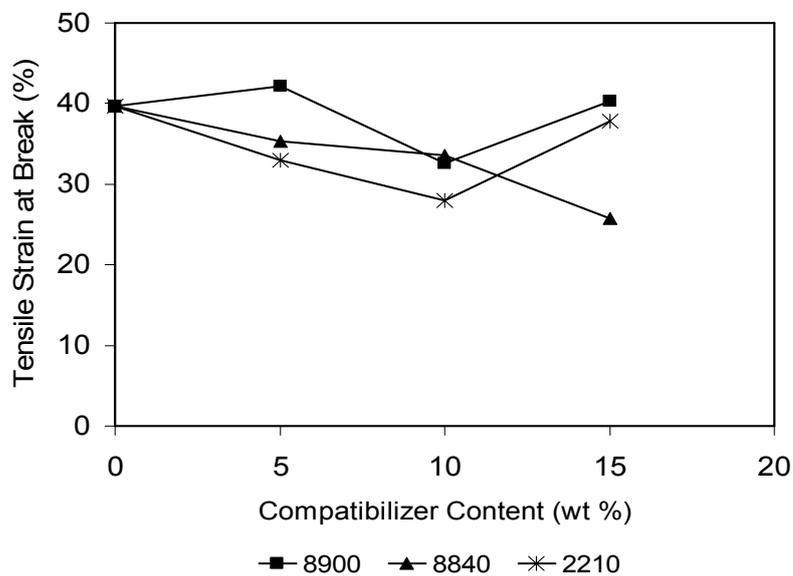
Figure 4.34 Effect of compatibilizer content on tensile strain at break values of LDPE/compatibilizer blends.

The tensile properties of the 2 wt % of organoclay and 5 wt % of compatibilizer loaded polymer/layered silicate nanocomposites are observed in Figures 4.35, 4.36, and 4.37. In the figures, the first and second bars belong to the neat LDPE and LDPE/compatibilizer blends with a 5 wt % loading. It is seen that with a 5 wt % loading of compatibilizer, the tensile strength and tensile modulus values of the virgin LDPE decreases since the compatibilizers have lower tensile strength and tensile modulus.

The tensile strength results of ternary nanocomposites prepared with AO4 sequence, containing different compatibilizer and organoclay types are shown in Figure 4.35. In thermoplastic-based nanocomposites (intercalated or exfoliated) the stress at break value expresses the ultimate strength that the material can bear before break, and varies strongly depending on the nature of the interactions between the polymer matrix and the filler [2]. Usually rigid particulate fillers decrease the tensile strength of a material, unless good adhesion is attained at the interface [55]. In Figure 4.35 remarkably improved tensile strength values are easily observed for ternary nanocomposites which are the result of the well dispersion of the silicate layers throughout the LDPE matrix.

It is clearly seen in Figure 4.36 that the tensile modulus, expressing the stiffness of the material at the start of a tensile test, has shown to be strongly improved when ternary nanocomposites are formed. The extent of the improvement of the modulus depends directly upon the average length of dispersed clay particles. Thus the main reason for the drastic improvement in tensile modulus in LDPE nanocomposites is the strong interaction between the well dispersed silicate layers and the matrix via formation of the hydrogen bonds between the functional groups of compatibilizers and the hydroxyl groups of organoclay [31]. In other words, the possible reactions between the functional groups of compatibilizers (GMA, MAH), and the groups on the organoclay surface (OH⁻), increase the adhesion of the polymer matrix and the organoclay. Due to this improvement, the stresses are much more effectively transferred from polymer matrix to the inorganic filler, and thus a higher increase in tensile modulus is expected [32].

When compared with the tensile strength and tensile modulus of LDPE/organoclay nanocomposites, ternary LDPE/compatibilizer/organoclay nanocomposites are characterized by larger strength and modulus increases for the same clay loading. These results are expected based on the morphological analysis results described earlier. All of these nanocomposites are either intercalated or exfoliated.

Among the ternary LDPE/E-MA-GMA/organoclay nanocomposites, the maximum increase in tensile strength and tensile modulus values were observed for the ones prepared with organoclay 15A. The improvement with respect to neat LDPE was 43 % for tensile strength and 44 % for tensile modulus. In the nanocomposites containing E-GMA, although each organoclay type showed improvement in mechanical properties, the highest improvement was achieved with the addition of 15A with 53 % increase in tensile strength and 54 % increase in tensile modulus. Lastly, in LDPE/E-nBA-MAH/organoclay nanocomposites, the highest improvement was achieved with 30B. The tensile strength and tensile modulus of the material was increased by 44 % and 72 % respectively. The striking increase in modulus of LDPE/E-nBA-MAH/30B nanocomposite could be due to the increased reaction possibility owing to the additional hydroxyl groups of organic modifier of 30B and strong interaction between the polar compatibilizer and silicate layers. In addition to these, XRD analysis results also support that better dispersion was achieved with nanocomposites containing 30B with the highest basal spacing values.

With an increase of 9.6 % in tensile strength and 11 % increase in tensile modulus the lowest improvement was observed for LDPE/E-MA-GMA/25A nanocomposites. When comparing with LDPE/E-MA-GMA/15A nanocomposites, 15A contains two long alkyl chains instead of one, which enhances the increase of the basal spacing of the layered silicates.

Figure 4.37 shows the tensile strain at break values of LDPE/compatibilizer/organoclay nanocomposites. It is observed that for the nanocomposites that have the best tensile strength and tensile modulus values, there is no a significant change in the tensile strain at break values. It is possible to say that the mechanical improvement was

achieved with suitable compositions of nanocomposites, as explained in the previous paragraphs.
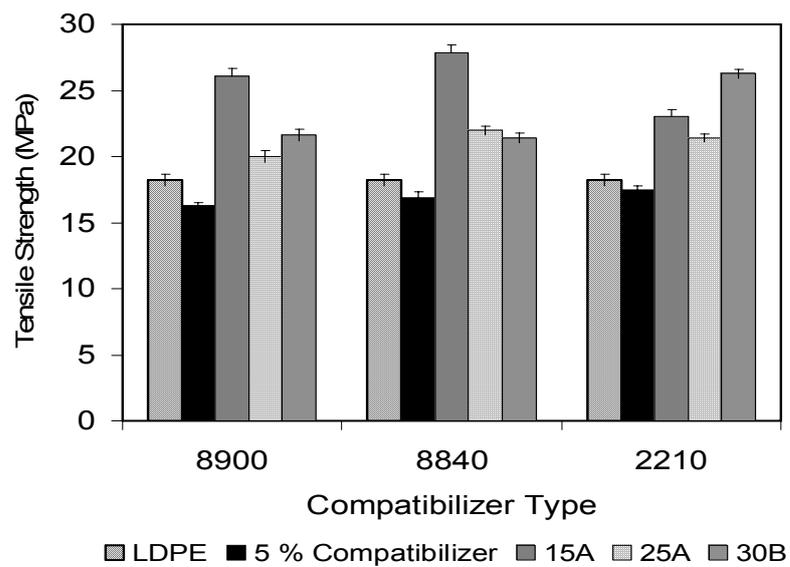
Figure 4.35 Tensile strength values of ternary LDPE/compatibilizer/organoclay nanocomposites.
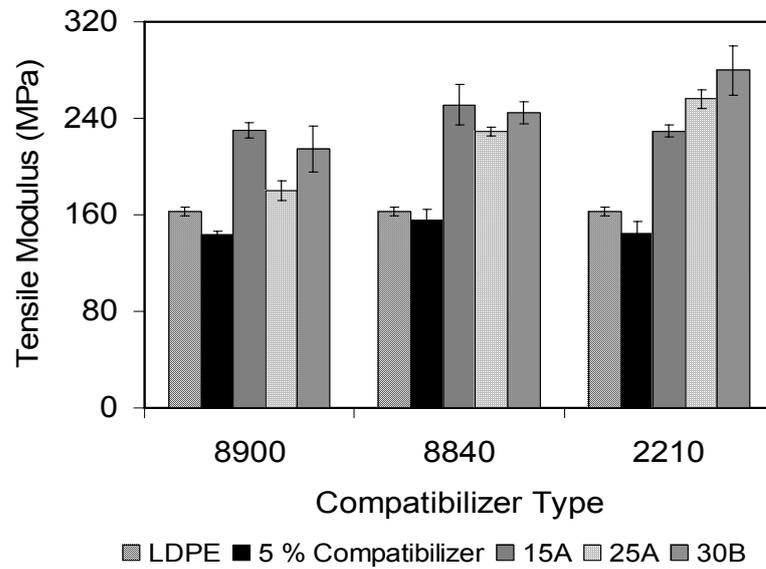
Figure 4.36 Tensile modulus values of ternary LDPE/compatibilizer/organoclay nanocomposites.
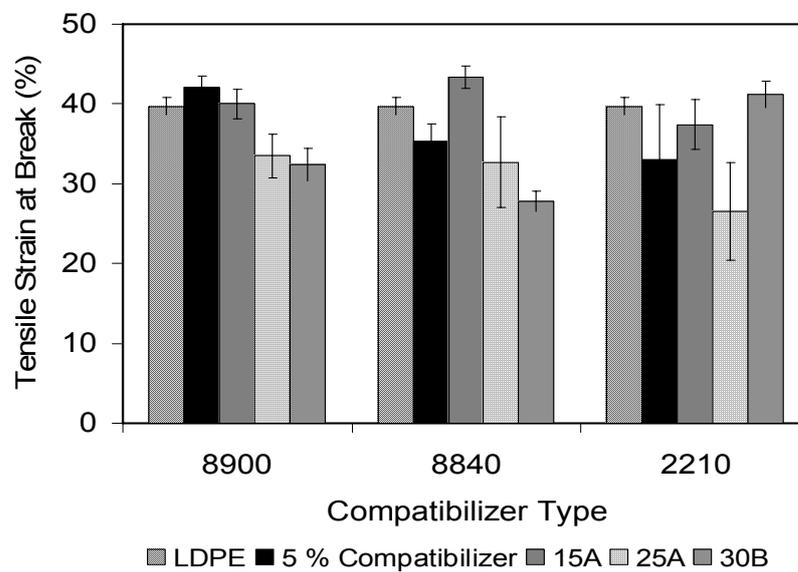
Figure 4.37 Tensile strain at break values of ternary LDPE/compatibilizer/organoclay nanocomposites.

In order to investigate the effect of addition order on mechanical properties of nanocomposites, three different compositions were prepared; LDPE/E-MA-GMA/15A (93+5+2 wt %), LDPE/E-MA-GMA/15A (88+10+2 wt %), and LDPE/E-nBA-MAH/30B (93+5+2 wt %). Figures 4.38 through 4.46 show the tensile properties of these nanocomposites. In order to distinguish the effect of addition order on properties, the tensile values of neat LDPE, LDPE/organoclay, and LDPE/compatibilizer blends are also given with the values of ternary nanocomposites on the same figures.

In this study four different addition order sequences were performed to obtain the ternary nanocomposites. They can be summarized as:

AO1: (CoC)P
AO2: (PC)Co
AO3: (PCo)C
AO4: (PCOC)

where P, Co, and C refer to LDPE, compatibilizer, and organoclay respectively. The parenthesis denotes the first run of extrusion. In the second run of extrusion process the third material was added to the system.
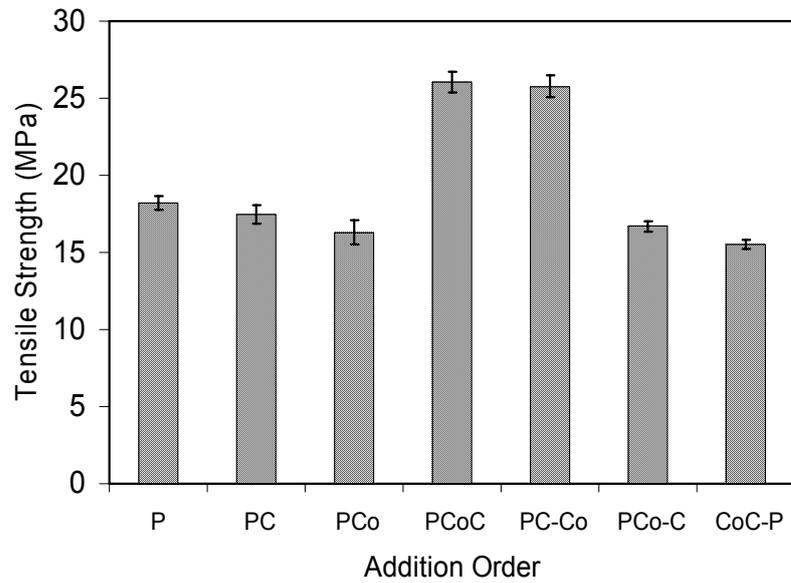
Figure 4.38 Effect of addition order on tensile strength of LDPE/ E-MA-GMA /15A nanocomposites containing 5 wt % compatibilizer and 2 wt % organoclay.
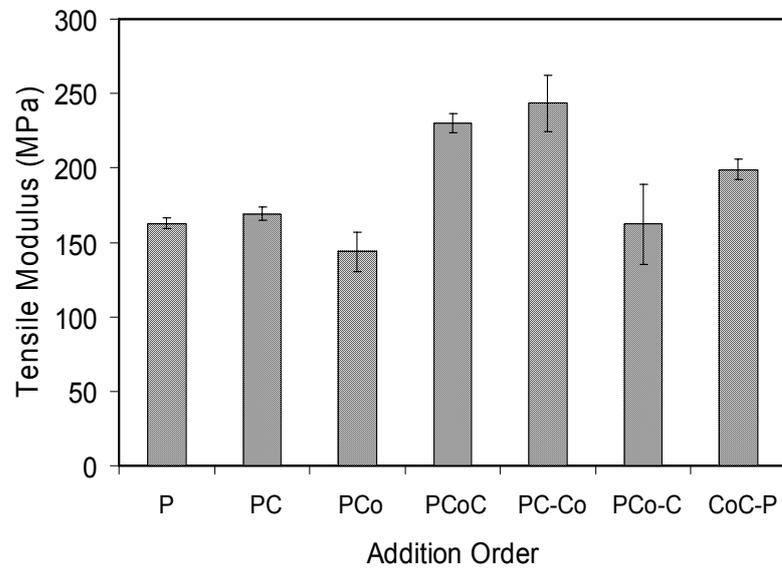
Figure 4.39 Effect of addition order on tensile modulus of LDPE/ E-MA-GMA /15A nanocomposites containing 5 wt % compatibilizer and 2 wt % organoclay.
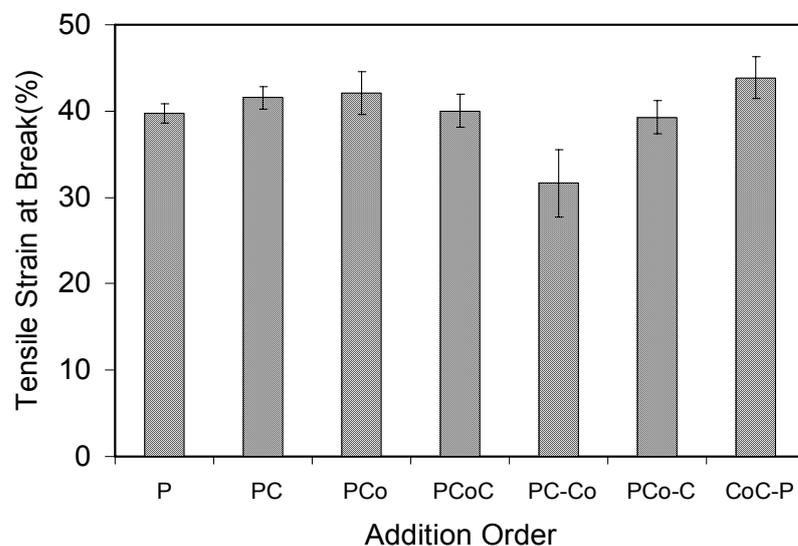
Figure 4.40 Effect of addition order on tensile strain at break value of LDPE/ E-MA-GMA /15A nanocomposites containing 5 wt % compatibilizer and 2 wt % organoclay.
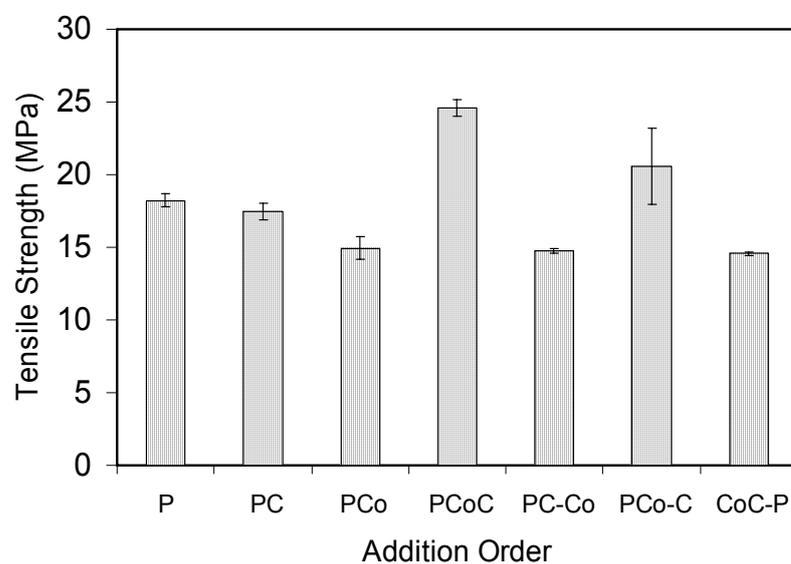
Figure 4.41 Effect of addition order on tensile strength of LDPE/ E-MA-GMA /15A nanocomposites containing 10 wt % compatibilizer and 2 wt % organoclay.
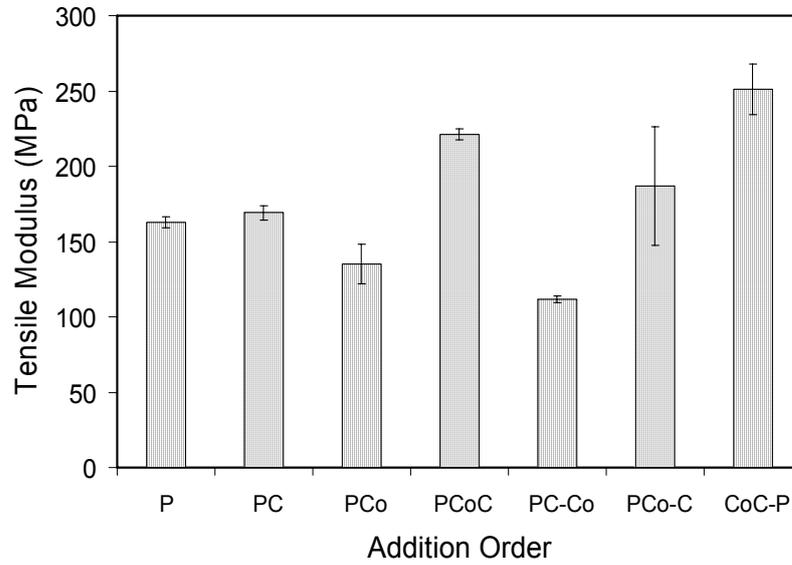
Figure 4.42 Effect of addition order on tensile modulus of LDPE/ E-MA-GMA /15A nanocomposites containing 10 wt % compatibilizer and 2 wt % organoclay.
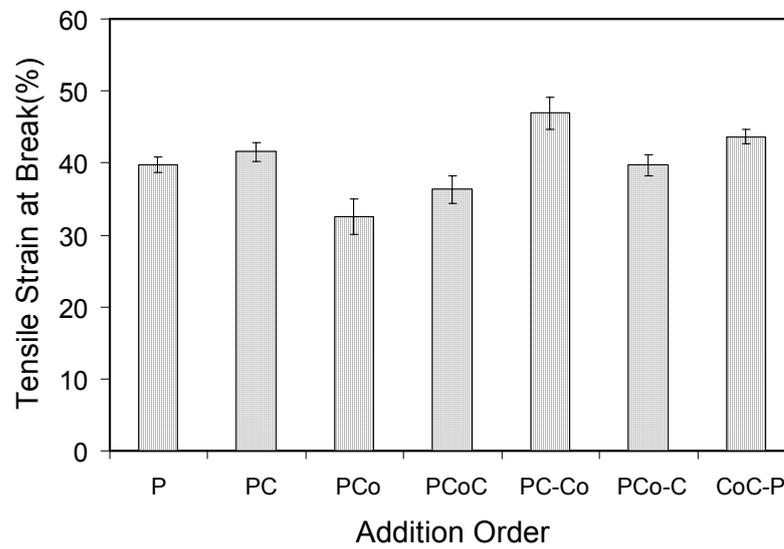
Figure 4.43 Effect of addition order on tensile strain at break value of LDPE/ E-MA-GMA /15A nanocomposites containing 10 wt % compatibilizer and 2 wt % organoclay.
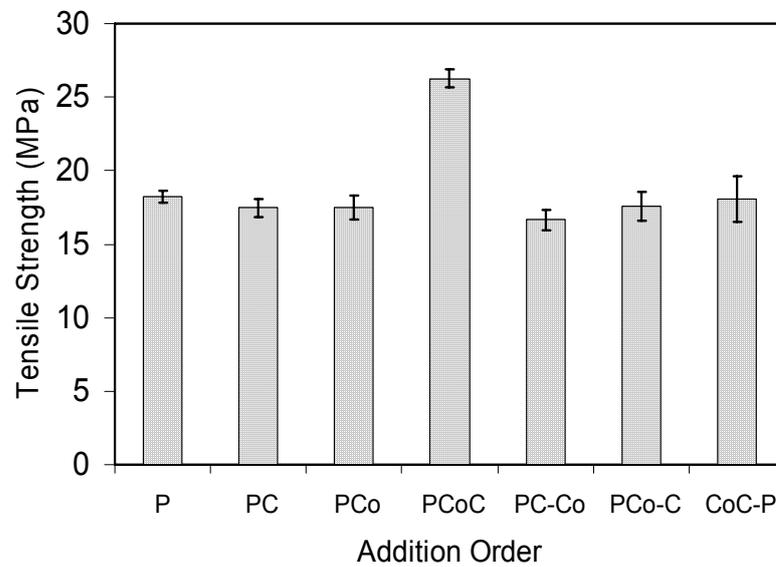
Figure 4.44 Effect of addition order on tensile strength of LDPE/ E-nBA-MAH/30B nanocomposites containing 5 wt % compatibilizer and 2 wt % organoclay.
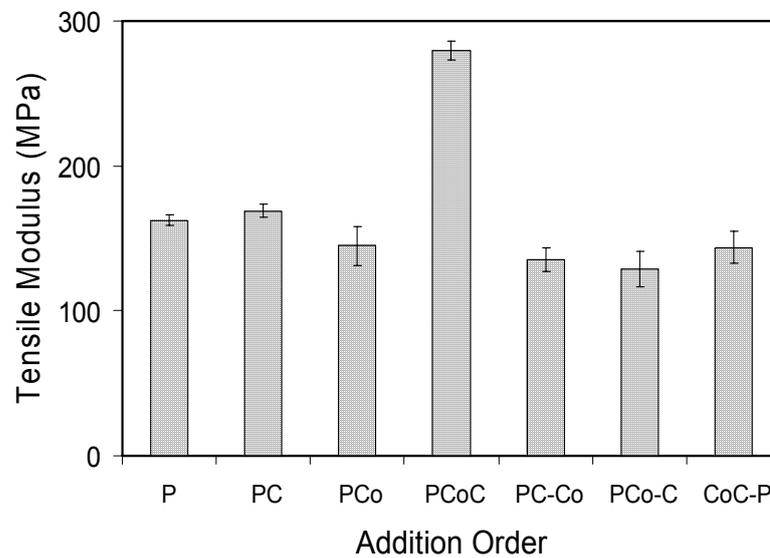
Figure 4.45 Effect of addition order on tensile modulus of LDPE/ E-nBA-MAH/30B nanocomposites containing 5 wt % compatibilizer and 2 wt % organoclay.
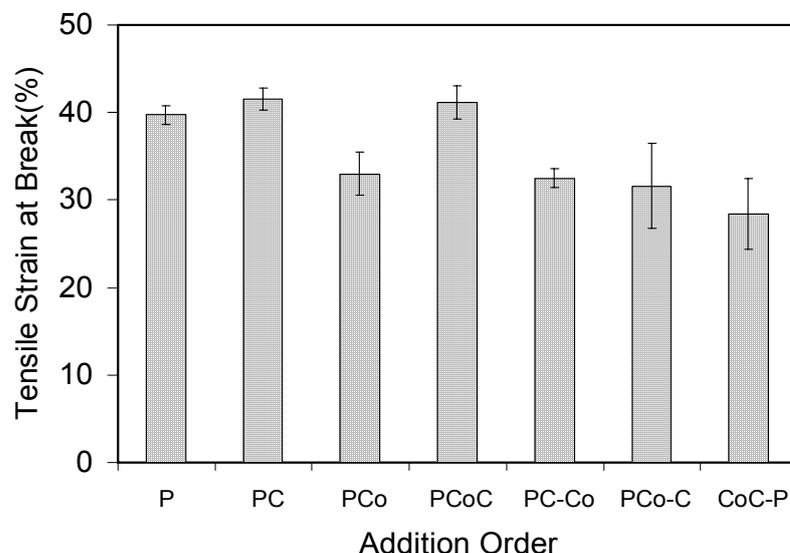
Figure 4.46 Effect of addition order on tensile strain at break value of LDPE/ E-nBA-MAH/30B nanocomposites containing 5 wt % compatibilizer and 2 wt % organoclay.

Based on the tensile properties, PCoC (AO4) mixing order, is seem to be the best addition sequence in which all the materials were fed to the extruder in the first run. In general, these nanocomposites showed the highest improvement in tensile strength and tensile modulus when compared to nanocomposites prepared with other addition order sequences. In addition to these, elongation behavior of these nanocomposites was not poor which is an evidence of better dispersion of the silicate layers in the polymer matrix. In the case of AO1 mixing order, compatibilizer and the organoclay were mixed in the first run of extrusion process. Since viscosity of the compatibilizer is much lower than the LDPE, it can be said that in the first run, compatibilizer was unable to apply additional shear to organoclay to disperse them and so the intercalation of compatibilizer into the clay galleries did not occur and this caused a decrease in the reaction possibility with the organoclay. In the AO2 mixing order, organoclay and LDPE were mixed in the first run and compatibilizer was added to this mixture in the second run. In this case, it was possible to provide additional shear by highly viscous polymer matrix which enhanced the dispersion of clay, but this may hinder the possible reactions of functional groups of compatibilizer with organoclay

since polymer initially surrounded the organoclay. For AO3, LDPE and compatibilizer were compounded in the first run and then organoclay was added. In this addition order sequence, the organoclay was subjected to the extrusion process only once so shear was applied to the organoclay to open the platelets once. This shear was not sufficient to open the organoclay layers enough and so lower interaction of the clay layers and polymer matrix occurred. This may be the cause of the lower tensile properties in comparison to the AO4 results which provided twice extrusion of the organoclay.

4.3.2 Flexural properties

Flexural properties were measured by three point loading system and results reported here are the average of at least five samples. The flexural strength and flexural modulus of all samples are given in Figures 4.47 through 4. 60.

The flexural test involves both tension and compression of the specimen. Due to the nature of the flexural test, higher values of flexural strength and modulus are expected than the tensile strength and tensile modulus. However, it was observed that although the flexural modulus values are significantly higher than the tensile modulus values, flexural strength values were lower than the tensile strength for all samples. Considering the stress-strain diagrams of both tests, no yield was observed during the tensile test and stress hardening occurred until the fracture of the sample. However, no fracture was observed for the flexural tests and after a maximum value, decrease in the applied force occurred. The flexural tests were ended manually when the specimen touched the side walls of the test machine and the applied force started began to increase.

The effect of organoclay content on flexural strength is similar to tensile test results as seen in Figures 4.47 and 4.48. Increase of organoclay content increased the flexural strength values, however after a certain amount of organoclay loading, agglomerates of clay may occur and that decreased the flexural strength.

Flexural modulus can be expressed as the material's stiffness when flexed, and as in the case of the tensile modulus it highly depends on the degree of dispersion of the silicate layers in the polymer matrix. Addition of rigid clay particles generally increased the flexural modulus as seen in the Figures 4.49 and 4.50.

Figure 4.51 and 4.52 belong to flexural properties of the LDPE/compatibilizer blends. Generally, increase in organoclay content resulted in decrease in both flexural strength and modulus as expected.

Flexural properties of ternary nanocomposites are given in Figures 4.53 and 4.54. The effect of compatibilizer on dispersion of silicate layers is easily observed when comparing the flexural test results of ternary nanocomposites with binary nanocomposites as in the case of the tensile properties. The highest flexural tensile and flexural modulus values also belong to LDPE/E-MA-GMA/15A, LDPE/GMA/15A and LDPE/nBA/MAH nanocomposites owing to the factors explained in the previous section. The improvement of flexural strength and flexural modulus of these nanocomposites are; 22 % and 14.6 % for LDPE/E-MA-GMA/15A; 34.5 % and 13.6 % for LDPE/GMA/15A; and 36.6 % and 17.7 % for LDPE/nBA/MAH nanocomposites respectively.

To consider the effect of addition order of materials on flexural properties, it is seen from Figures 4.55 through 4.60, that there are remarkable differences in properties according to addition order. In general AO4 is the best among the others. The highest improvement was achieved with nanocomposites prepared with this sequence because of the factors explained in tensile properties section. Moreover, decrease in flexural properties was observed for nanocomposites prepared with other addition order sequences.
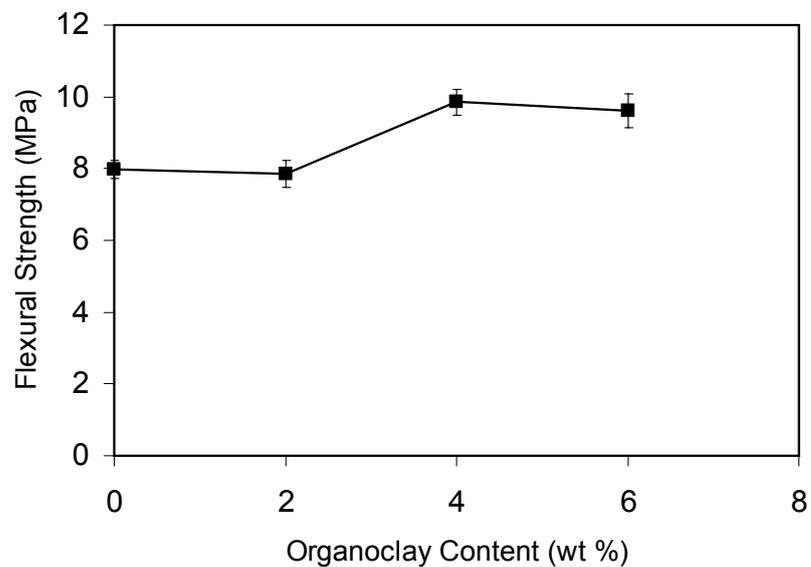
Figure 4.47 Effect of organoclay content on flexural strength of LDPE/15A nanocomposites.
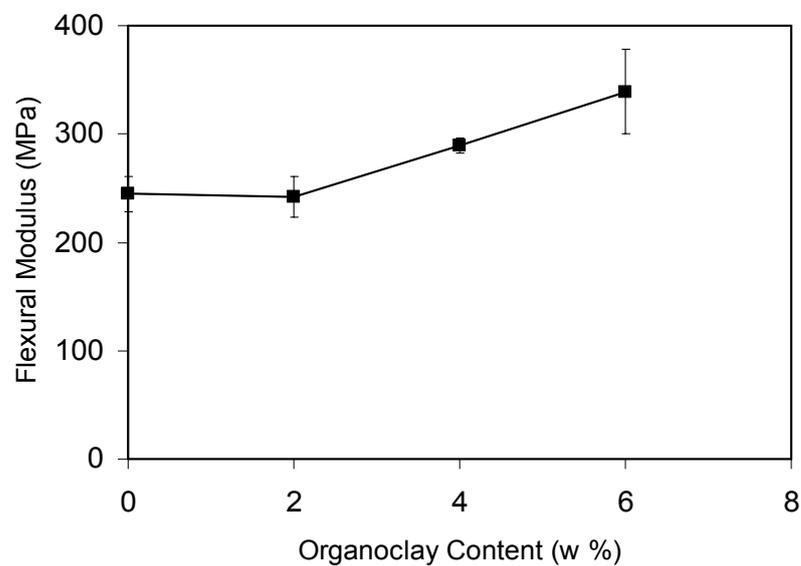
Figure 4.48 Effect of organoclay content on flexural modulus of LDPE/15A nanocomposites.
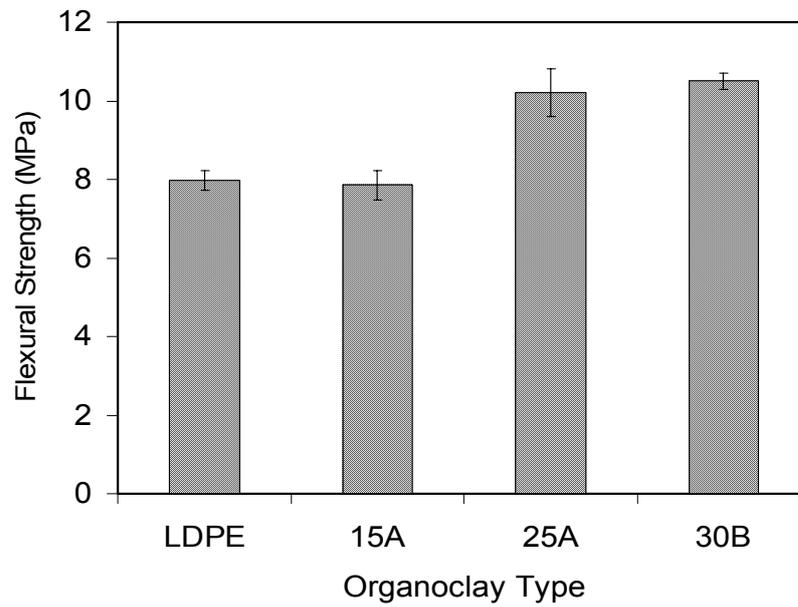
Figure 4.49 Flexural strength of LDPE/organoclay nanocomposites, containing 2 wt % organoclay.
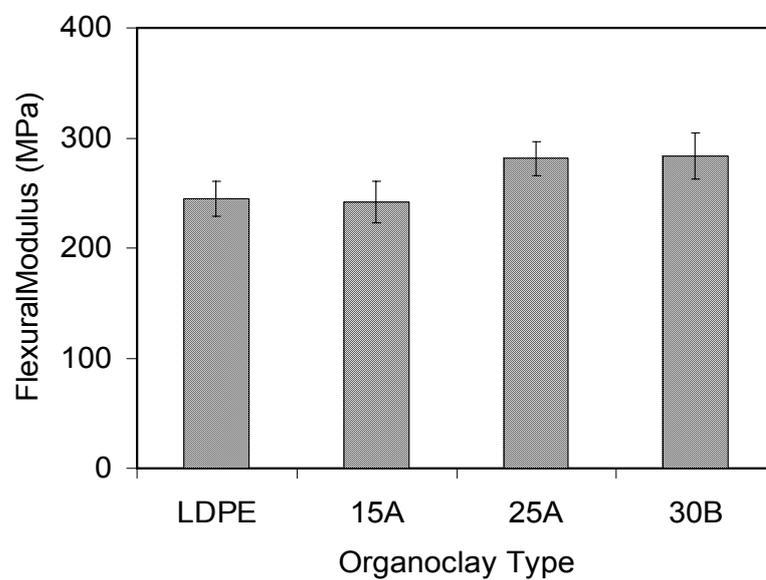
Figure 4.50 Flexural modulus of LDPE/organoclay nanocomposites, containing 2 wt % organoclay.
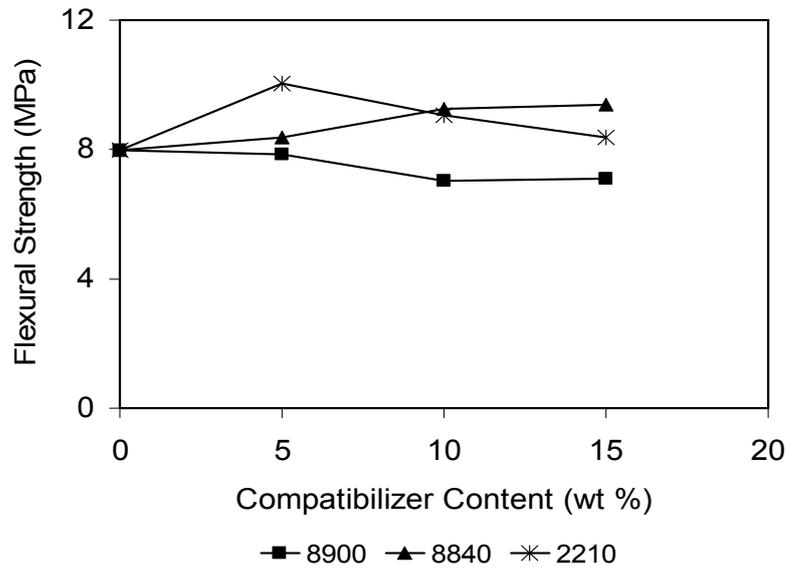
Figure 4.51 Effect of compatibilizer content on flexural strength of LDPE/compatibilizer blends.
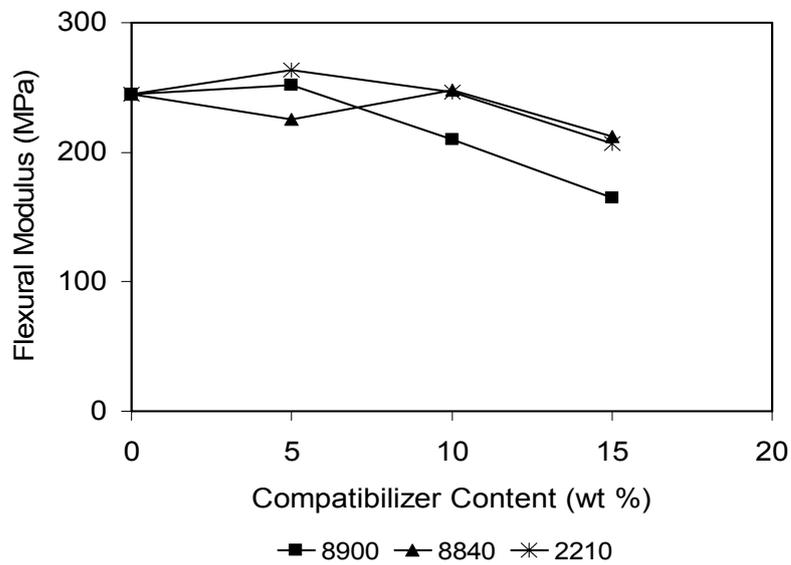
Figure 4.52 Effect of compatibilizer content on flexural modulus of LDPE / compatibilizer blends.
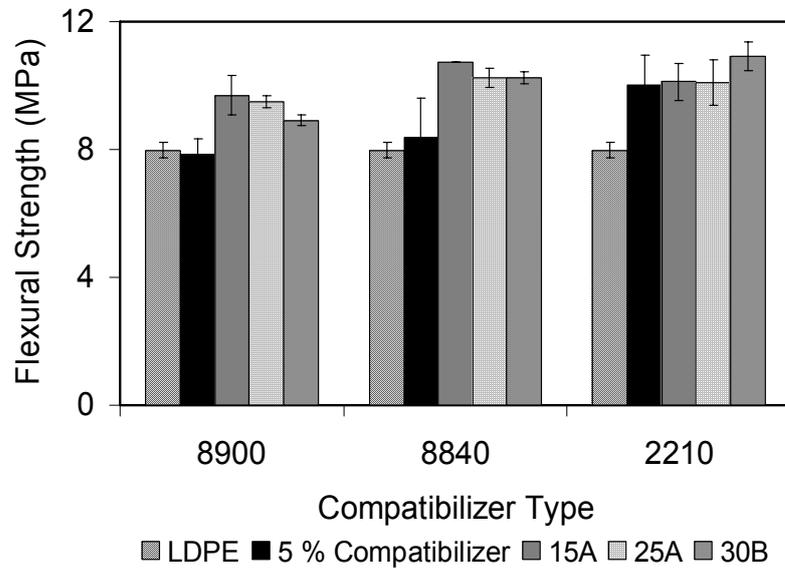
Figure 4.53 Flexural strength values of ternary LDPE/compatibilizer/organoclay nanocomposites.
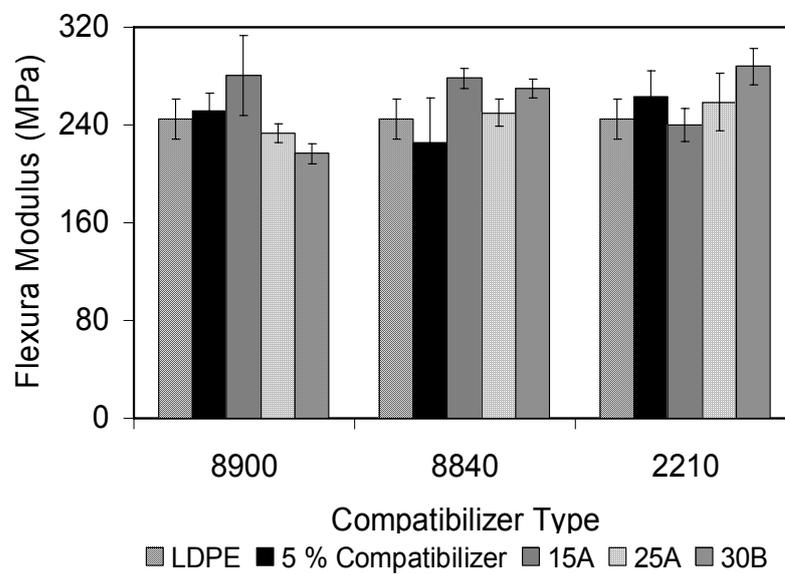
Figure 4.54 Flexural modulus values of ternary LDPE/compatibilizer/organoclay nanocomposites.
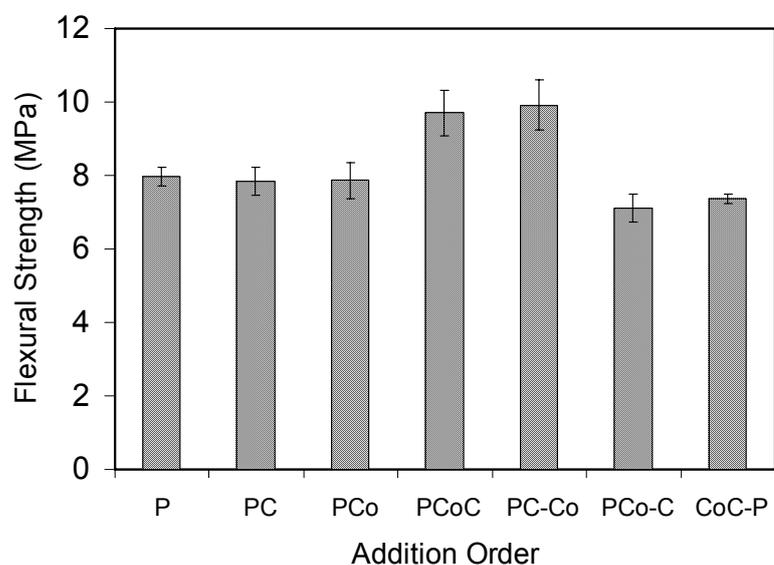
Figure 4.55 Effect of addition order on flexural strength of LDPE/ E-MA-GMA /15A nanocomposites containing 5 wt % compatibilizer and 2 wt % organoclay.
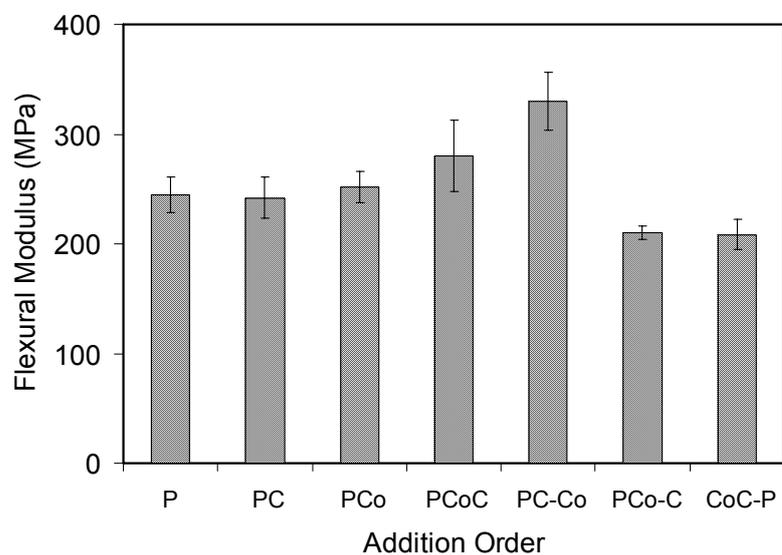
Figure 4.56 Effect of addition order on flexural modulus of LDPE/ E-MA-GMA /15A nanocomposites containing 5 wt % compatibilizer and 2 wt % organoclay.
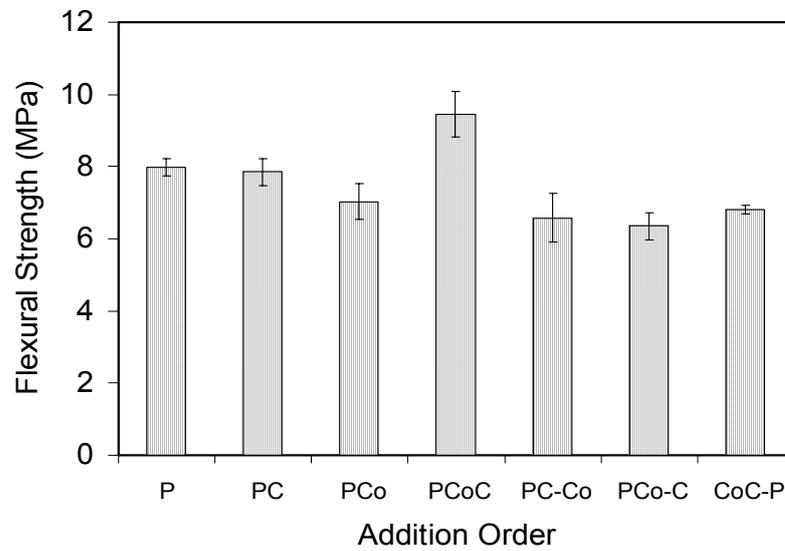
Figure 4.57 Effect of addition order on flexural strength of LDPE/ E-MA-GMA /15A nanocomposites containing 10 wt % compatibilizer and 2 wt % organoclay.
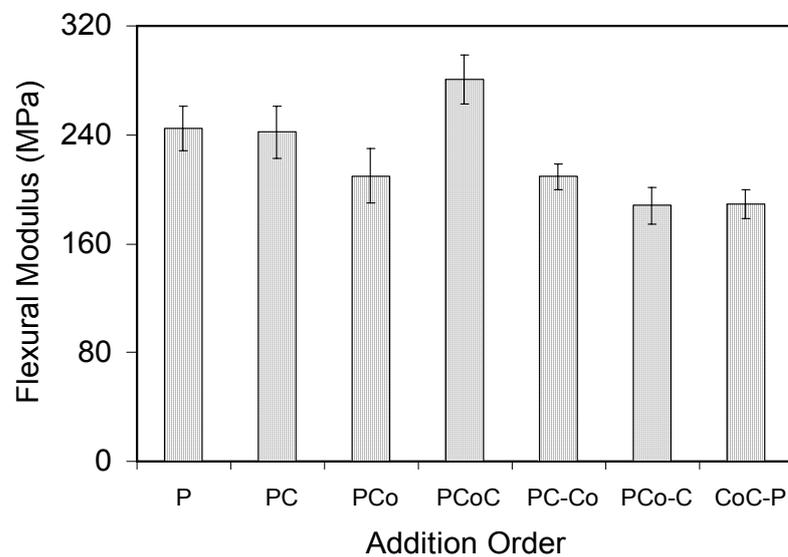
Figure 4.58 Effect of addition order on flexural modulus of LDPE/ E-MA-GMA /15A nanocomposites containing 10 wt % compatibilizer and 2 wt % organoclay.
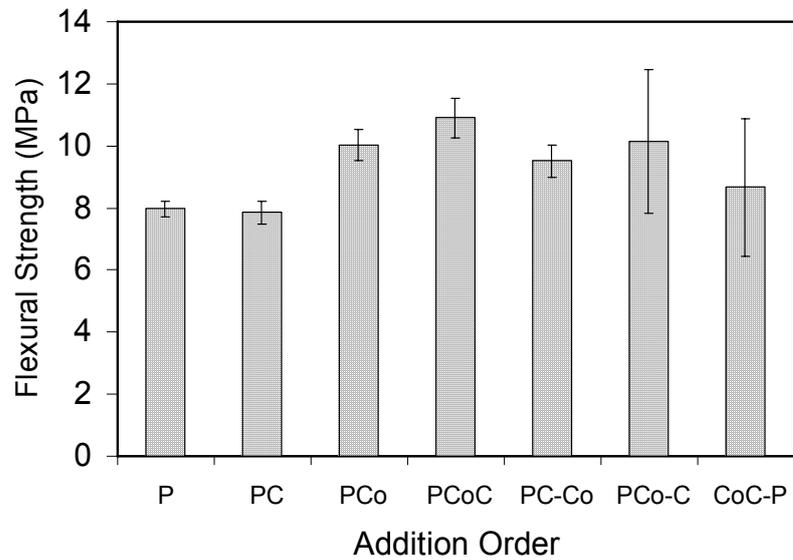
Figure 4.59 Effect of addition order on flexural strength of LDPE/ E-nBA-MAH/30B nanocomposites containing 5 wt % compatibilizer and 2 wt % organoclay.
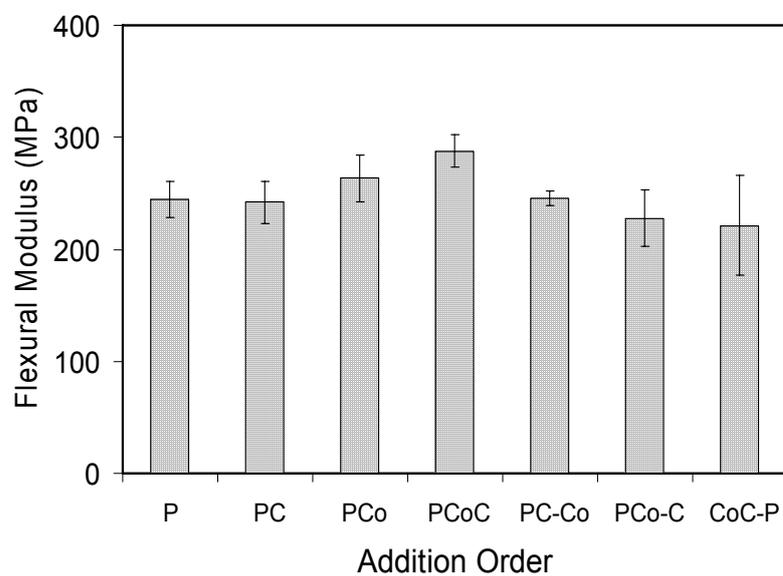
Figure 4.60 Effect of addition order on flexural modulus of LDPE/ E-nBA-MAH/30B nanocomposites containing 5 wt % compatibilizer and 2 wt % organoclay.

4.4 Flow Characteristics

Melt flow index (MFI) was performed in order to investigate the flow behavior of the samples, which is inversely related to melt viscosity. The test was carried out under a specified load of 2.16 kg and a specified temperature of 270°. There are several factors that influence the MFI as molecular weight, the presence of co-monomers, the degree of chain branching as well as heat transfer in polymer processing. The differences in MFI values are so small that it is difficult to have exact conclusions about the flow properties of the samples.

MFI values of pure materials are given in Table 4.4. It is seen that MFI of neat LDPE increased (viscosity decrease) during the extrusion process. This may be due to the decrease in the molecular weight of the LDPE due to the applied shear during extrusion.

Table 4.4 MFI values of pure materials

Material	MFI (g/10 min)
LDPE (not extruded)	1.86
LDPE (twice extruded)	2.84
E-MA-GMA	36.19
E-GMA	30.64
E-nBA-MAH	49.72

Addition of organoclay decreased the MFI value of 2.84 which indicates a higher viscosity as expected. Here, the clay particles act as fillers causing an increase in viscosity and dispersed clay particles further prevent the flow of the polymer chains. The MFI of compatibilizers are much greater than the MFI of pure LDPE, so it was expected that MFI values would increase (viscosity would decrease) with increasing concentration of the compatibilizers. However, the situation was opposite for all LDPE/compatibilizer blends. Non-polar structure of LDPE could lead in the easy flow of the polymer on the surface of the walls of the MFI machine and viscosity decreases.

However the addition of the polar compatibilizer to the LDPE increases the polarity and they could stick on the walls and resulted in decrease in MFI. The MFI results of LDPE/organoclay nanocomposites and LDPE/compatibilizer blends are given in Table 4.5 and Table 4.6 respectively.

Table 4.5 MFI values of LDPE/organoclay nanocomposites

Composition	Organoclay wt %	MFI (g/10 min)
LDPE + 15A	2	2.29
LDPE + 15A	4	2.22
LDPE + 15A	6	2.30
LDPE + 25A	2	2.02
LDPE + 30B	2	1.89

Table 4.6 MFI values of LDPE/compatibilizer blends

Composition	Compatibilizer wt %	MFI (g/10 min)
LDPE + 8900	5	1.57
LDPE + 8900	10	1.12
LDPE + 8900	15	1.05
LDPE + 8840	5	1.86
LDPE + 8840	10	1.78
LDPE + 8840	15	1.74
LDPE + 2210	5	2.09
LDPE + 2210	10	2.20
LDPE + 2210	15	2.57

MFI values of ternary nanocomposites are shown in Table 4.7. It is observed that MFI of ternary nanocomposites prepared with AO4 mixing order are lower than the neat LDPE, indicating that melt viscosity increased. It is obvious that the effect of

organoclay is dominant to the effect of compatibilizer on MFI of the ternary nanocomposites. These results are also the evidence of better dispersion of organoclay due to the addition of compatibilizer to the system. Moreover, XRD results support the well dispersion of clay by intercalated structures of ternary nanocomposites.

Table 4.7 MFI values of ternary LDPE/compatibilizer/organoclay nanocomposites produced with AO4 sequence.

Composition	Compatibilizer wt %	Organoclay wt %	MFI (g/10 min)
LDPE+8900+15A	5	2	1.76
LDPE+8840+15A	5	2	1.81
LDPE+2210+15A	5	2	2.32
LDPE+8900+25A	5	2	1.85
LDPE+8840+25A	5	2	1.89
LDPE+2210+25A	5	2	2.24
LDPE+8900+30B	5	2	2.05
LDPE+8840+30B	5	2	2.28
LDPE+2210+30B	5	2	2.57

The effect of addion order on melt flow index is given in Table 4.8. Decrease in melt flow index (increase in viscosity) was observed for nanocomposites containing E-MA-GMA, and organoclay 15A. On the other hand owing to the increase in MFI, it can be said that the compatibilizer effect on MFI was dominant for nanocomposites containing E-nBA-MAH and 30B and produced with AO1 and AO3 mixing orders.

Table 4.8 MFI values of ternary LDPE/compatibilizer/organoclay nanocomposites produced with different addition orders.

Composition	Compatibilizer wt %	Organoclay wt %	MFI (g/10 min)
LDPE / Lotader® 8900 / Cloisite® 15A			
AO1: (CoC)-P	5	2	2.00
AO2: (PC)-Co	5	2	1.68
AO3: (PCo)-C	5	2	1.51
AO4: (PCoC)	5	2	1.76
LDPE / Lotader® 8900 / Cloisite® 15A			
AO1: (CoC)-P	10	2	0.84
AO2: (PC)-Co	10	2	0.87
AO3: (PCo)-C	10	2	0.81
AO4: (PCoC)	10	2	1.02
LDPE / Lotader® 2210 / Cloisite® 30B			
AO1: (CoC)-P	5	2	3.05
AO2: (PC)-Co	5	2	3.32
AO3: (PCo)-C	5	2	2.84
AO4: (PCoC)	5	2	2.57

CHAPTER 5

CONCLUSIONS

Ternary nanocomposites of low density polyethylene have been produced with different compatibilizers, and organoclays by means of melt compounding method. Effects of compatibilizer, organoclay, and the addition order of the components, on the morphology, thermal properties, mechanical properties, as well as flow behavior were investigated.

Considering the morphology of 2 wt % organoclay loaded LDPE/organoclay nanocomposites, intercalation of polymer was observed only for LDPE/25A nanocomposites. In addition to this, increase in organoclay content does not favor the dispersion of the clay, but decreases the degree of dispersion. X-ray analyses obviously show the positive effect of addition of compatibilizer to LDPE/organoclay nanocomposites, on dispersion of the organoclay particles. 5 wt % compatibilizer loading to the LDPE/organoclay nanocomposites resulted in a shift to smaller angles, and diffraction peaks that are broader and lower in height in comparison to those of the neat organoclay and LDPE/ organoclay nanocomposites. The highest increase of the basal spacing for ternary nanocomposites obtained for LDPE/E-nBA-MAH/organoclay nanocomposites were 83 %, 198 %, and 206 % for samples containing 15A, 25A and 30B respectively. It was difficult to distinguish the effect of addition order procedure on morphology of ternary nanocomposites, since there is only slight difference in d-spacing of the clay platelets.

From SEM micrographs, it is seen that, the smooth surface of the pristine LDPE disappeared when melt blended with either organoclay or compatibilizer. Increase in organoclay content resulted in shorter and closer crack propagation lines instead of straight propagation lines. In SEM micrographs of ternary nanocomposites, the smooth structure of neat LDPE is not detected and many shorter and closer, circular, non

linear crack propagation lines are the evidence of the well dispersion of organoclay throughout the matrix. Due to poor dispersion, agglomerates of clay particles were also detected in some SEM micrographs of samples which also possess poor mechanical properties. The effect of organoclay type and addition order on morphological structure of nanocomposites could not be investigated owing to the resemblance of the fractured surfaces of the samples.

DSC analysis showed that, the melting temperature (T_m) and percent crystallinity of LDPE did not change remarkably due to the addition of organoclay and compatibilizer. Thus it is concluded that addition of both organoclay and compatibilizer does not influence the melting behavior of the compositions, Also it is observed that the compatibilizers and organoclay types have no nucleation activity in LDPE.

Increase in organoclay content decreased the mechanical properties of the binary LDPE/organoclay nanocomposites due to the agglomeration of the organoclay particles. Also since compatibilizers have lower mechanical properties than the LDPE, generally poor mechanical properties were observed at high loading of compatibilizers in LDPE/compatibilizer blends.

The mechanical properties including the tensile strength, tensile modulus, tensile strain at break, flexural strength and flexural modulus, showed notable improvements for ternary LDPE/compatibilizer/organoclay nanocomposites with respect to neat LDPE and LDPE/organoclay nanocomposites. According to the results of the mechanical tests, LDPE/E-MA-GMA/15A, LDPE/E-GMA/15A and LDPE/E-nBA-MAH/30M nanocomposites showed the highest improvement in mechanical properties.

Based on tensile and flexural properties, PCoC (AO4) is the best addition sequence in which all the materials were simultaneously fed to the extruder in the first run.

MFI measurements showed that, the effect of organoclay is more dominant than the effect of compatibilizer on viscosity of the ternary nanocomposites. Thus with the addition of organoclay in the ternary nanocomposites the viscosity increased which is

also the evidence of better dispersion of organoclay owing to the addition of compatibilizer to the system.

REFERENCES

1. Akovali G., "Handbook of Composite Fabrication", Rapra Technology Ltd., Shawbury, UK, 2001.

2. Alexandre M. and Dubois P., "Polymer-layered Silicate Nanocomposites: Preparation, Properties and Uses of a New Class of Materials", Materials Science and Engineering, vol.28, 1-63, 2000.

3. Giannelis E.P., "Polymer Layered Silicate Nanocomposites" , Advanced Materials, vol.8, 29-35, 1996.

4. Bafna A. A., " Polyethylene-Clay Nanocomposites: Processing-Structure-Property Relationship", Ph. D. Thesis, University of Cincinnati, Ohio, USA, 2004.

5. Kroschwitz J. I., "Concise Encyclopedia of Polymer Science and Enginering", Wiley-Interscience Publication, New York, 1990.

6. Hambir S., Bulakh N., and Jog J.P., "Polypropylene / Clay Nanocomposites: Effect of Compatibilizer on the Thermal, Crystallization and Dynamic Behavior", Polymer Engineering and Science, vol.42 No.9, 1800-1807, 2002.

7. Wang K. H., Choi M. H., Koo C. M., Choi Y.S., Chung I. J., "Synthesis and Characterization of Maleated Polyethylene / Clay Nanocomposites", Polymer, vol.42, 9819-9826, 2001.

8. Li X., "Effect of Blending Sequence on the Microstructure and Properties of PBT/EVA-g-MAH / Organoclay Ternary Nanocomposites". Polymer Engineering and Science, vol.42, No.11,2156-2164, 2002.

9. Gopakumar T.G., Lee J.A., Kontopoulou M., Parent J.S., "Influence of Clay Exfoliation on the Physical Properties of Montmorillonite / Polyethylene Composites", Polymer, vol. 43, 5483-5491, 2002.

10. Kato M., Okamoto H., Hasegawa N., Tsukigase A. and Usuki A., " Preparation and Properties of Polyethylene-Clay Hybrids", Polymer Engineering and Science, vol.43 No.6, 1312-1316, 2003.

11. Liang G., Xu J., Bao S., Xu W., "Polyethylene/Maleic Anhydride Grafted Polyethylene/Organic-Montmorillonite Nanocomposites.I. Preparation, Microstructure, and Mechanical Properties", Journal of Applied Polymer Science, vol.91, 3974-3980, 2004.

12. Zhang J., Wilkie C.A., "Preparation and Flammability of Polyethylene-Clay Nanocomposites", Polymer Degradation and Stability, vol.80, 163-169, 2003.

13. Hotta S., Paul D.R., "Nanocomposites Formed From Linear Low Density Polyethylene and Organoclays", Polymer, vol.45, 7639-7654, 2004.

14. Zhai H., Xu W., Guo H., Zhou Z., Shen S., Song Q., " Preparation and Characterization of PE and PE-g-MAH/montmorillonite Nanocomposites", European Polymer Journal, vol. 40, No: 11, 2539-2545, 2004.

15. Morawiec J., Pawlak A., Slouf M., Galeski A., Piorkowska E., Krasnikowa N., "Preparation and Properties of Compatibilized LDPE/Organo-modified Montmorillonite Nanocomposites", European Polymer Journal, vol. 41, 1115-1122, 2005.

16. Zhong Y., Kee D.D., " Morphology and Properties of Layered Silicate-Polyethylene Nanocomposite Blown Films", Polymer Engineering and Science, 469-477, 2005.

17. Hasegawa, N., Okamoto, H., Kato, M., Usuki, A., "Preparation and Mechanical Properties of Polypropylene-Clay Hybrids Based on Modified Polypropylene and Organophilic Clay", Journal of Applied Polymer Science, vol. 78, 1918-1922, 2000.

18. http://www.unitedcomposites.net/usapages/whycomposites2.htm

19. Fried J.R., "Polymer Science and Technology", 2 nd. Edition, Prentice Hall PTR, 2003.

20. "Kirk-Othmer Encyclopedia of Chemical Technology", 4 th Edition, vol.7, 1-27, John Wiley and Sons, Inc., New York, 1993.

21. Strong A B., "Fundamentals of Composites Manufacturing: Materials, Methods and Applications", Society of Manufacturing Engineers, Publications Development Dept., Reference Publications Division, Dearborn, Michigan, 1989.

22. Harper C.A., "Handbook of Plastics, Elastomers & Composires", 4 th Edition, McGraw - Hill, Inc., 2002.

23. Callister W.D., "Material Science and Engineering; An Introduction, 4 th Edition, John Wiley and Sons, Inc.,NY,1997.

24. Chawla K. K., "Composite Materials: Science and Engineering", Springer-Verlag, New York, 1998.

25. Daniel I. and Ishai O., "Engineering Mechanics of Composite Materials", Oxford University Press Inc., New York, USA, 1994.

26. Mazumdar S.K., "Composites Manufacturing Materials, Product, and Process Engineering", CRC Press, USA., 2002.

27. Electronic Development Labs, Inc., http://www.edl-inc.com, fast accessed; July 2005.

28. Dennis H.R., Hunter D.L., Chang D., Kim S., White J.L. Cho J.W., Paul D.R., "Effect of Melt Processing Conditions on the Extent of Exfoliation in Organoclay-based Nanocomposites", Polymer, vol.42, 9513-9522, 2001.

29. Schmidt D., Shah D., Giannelis E.P., "New Advances in Polymer/layered Silicate Nanocomposites", Current Opinion in Solid State and Materials Science, vol.6,205-212, 2002.

30. Pinnavaia T.J., Beall G.W., "Polymer-Clay Nanocomposites", John Wiley and Sons, Ltd., England, 2000

31. Ray S.S. and Okamoto M., "Polymer/layered Silicate Nanocomposites: A Review from Preparation to Processing", Progress in Polymer Science, 2003.

32. Manias E., Touny A., Wu L., Strawhecker K., Lu B., Chung T.C., "Polypropylene/Montmorillonite Nanocomposites.Review of the Synthetic Routes and Materials Properties", Chemistry of Materials, vol.13, 3516-3523, 2001.

33. Giannelis, E.P., Krishnamoorti, R., Manias, E., "Polymer-Silicate Nanocomposites: Model Systems for Confined Polymers and Polymer Brushes", Advances in Polymer Science, vol.138, 108-147, 1999.

34. LeBaron P. C., Wang Z. and Pinnavaia T. J., "Polymer-layered Silicate Nanocomposites: An Overview", Applied Clay Science, vol.15, 11-29, 1999.

35. Kornmann X., "Synthesis and Characterization of Thermoset-Clay Nanocomposites", Ph. D. Thesis, Lulea University of Technology, Sweden, 2000.

36. Vaia, R. A., Ishii, H., Giannelis, E. P.,"Synthesis and Properties of Two-Dimensional Nanostructures by Direct Intercalation of Polymer Melts in Layered Silicates", Chemistry of Materials, vol. 5, 1694-1696, 1993.

37. Rubin I. I., "Handbook of Plastic Materials and Technology", John Wiley and Sons Inc., 27, New York, 1990

38. Salamone J. C., "Polymer Materials Encyclopedia", Boca Raton, CRC Press Inc., New York, 1996.

39. "Kirk-Othmer Encyclopedia of Chemical Technology", 4 th Edition, vol.17, 702-707, John Wiley and Sons, Inc., New York, 1993.

40. "Kirk-Othmer Encyclopedia of Chemical Technology", 4 th Edition, vol.17, 707-723, John Wiley and Sons, Inc., New York, 1993.

41. Mark Bishop's Chemistry Site, http://www.mpcfaculty.net/mark_bishop / polyethylene_ formation_complete.jpg; fast accessed July 2005.

42. Rubin I. I., "Handbook of Plastic Materials and Technology", John Wiley and Sons Inc., 28, New York, 1990

43. Seymour R. B., Carraher C. E., "Structure-Property Relationships in Polymers", Plenum Press, New York, 1984.

44. Fischer H.,"Polymer Nanocomposites: From Fundamental Research to Specific applications" Material Science and Engineering C", vol. 23, 763-772, 2003.

45. The Dow Chemical Company, http://www.dow.com, fast accessed July 2005.

46. Rodriguez F., " Principles of Polymer Systems", 4 th. Edition, McGraw Hill, Pub. , 1996.

47. Rauwendaal C. "Polymer Extrusion" , Third, revised edition, Hanser / Gardner Publications, Inc. Cincinnati, 1994.

48. Rubin I.I., "Handbook of Plastic Materials and Technology", John Wiley & Sons, Inc.,New York, 1990.

49. Özden G., "Synthesis and Characterization of Polystyrene Clay Nanocomposites", M.Sc. Thesis, Middle East Technical University, Ankara, TURKEY, 2004.

50. Polymer Processing.com, http://www.polymerprocessing.com; fast accessed July 2005.

51. Kılınç M., "Processing and Characterization of PET Based Composites", M.Sc. Thesis, Middle East Technical University, Ankara, TURKEY, 2004.

52. Allock H.R., Lampe F.W., "Contemporary Polymer Chemistry", 2nd Edition, Prentice Hall., 1990.

53. Braggs Law, http://www.eserc. stonybrook.edu/ProjectJava/Bragg, fast accessed July 2005.

54. "Kirk-Othmer Encyclopedia of Chemical Technology", 4 th Edition, vol.16, John Wiley and Sons, Inc., New York, 1993.

55. Nielsen L. E ., Landel R. F ., "Mechanical Properties of Polymers and Composites", 2nd Edition, Marcel Decker, Inc., New York, 1994.

56. ASTM D638-91a, Standard Test Method for Tensile Properties of Plastics, "Annual Book of ASTM Standards", vol.08.01, 174-182, Philadelphia, USA ,1993.

57. Matweb material data, rhttp://www.matweb.com/reference/tensilestrength.asp; last accessed, July 2500.

58. Billmeyer J., Fred W., "Textbook of Polymer Science", 3rd Edition, John Wiley & Sons, Inc., 1984.

59. ASTM D790M-92, Standard Test Methods for Flexural Properties of Unreinforced Plastics and Electrical Insulating Materials, " Annual Book of Standards", vol. 08.01, 284-292, Philadelphia, USA ,1993.

60. Vaia, R.A., Jandt, K.D., Kramer, E.J., Giannelis E.P., "Microstructural Evolution of Melt Intercalated Polymer-Organically Modified Layered Silicates Nanocomposites", Chemistry of Materials, vol. 8, 2628-2635. 1996.

61. Dennis, H.R., Hunter, D.L., Chang, D., Kim, S., White, J.L., Cho, J.W., Paul, D.R., 2001. Effect of Melt Processing Conditions on the Extent of Exfoliation in Organoclay-Based Nanocomposites, Polymer, 42, 9513-9522.

62. Yoon J. T., Jo W. H., Lee M. S., Ko M.B, "Effects of Comonomers and Shear on the Melt Intercalation of Styrenics/Clay Nanocomposites", Polymer,vol. 42, 329-336, 2001.

63. A. Morgan, J. Gilman "Characterization of Polymer-layered Silicate (clay) Nanocomposites by Transmission Electron Microscopy and X-ray Diffraction: A Comparative Study", Journal of Applied Polymer Science ., vol. 87, 1329-1338, 2003.
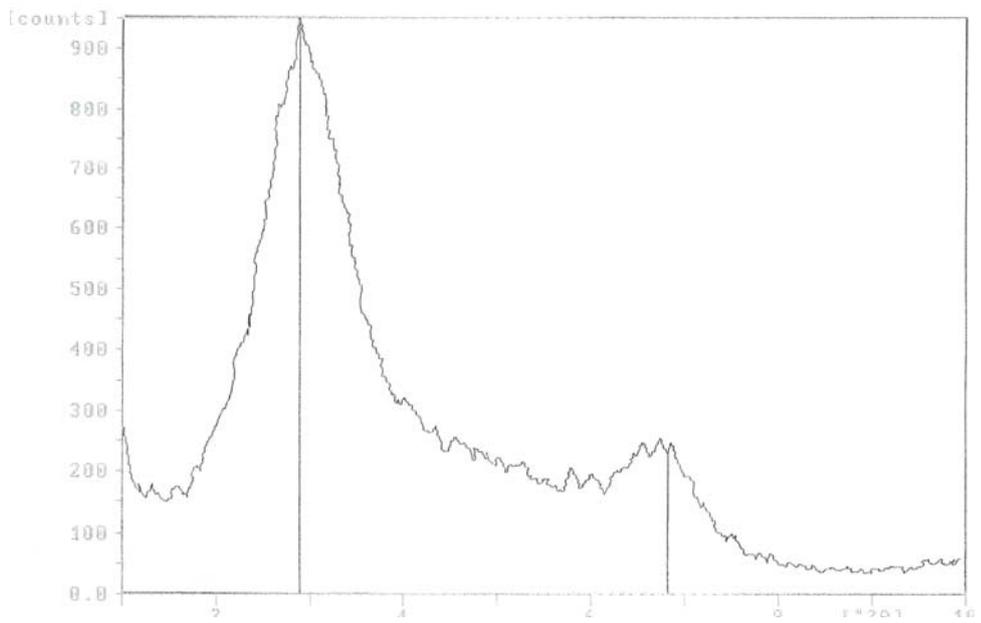
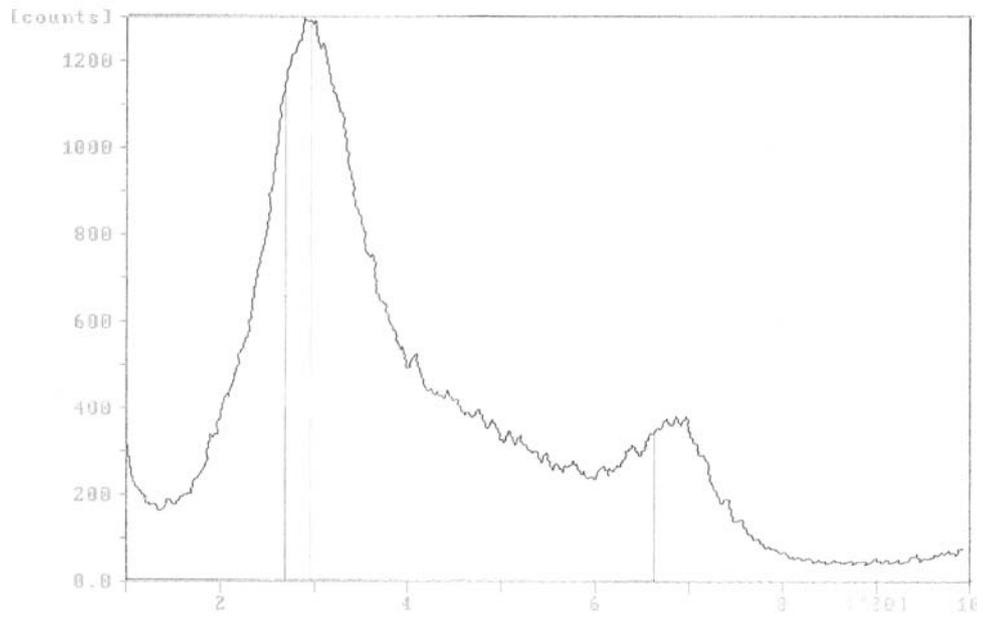# APPENDIX A

X-Ray Analysis
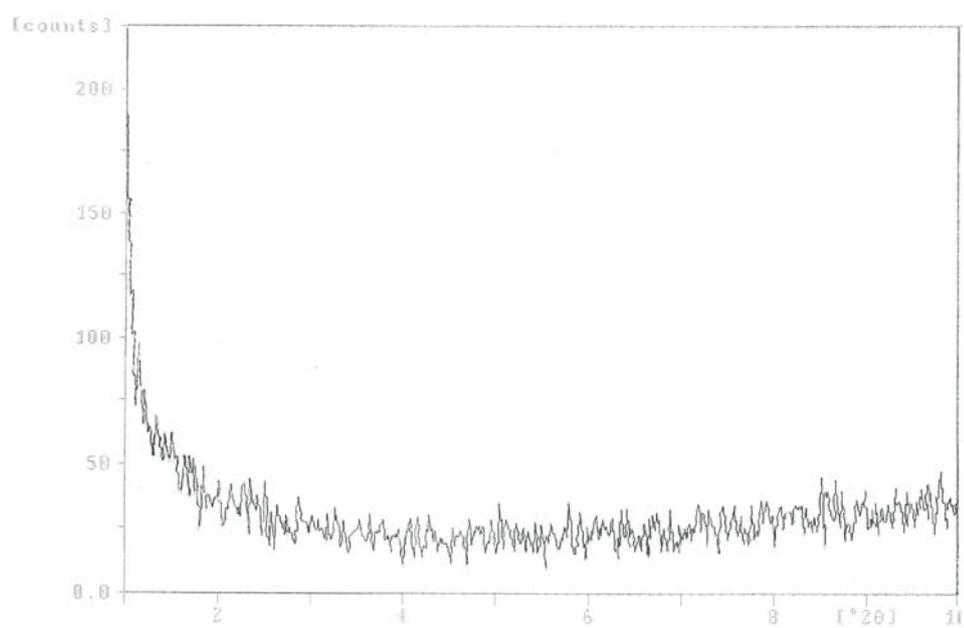
Figure A.1 X-Ray diffraction pattern of pure low density polyethylene (LDPE)

.
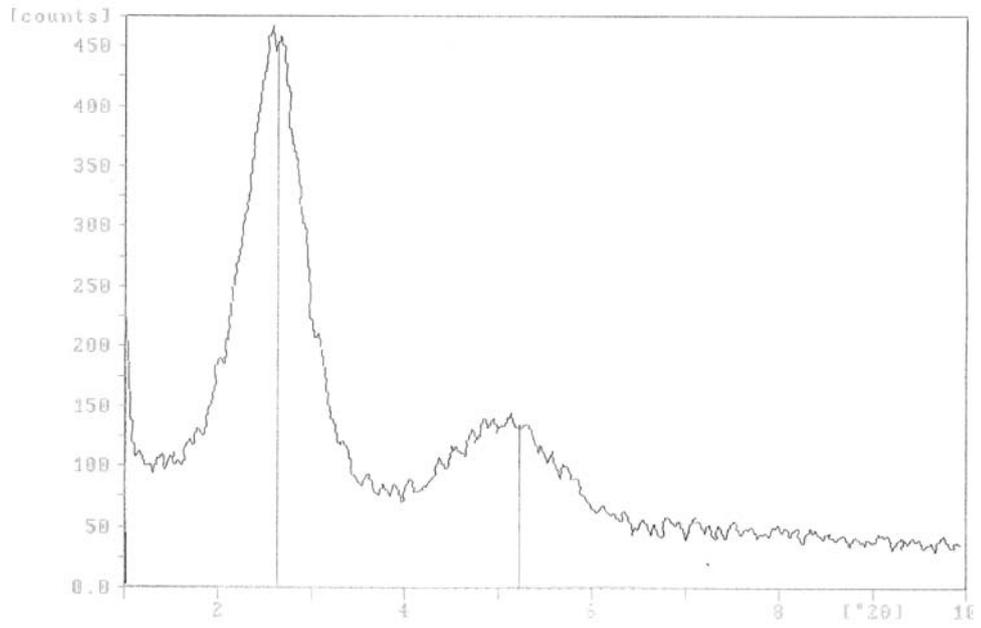
Figure A.2 X-Ray diffraction pattern of nanocomposite containing 2 wt. %
Cloisite® 15A .

Figure A.3 X-Ray diffraction pattern of nanocomposite containing 4 wt. %
Cloisite® 15A .

Figure A.4 X-Ray diffraction pattern of nanocomposite containing 6 wt. %
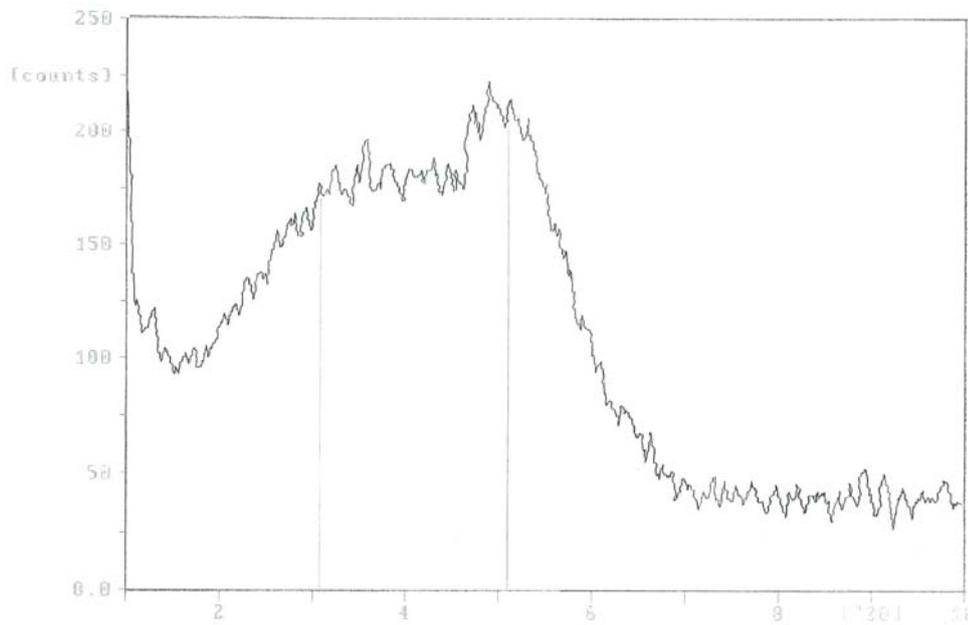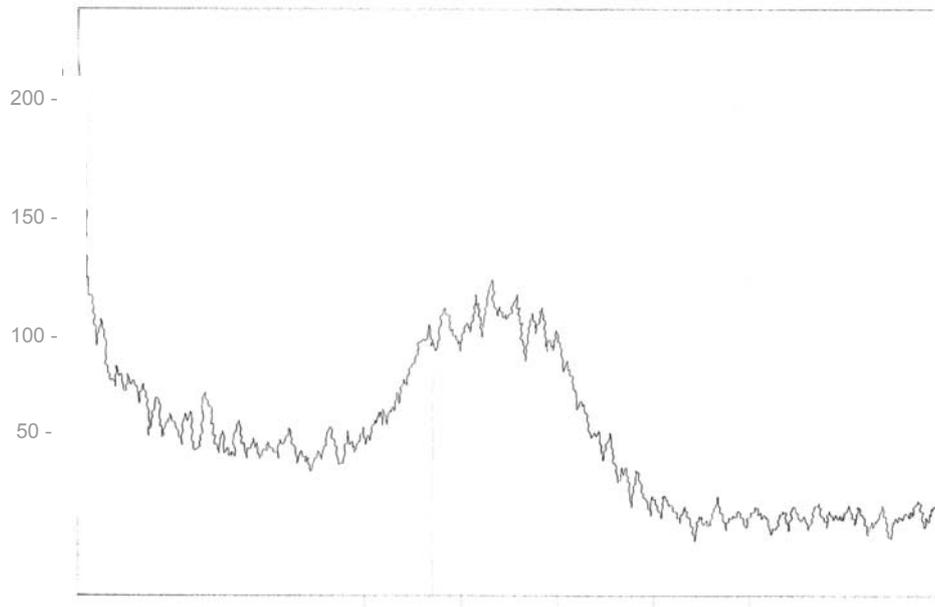Cloisite® 15A .

Figure A.5 X-Ray diffraction pattern of nanocomposite containing 2 wt. %
Cloisite® 25A .

Figure A.6 X-Ray diffraction pattern of nanocomposite containing 2 wt. %
Cloisite® 30B .
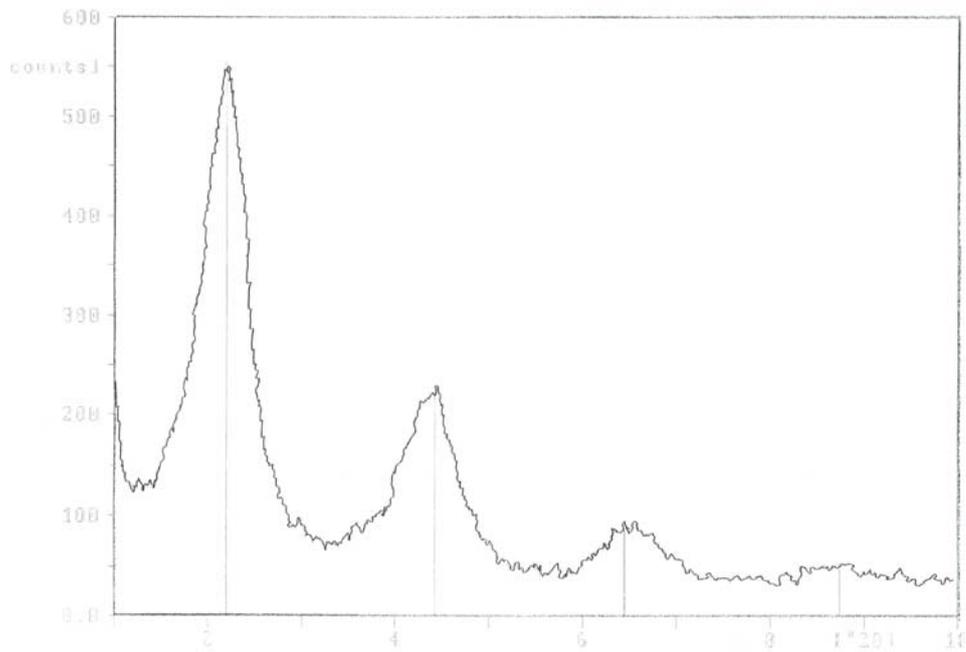
Figure A.7 X-Ray diffraction pattern of nanocomposite produced with AO4 sequence,
containing 2 wt. % Cloisite® 15A and 5 wt. % Lotader® AX 8900 .
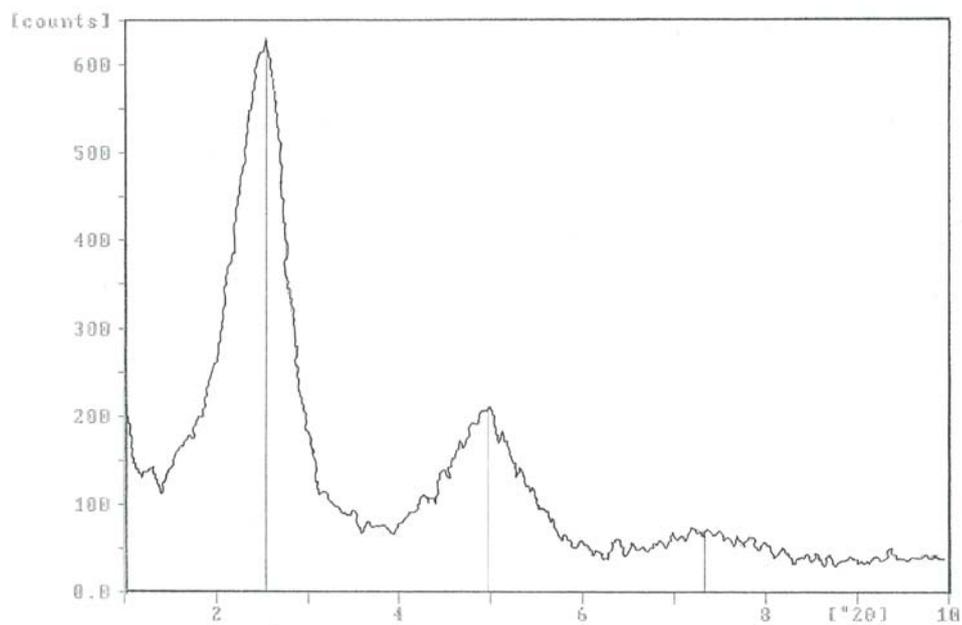
Figure A.8 X-Ray diffraction pattern of nanocomposite produced with AO4 sequence, containing 2 wt. % Cloisite® 15A and 5 wt. % Lotader® AX 8840 .
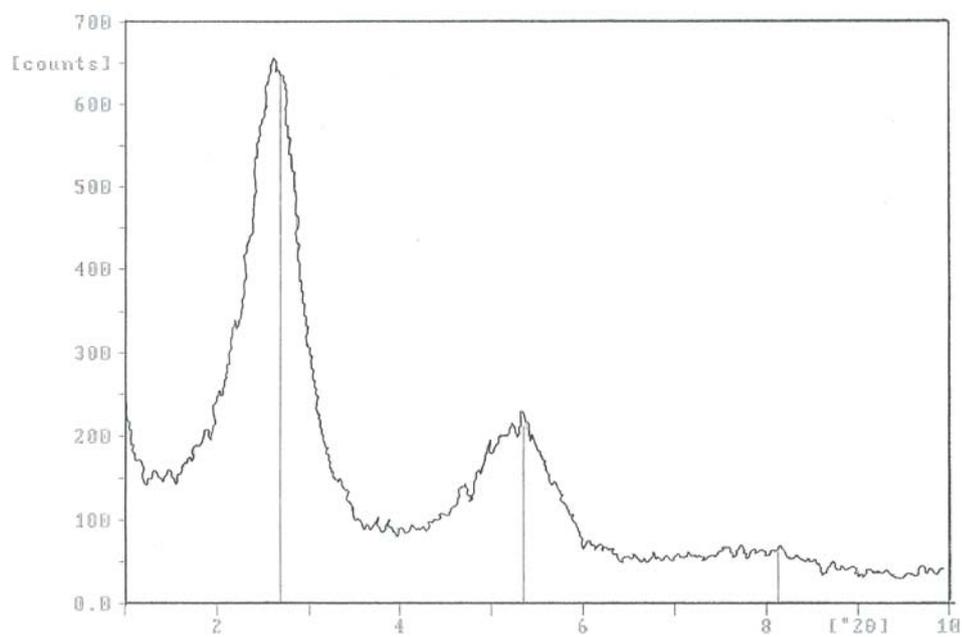
Figure A.9 X-Ray diffraction pattern of nanocomposite containing 2 wt. % Cloisite® 15A and 5 wt. % Lotader® 2210 .

Figure A.10 X-Ray diffraction pattern of nanocomposite containing 2 wt. % Cloisite®
25A and 5 wt. % Lotader® AX 8900 .

Figure A.11 X-Ray diffraction pattern of nanocomposite produced with AO4 sequence,
containing 2 wt. % Cloisite® 25A and 5 wt. % Lotader® AX 8840.

Figure A.12 X-Ray diffraction pattern of nanocomposite produced with AO4 sequence, containing 2 wt. % Cloisite® 25A and 5 wt. % Lotader® 2210 .
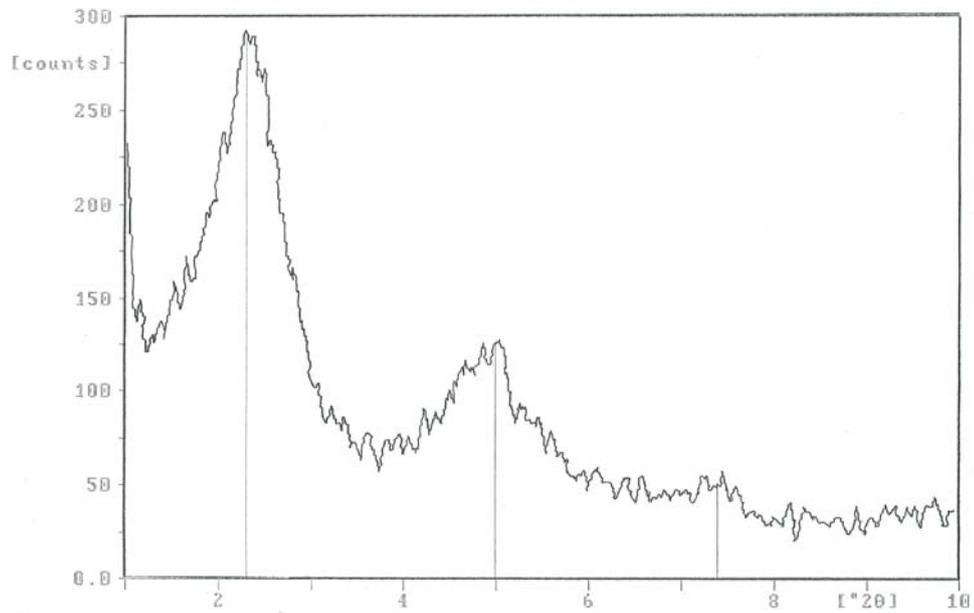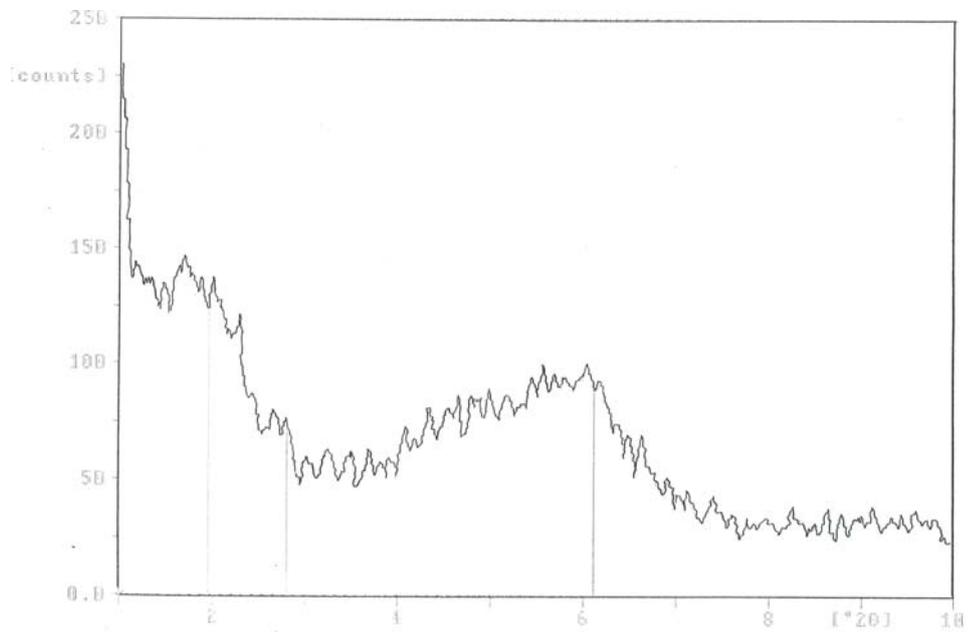

Figure A.13 X-Ray diffraction pattern of nanocomposite produced with AO4 sequence, containing 2 wt. % Cloisite® 30B and 5 wt. % Lotader® AX 8900 .

Figure A.14 X-Ray diffraction pattern of nanocomposite produced with AO4 sequence, containing 2 wt. % Cloisite® 30B and 5 wt. % Lotader® AX 8840 .

Figure A.15 X-Ray diffraction pattern of nanocomposite produced with AO4 sequence, containing 2 wt. % Cloisite® 30B and 5 wt. % Lotader® 2210 .
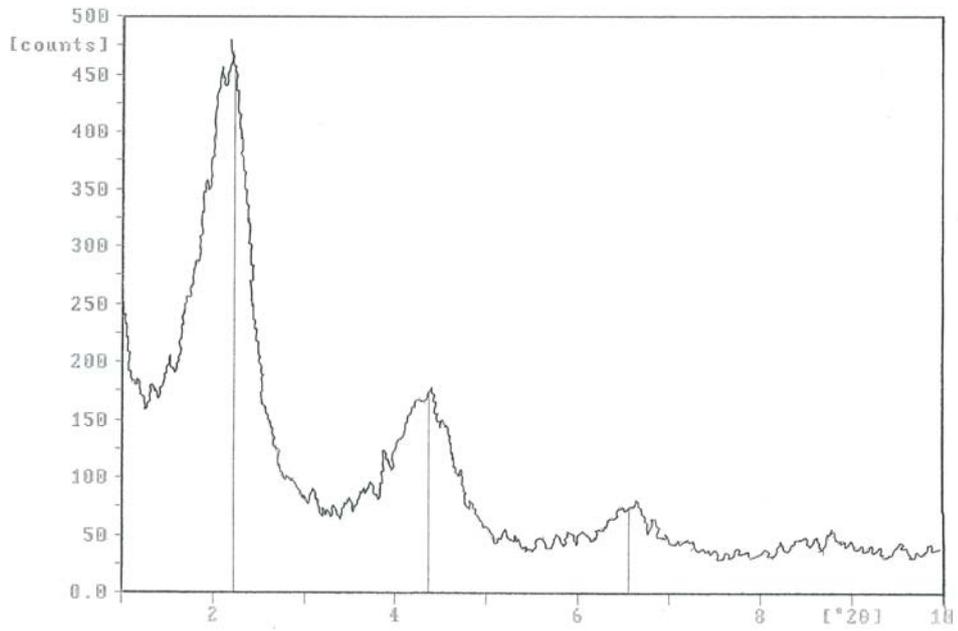
Figure A.16 X-Ray diffraction pattern of nanocomposite produced with AO1 sequence, containing 2 wt. % Cloisite® 15A and 5 wt. % Lotader® AX 8900.
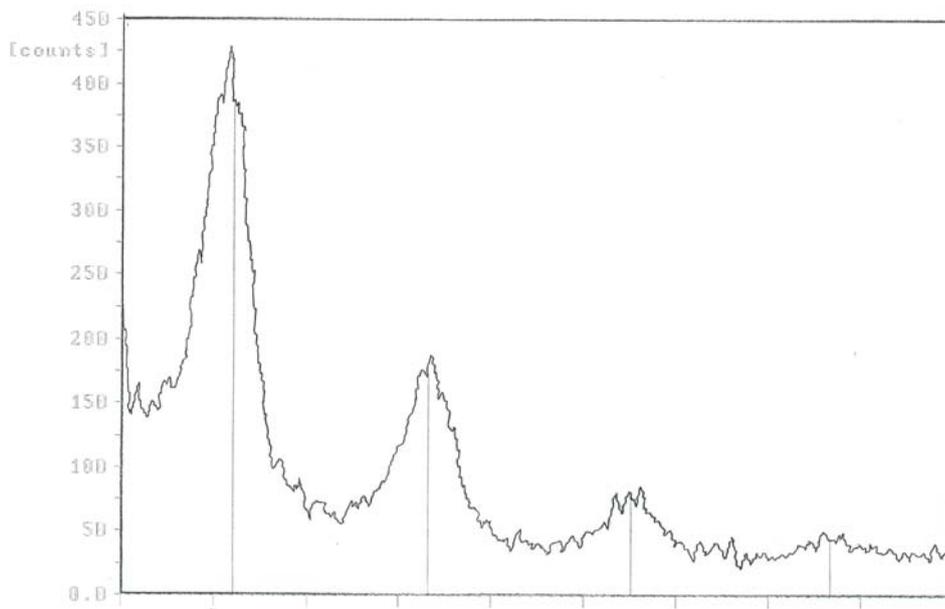
Figure A.17 X-Ray diffraction pattern of nanocomposite produced with AO2 sequence, containing 2 wt. % Cloisite® 15A and 5 wt. % Lotader® AX 8900.
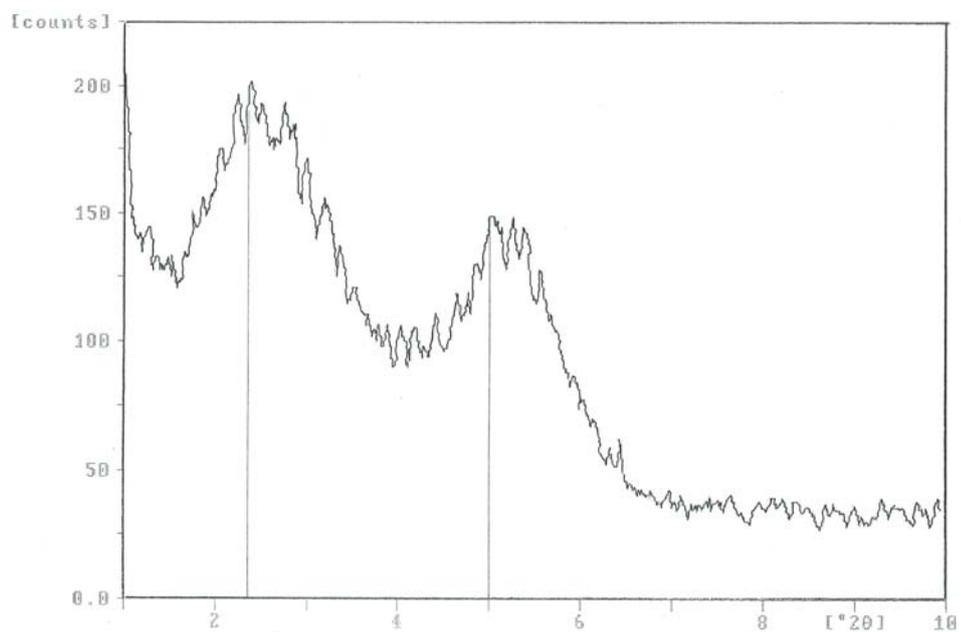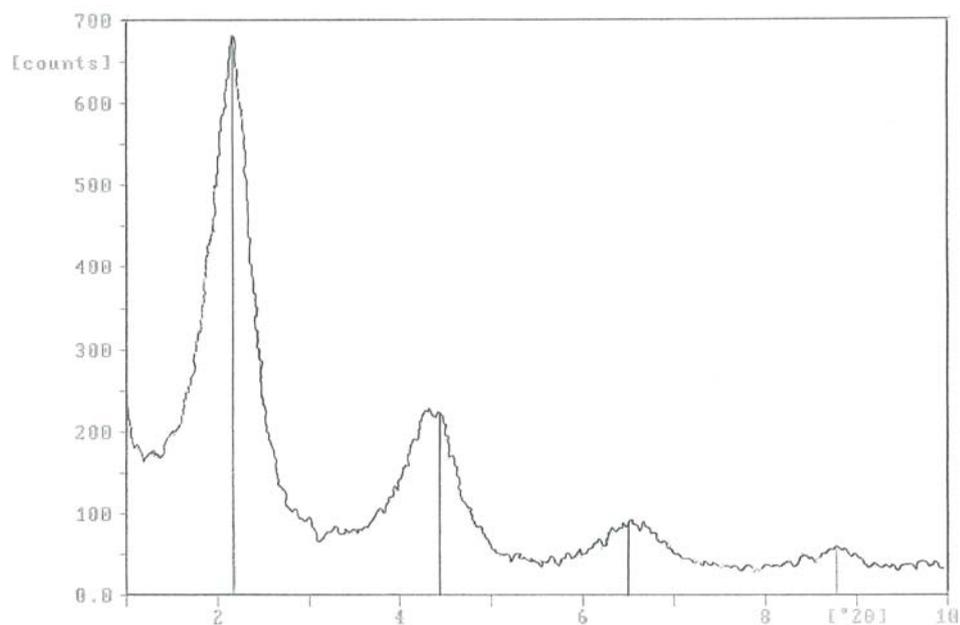
Figure A.18 X-Ray diffraction pattern of nanocomposite produced with AO3 sequence, containing 2 wt. % Cloisite® 15A and 5 wt. % Lotader® AX 8900.
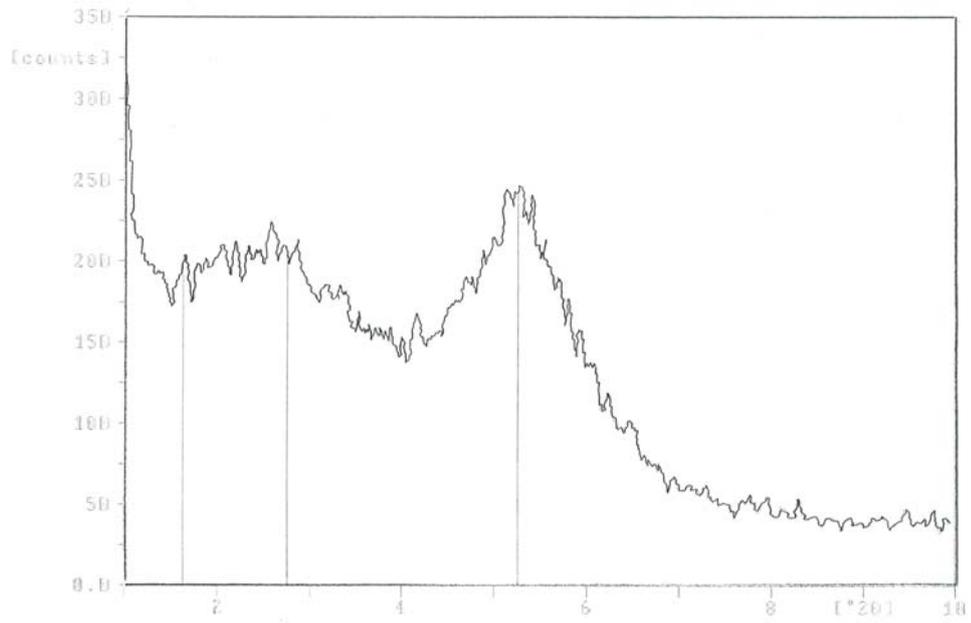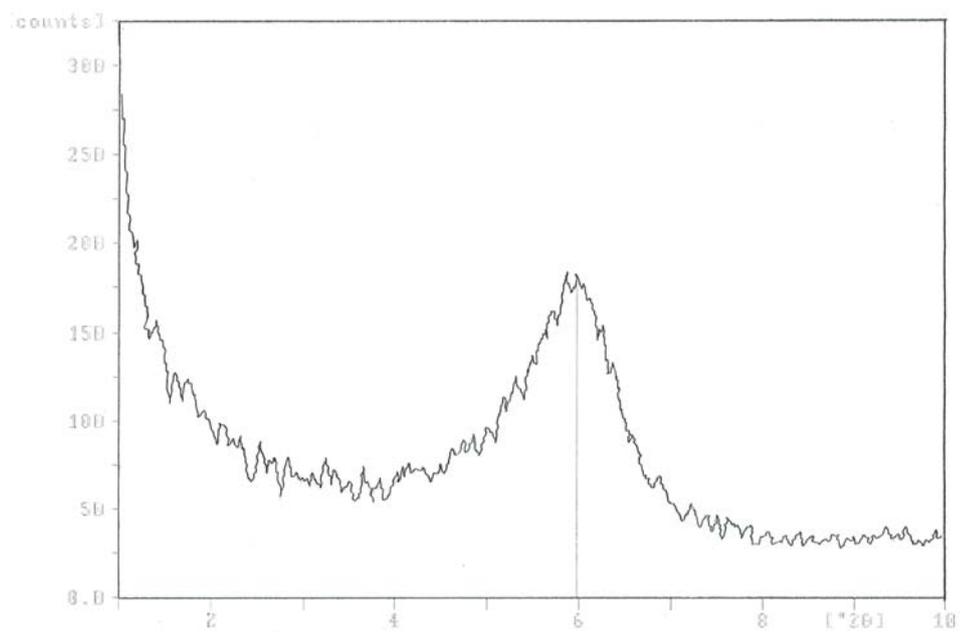

Figure A.19 X-Ray diffraction pattern of nanocomposite produced with AO1 sequence, containing 2 wt. % Cloisite® 30B and 5 wt. % Lotader® AX 8900.
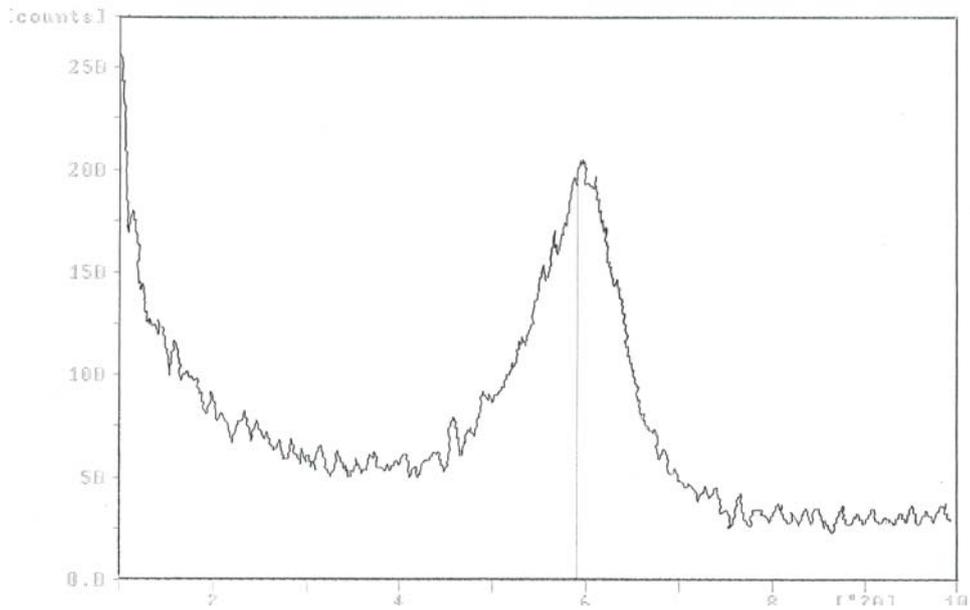
Figure A.20 X-Ray diffraction pattern of nanocomposite produced with AO2 sequence, containing 2 wt. % Cloisite® 30B and 5 wt. % Lotader® 2210.
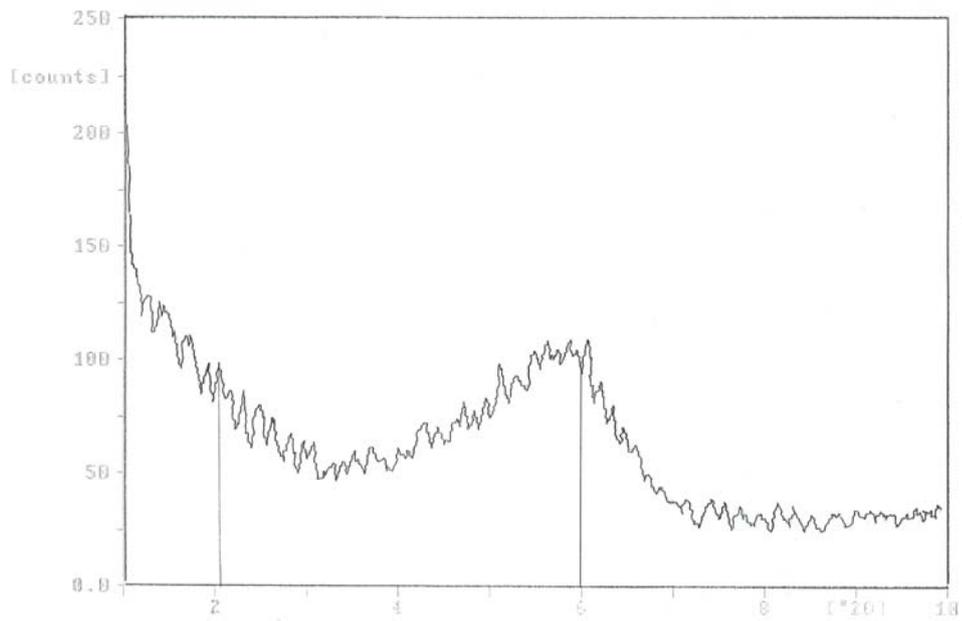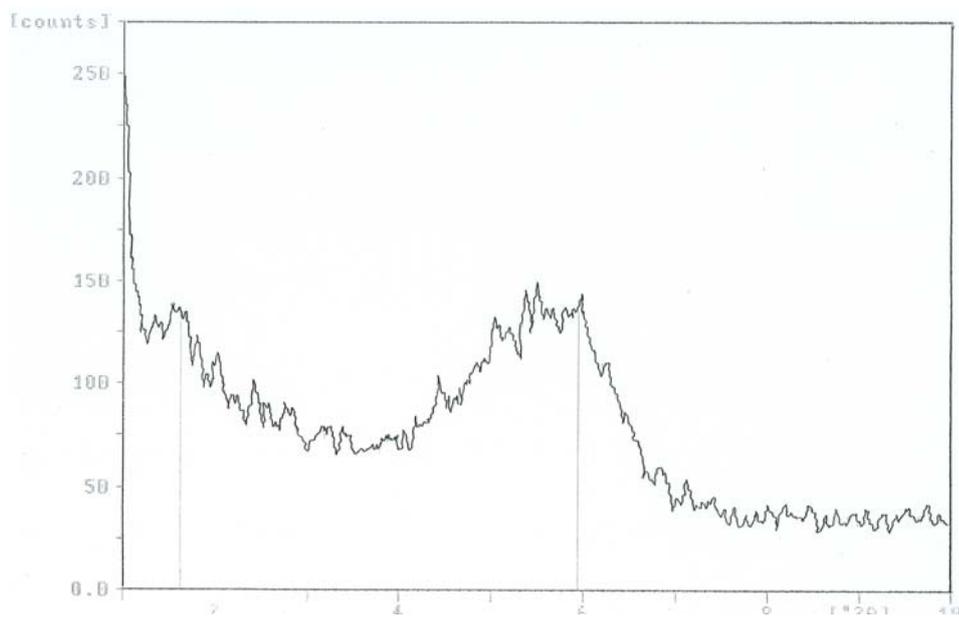

Figure A.21 X-Ray diffraction pattern of nanocomposite produced with AO3 sequence, containing 2 wt. % Cloisite® 30B and 5 wt. % Lotader® 2210.

DSC Analysis

Figure B.1 DSC thermogram of pure low density polyethylene (LDPE)

.
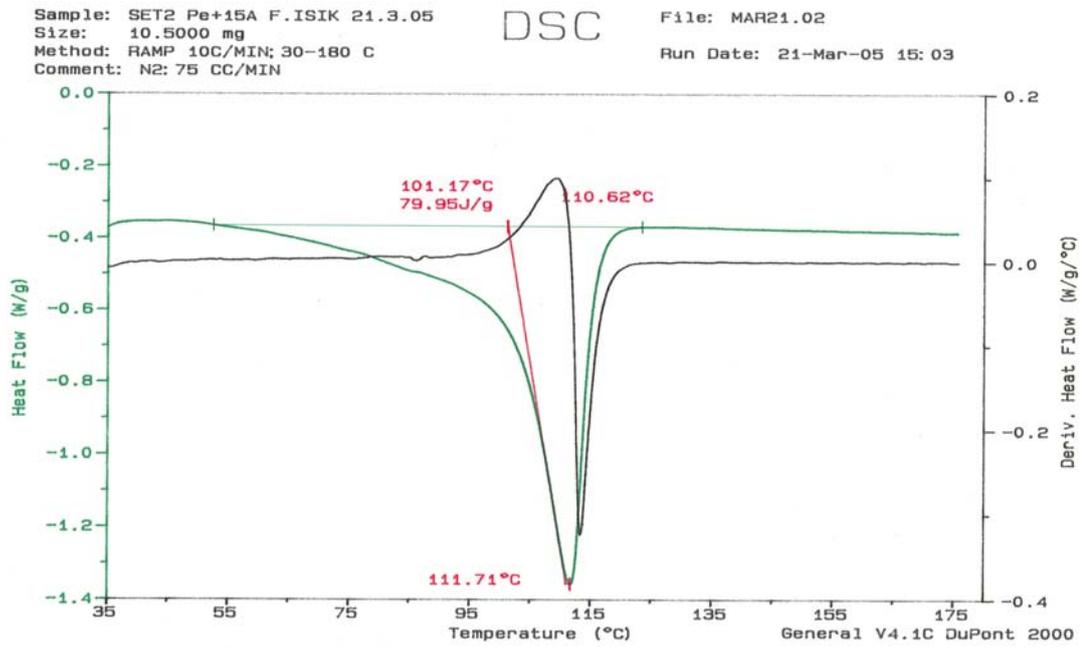
Figure B.2 DSC thermogram of nanocomposite containing 2 wt. % Cloisite® 15A
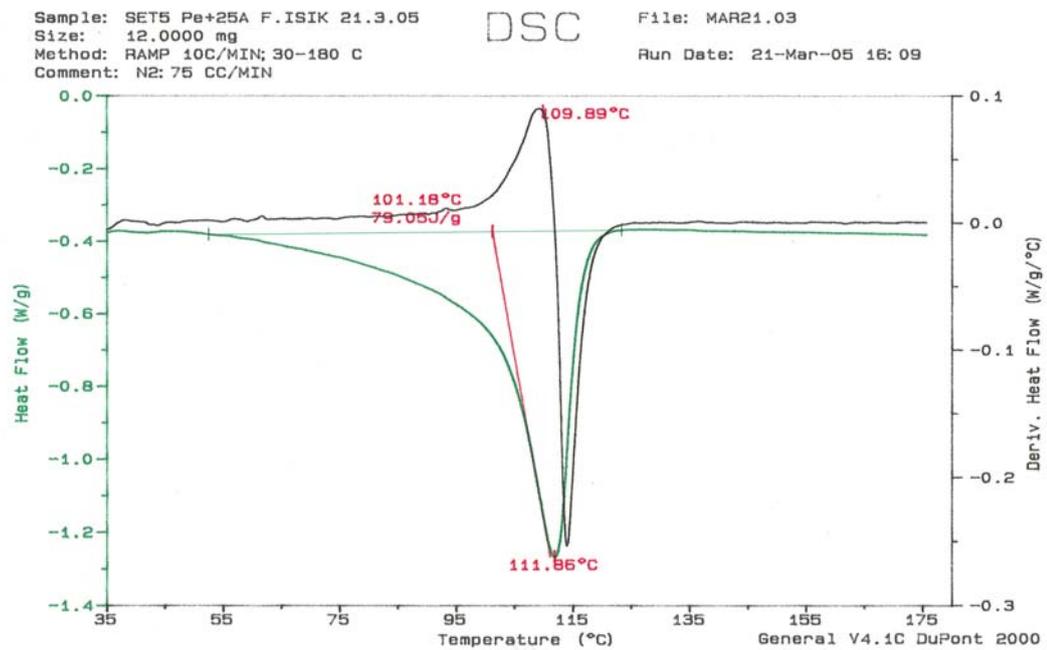
Figure B.3 DSC thermogram of nanocomposite containing 2 wt. % Cloisite® 25A .
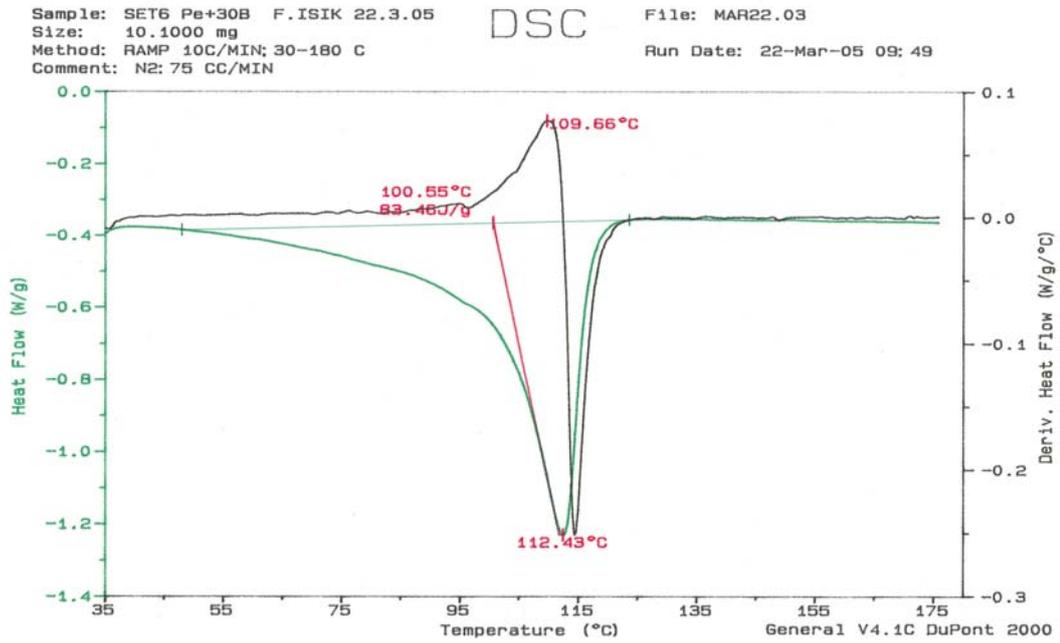
Figure B.4 DSC thermogram of nanocomposite containing 2 wt. % Cloisite® 30B .
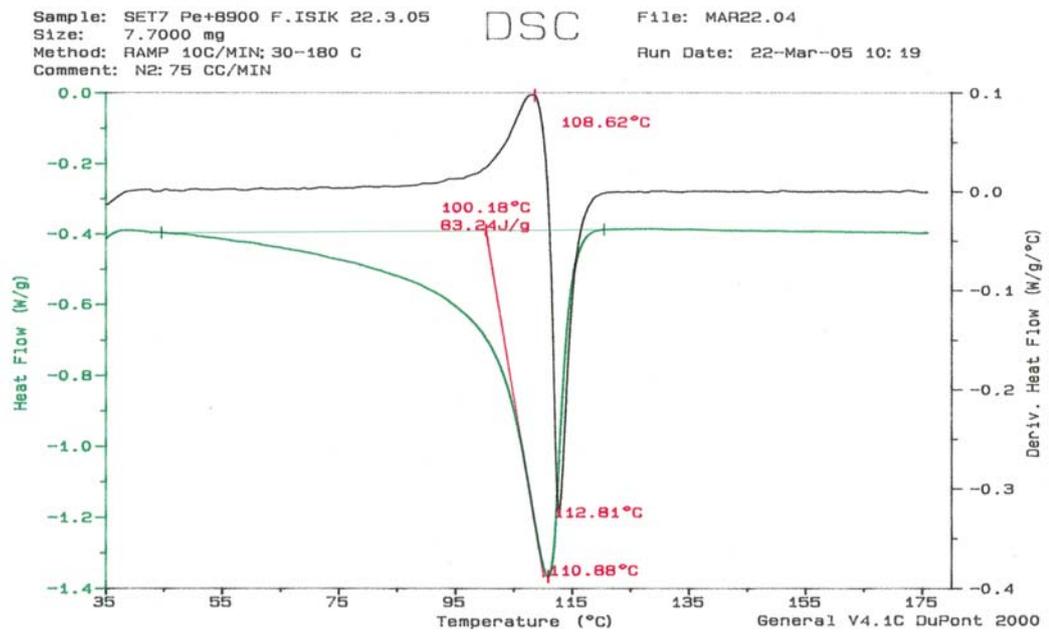
Figure B.5 DSC thermogram of composite containing 5 wt. % Lotader® AX 8900 .
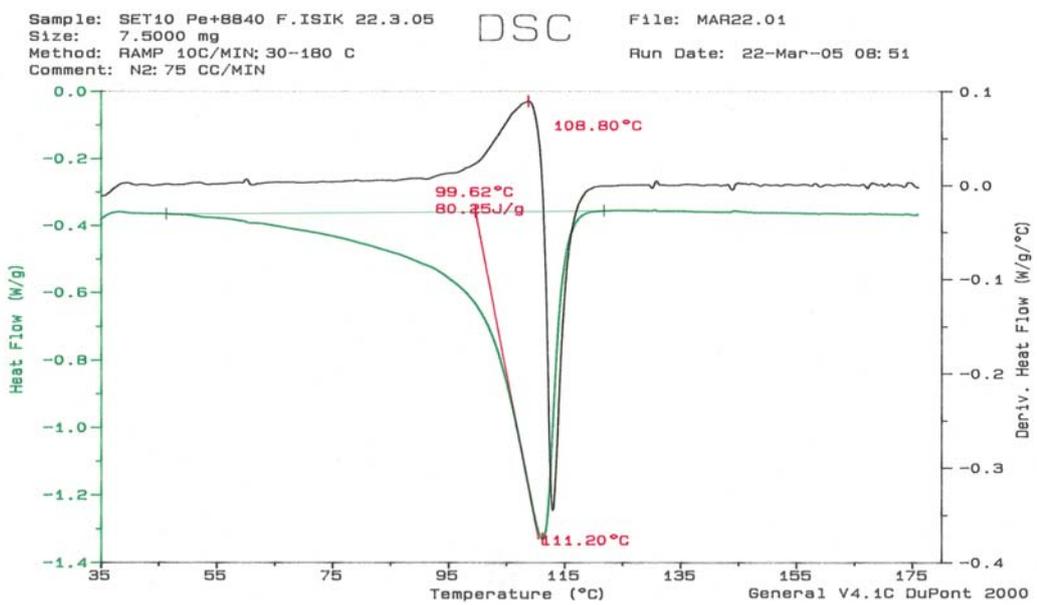
Figure B.6 DSC thermogram of composite containing 5 wt. % Lotader® AX 8840 .
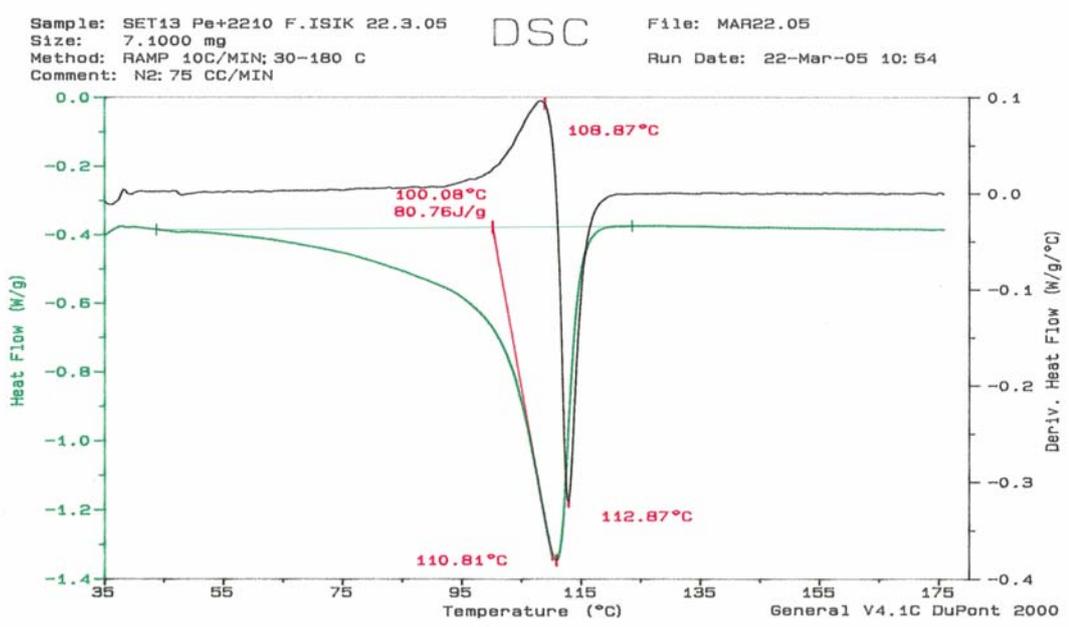
Figure B.7 DSC thermogram of composite containing 5 wt. % Lotader® 2210 .
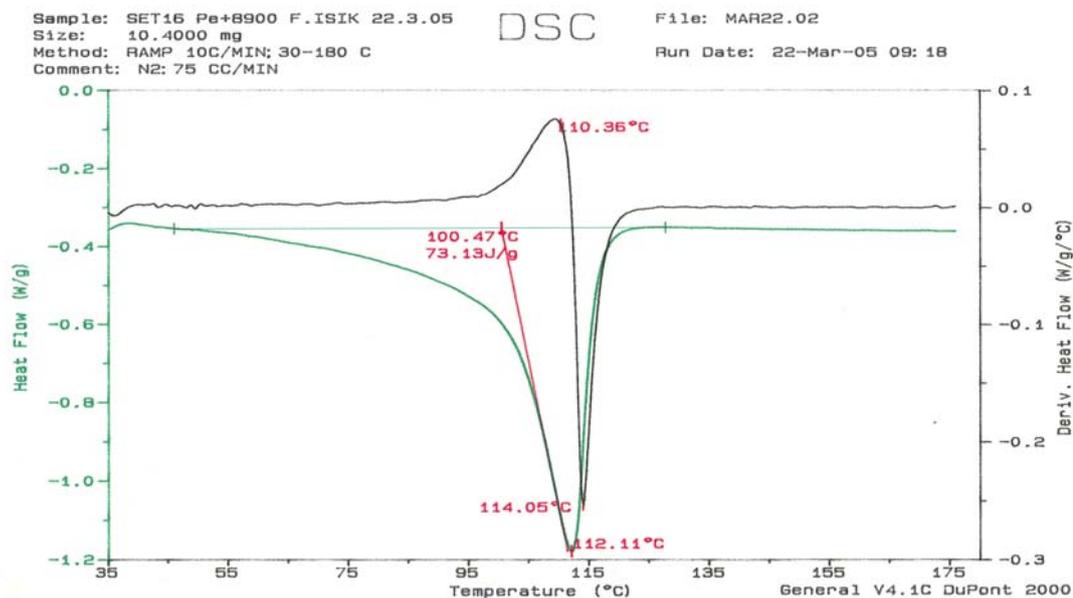
Figure B.8 DSC thermogram of nanocomposite produced with AO4 sequence, containing 2 wt. % Cloisite® 15A, and 5 wt. % Lotader® AX 8900 .
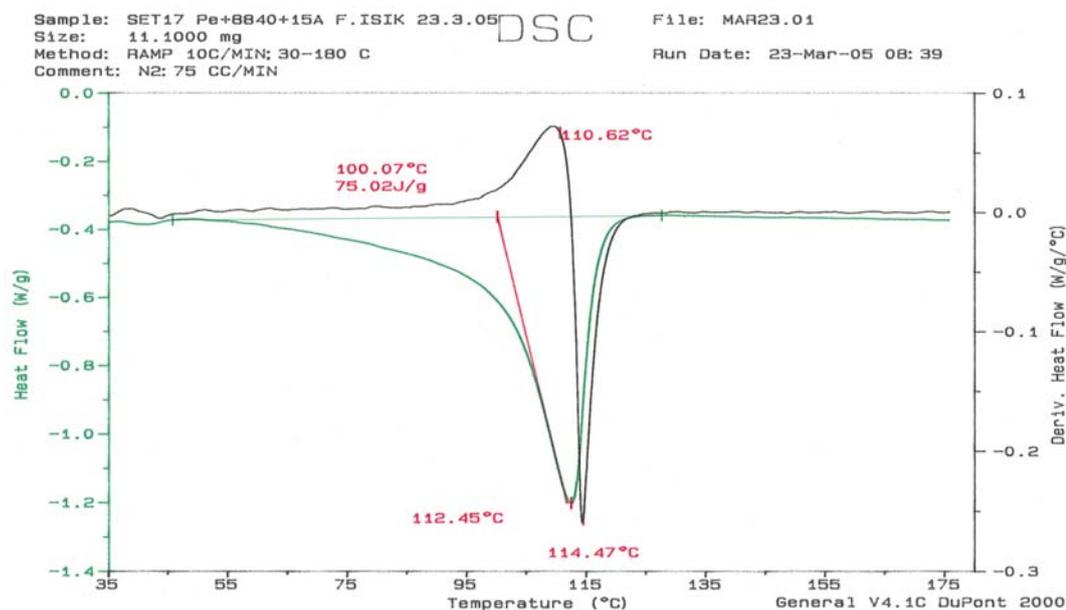
Figure B.9 DSC thermogram of nanocomposite produced with AO4 sequence, containing 2 wt. % Cloisite® 15A, and 5 wt. % Lotader® AX 8840 .
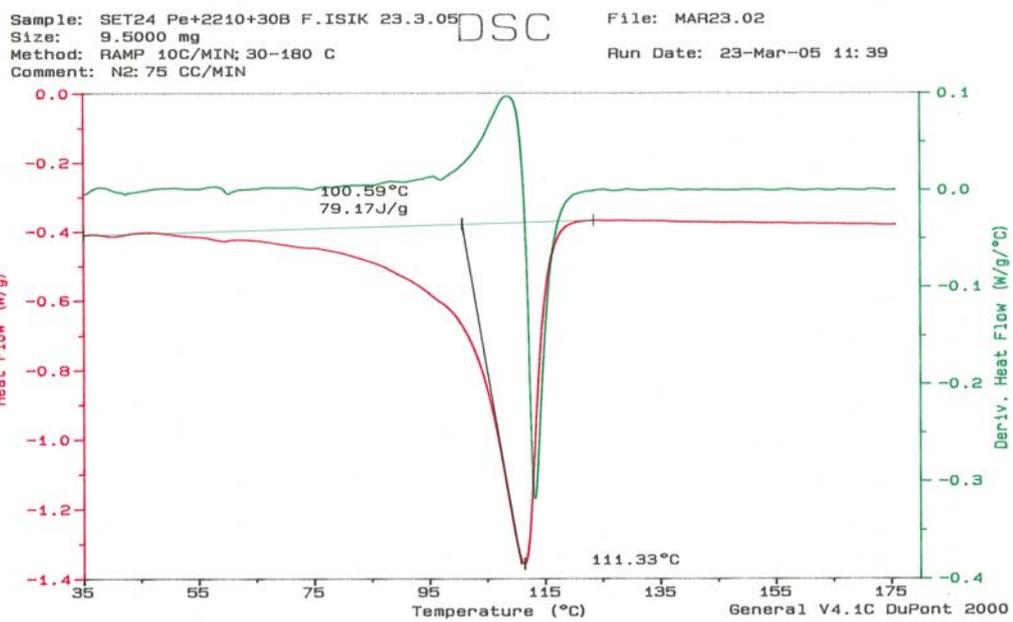
Figure B.10 DSC thermogram of nanocomposite produced with AO4 sequence, containing 2 wt. % Cloisite® 30B, and 5 wt. % Lotader® 2210 .
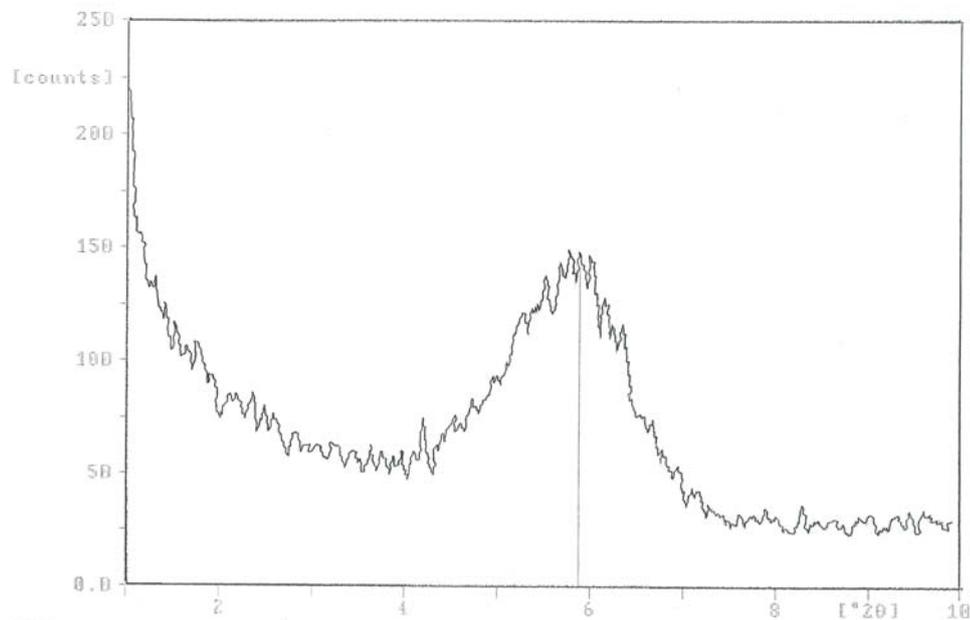
APPENDIX C

Mechanical Test Results

Table C.1 Tensile strength data for all samples

Composition	Organoclay wt %	Tensile Strength (MPa)	St. Dev.
LDPE	-	18.2	0.4

LDPE/Organoclay

Composition	Organoclay wt %	Tensile Strength (MPa)	St. Dev.
LDPE+15A	2	17.5	0.6
LDPE+15A	4	19.7	1.6
LDPE+15A	6	16.1	0.9
LDPE+25A	2	21.5	1.1
LDPE+30B	2	18.2	0.5

LDPE/Compatibilizer

Composition	Compatibilizer wt %	Tensile Strength (MPa)	St. Dev.
LDPE + 8900	5	16.3	0.3
LDPE + 8900	10	14.9	0.8
LDPE + 8900	15	13.5	0.4
LDPE + 8840	5	16.9	0.5
LDPE + 8840	10	18.2	1.1
LDPE + 8840	15	17.1	1.3
LDPE + 2210	5	17.5	0.3
LDPE + 2210	10	21.6	0.4
LDPE + 2210	15	20.1	1.0

Table C.2 Tensile strength data for all samples (Cont'd)

Composition	Organoclay wt %	Tensile Strength (MPa)	St. Dev.
Ternary Compositions Prepared with AO4 Sequence (PCoC) [*]			
LDPE+8900+15A	2	26.0	0.6
LDPE+8840+15A	2	27.9	0.6
LDPE+2210+15A	2	23.0	0.5
LDPE+8900+25A	2	20.0	0.5
LDPE+8840+25A	2	22.0	0.3
LDPE+2210+25A	2	21.4	0.3
LDPE+8900+30B	2	21.6	0.5
LDPE+8840+30B	2	21.4	0.4
LDPE+2210+30B	2	26.3	0.3
LDPE/8900/15A Nanocomposites [*]			
AO1 (CoC)+P	2	15.6	0.3
AO2 (P+C)+Co	2	25.8	0.7
AO3 (P+Co)+C	2	16.7	0.3
AO4 (PCoC)	2	26.0	0.6
LDPE/8900/15A Nanocomposites [**]			
AO1 (CoC)+P	2	14.6	0.2
AO2 (P+C)+Co	2	14.8	2.6
AO3 (P+Co)+C	2	20.6	0.1
AO4 (PCoC)	2	24.6	0.6
LDPE /2210/30B Nanocomposites [*]			
AO1 (CoC)+P	2	18.1	1.5
AO2 (P+C)+Co	2	16.6	0.9
AO3 (P+Co)+C	2	17.6	1.0
AO4 (PCoC)	2	26.3	0.3

* 5 wt % compatibilizer loaded nanocomposites

** 10 wt % compatibilizer loaded nanocomposites

Table C.3 Tensile modulus data for all samples

Composition	Organoclay wt %	Tensile Modulus (MPa)	St. Dev.
LDPE	-	162.6	3.6

LDPE/Organoclay

Composition	Organoclay wt %	Tensile Modulus (MPa)	St. Dev.
LDPE+15A	2	169.1	4.6
LDPE+15A	4	233.2	48.3
LDPE+15A	6	227.0	8.6
LDPE+25A	2	202.6	24.9
LDPE+30B	2	197.3	10.7

LDPE/Compatibilizer

Composition	Compatibilizer wt %	Tensile Modulus (MPa)	St. Dev.
LDPE + 8900	5	143.9	2.9
LDPE + 8900	10	134.9	13.3
LDPE + 8900	15	114.2	4.5
LDPE + 8840	5	155.4	9.2
LDPE + 8840	10	162.7	24.1
LDPE + 8840	15	152.0	11.7
LDPE + 2210	5	144.9	9.3
LDPE + 2210	10	221.4	9.7
LDPE + 2210	15	187.3	19.1

Table C.4 Tensile modulus data for all samples (Cont'd)

Composition	Organoclay wt %	Tensile Modulus (MPa)	St. Dev.
Ternary Compositions Prepared with AO4 Sequence (PCoC)[*]			
LDPE+8900+15A	2	230.3	6.6
LDPE+8840+15A	2	251.1	16.9
LDPE+2210+15A	2	229.3	4.9
LDPE+8900+25A	2	180.0	7.9
LDPE+8840+25A	2	229.3	3.8
LDPE+2210+25A	2	256.2	7.8
LDPE+8900+30B	2	214.5	19.3
LDPE+8840+30B	2	244.4	9.3
LDPE+2210+30B	2	279.8	20.6
LDPE/8900/15A Nanocomposites [*]			
AO1 (CoC)+P	2	199.0	6.9
AO2 (P+C)+Co	2	243.3	19.1
AO3 (P+Co)+C	2	162.1	26.6
AO4 (PCoC)	2	230.3	6.6
LDPE/8900/15A Nanocomposites [**]			
AO1 (CoC)+P	2	251.0	2.1
AO2 (P+C)+Co	2	111.5	39.6
AO3 (P+Co)+C	2	186.8	16.6
AO4 (PCoC)	2	221.1	3.9
LDPE /2210/30B Nanocomposites [*]			
AO1 (CoC)+P	2	143.6	11.0
AO2 (P+C)+Co	2	135.6	8.1
AO3 (P+Co)+C	2	128.7	12.1
AO4 (PCoC)	2	279.8	20.6

* 5 wt % compatibilizer loaded nanocomposites

** 10 wt % compatibilizer loaded nanocomposites

Table C.5 Tensile strain at break data for all samples

Composition	Organoclay wt %	Tensile Strain at Break (%)	St. Dev.
LDPE	-	39.7	1.1

LDPE/Organoclay			
LDPE+15A	2	41.5	1.3
LDPE+15A	4	33.5	7.1
LDPE+15A	6	27.2	1.4
LDPE+25A	2	30.2	6.1
LDPE+30B	2	23.7	3.2

LDPE/Compatibilizer			
Composition	**Compatibilizer wt %**	**Tensile Strain at Break (%)**	**St. Dev.**
LDPE + 8900	5	42.1	1.3
LDPE + 8900	10	32.5	2.5
LDPE + 8900	15	40.3	1.7
LDPE + 8840	5	35.4	2.2
LDPE + 8840	10	33.6	4.0
LDPE + 8840	15	25.7	2.3
LDPE + 2210	5	33.0	6.9
LDPE + 2210	10	28.0	1.9
LDPE + 2210	15	37.8	3.1

Table C.6 Tensile strain at break data for all samples (Cont'd)

Composition	Organoclay wt %	Tensile Strain at Break (%)	St. Dev.
Ternary Compositions Prepared with AO4 Sequence (PCoC)[*]			
LDPE+8900+15A	2	40.0	1.9
LDPE+8840+15A	2	43.4	1.4
LDPE+2210+15A	2	37.4	3.1
LDPE+8900+25A	2	33.5	2.7
LDPE+8840+25A	2	32.7	5.6
LDPE+2210+25A	2	26.5	6.1
LDPE+8900+30B	2	32.4	2.0
LDPE+8840+30B	2	27.8	1.3
LDPE+2210+30B	2	41.2	1.6
LDPE/8900/15A Nanocomposites [*]			
AO1 (CoC)+P	2	43.9	2.4
AO2 (P+C)+Co	2	31.7	3.9
AO3 (P+Co)+C	2	39.3	1.9
AO4 (PCoC)	2	40.0	1.9
LDPE/8900/15A Nanocomposites [**]			
AO1 (CoC)+P	2	43.7	2.3
AO2 (P+C)+Co	2	46.9	1.5
AO3 (P+Co)+C	2	39.7	0.9
AO4 (PCoC)	2	36.3	1.9
LDPE /2210/30B Nanocomposites [*]			
AO1 (CoC)+P	2	28.4	4.0
AO2 (P+C)+Co	2	32.5	1.1
AO3 (P+Co)+C	2	31.6	4.9
AO4 (PCoC)	2	41.2	1.6

* 5 wt % compatibilizer loaded nanocomposites

** 10 wt % compatibilizer loaded nanocomposites

Table C.7 Flexural strength data for all samples

Composition	Organoclay wt %	Flexural Strength (MPa)	St. Dev.
LDPE	-	8.0	0.3

LDPE/Organoclay

Composition	Organoclay wt %	Flexural Strength (MPa)	St. Dev.
LDPE+15A	2	7.9	0.4
LDPE+15A	4	9.9	0.4
LDPE+15A	6	9.6	0.5
LDPE+25A	2	10.2	0.6
LDPE+30B	2	10.5	0.2

LDPE/Compatibilizer

Composition	Compatibilizer wt %	Flexural Strength (MPa)	St. Dev.
LDPE + 8900	5	7.9	0.5
LDPE + 8900	10	7.0	0.3
LDPE + 8900	15	7.1	0.2
LDPE + 8840	5	8.4	1.2
LDPE + 8840	10	9.3	0.3
LDPE + 8840	15	9.4	0.1
LDPE + 2210	5	10.0	0.9
LDPE + 2210	10	9.1	0.3
LDPE + 2210	15	8.4	0.4

Table C.8 Flexural strength data for all samples (Cont'd)

Composition	Organoclay wt %	Flexural Strength (MPa)	St. Dev.
Ternary Compositions Prepared with AO4 Sequence (PCoC)[*]			
LDPE+8900+15A	2	9.7	0.7
LDPE+8840+15A	2	10.7	0.1
LDPE+2210+15A	2	10.1	0.6
LDPE+8900+25A	2	9.5	0.2
LDPE+8840+25A	2	10.2	0.3
LDPE+2210+25A	2	10.1	0.7
LDPE+8900+30B	2	8.9	0.2
LDPE+8840+30B	2	10.2	0.2
LDPE+2210+30B	2	10.9	0.5
LDPE/8900/15A Nanocomposites [*]			
AO1 (CoC)+P	2	7.4	0.1
AO2 (P+C)+Co	2	9.9	0.7
AO3 (P+Co)+C	2	7.1	0.4
AO4 (PCoC)	2	9.7	0.6
LDPE/8900/15A Nanocomposites [**]			
AO1 (CoC)+P	2	6.8	0.3
AO2 (P+C)+Co	2	6.6	0.4
AO3 (P+Co)+C	2	6.4	0.1
AO4 (PCoC)	2	9.5	0.7
LDPE /2210/30B Nanocomposites [*]			
AO1 (CoC)+P	2	8.7	2.2
AO2 (P+C)+Co	2	9.5	0.5
AO3 (P+Co)+C	2	10.2	2.3
AO4 (PCoC)	2	10.9	0.5

* 5 wt % compatibilizer loaded nanocomposites

** 10 wt % compatibilizer loaded nanocomposites

Table C.9 Flexural Modulus data for all samples

Composition	Organoclay wt %	Flexural Modulus (MPa)	St. Dev.
LDPE	-	244.7	16.3

LDPE/Organoclay			
LDPE+15A	2	241.9	19.1
LDPE+15A	4	289.5	6.9
LDPE+15A	6	338.8	39.0
LDPE+25A	2	281.4	15.3
LDPE+30B	2	283.9	20.8

LDPE/Compatibilizer			
Composition	Compatibilizer wt %	Flexural Modulus (MPa)	St. Dev.
LDPE + 8900	5	251.7	14.3
LDPE + 8900	10	209.9	20.0
LDPE + 8900	15	164.8	7.3
LDPE + 8840	5	225.4	36.6
LDPE + 8840	10	247.7	30.8
LDPE + 8840	15	212.5	11.8
LDPE + 2210	5	263.6	20.8
LDPE + 2210	10	246.5	7.4
LDPE + 2210	15	206.4	9.9

Table C.10 Flexural Modulus data for all samples (Cont'd)

Composition	Organoclay wt %	Flexural Modulus (MPa)	St. Dev.
Ternary Compositions Prepared with AO4 Sequence (PCoC)[*]			
LDPE+8900+15A	2	280.4	18.1
LDPE+8840+15A	2	278.1	7.8
LDPE+2210+15A	2	239.9	10.5
LDPE+8900+25A	2	233.3	7.5
LDPE+8840+25A	2	249.8	11.2
LDPE+2210+25A	2	258.5	23.8
LDPE+8900+30B	2	216.4	7.2
LDPE+8840+30B	2	269.9	7.9
LDPE+2210+30B	2	287.9	14.8
LDPE/8900/15A Nanocomposites [*]			
AO1 (CoC)+P	2	208.5	14.0
AO2 (P+C)+Co	2	330.0	26.5
AO3 (P+Co)+C	2	209.9	6.2
AO4 (PCoC)	2	280.4	32.7
LDPE/8900/15A Nanocomposites [**]			
AO1 (CoC)+P	2	189.2	9.5
AO2 (P+C)+Co	2	209.4	13.7
AO3 (P+Co)+C	2	188.0	10.4
AO4 (PCoC)	2	280.7	18.1
LDPE /2210/30B Nanocomposites [*]			
AO1 (CoC)+P	2	221.0	44.7
AO2 (P+C)+Co	2	245.5	6.7
AO3 (P+Co)+C	2	227.6	25.2
AO4 (PCoC)	2	287.9	14.8

* 5 wt % compatibilizer loaded nanocomposites

** 10 wt % compatibilizer loaded nanocomposites